

PM_{2.5} State Implementation Plan

Meteorological Modeling

Prepared by:

Dr. Erik Crosman
Christopher Foster, M.S.

Department of Atmospheric Sciences
University of Utah
135 S 1460 E Rm 819 WBB
Salt Lake City, UT

For

Patrick Barickman
Utah Division of Air Quality
195 North 1950 West
Salt Lake City, Utah 84116

16 November, 2016
Updated 2 March, 2017

Summary

This technical support document summarizes the meteorological modeling used by the Utah Division of Air Quality for their wintertime PM_{2.5} State Implementation Plan. Research over the past 4 years have led to improved meteorological simulations for cold-air pool episodes in northern Utah. This document describes in depth the Weather Research and Forecasting (WRF) model configuration and improvements to surface parameters and the model surface state (e.g., snow cover, vegetation depth and albedo). Three simulations of persistent cold-air pools are run for January 2011, December 2013, and February 2016. Extensive observations from the persistent cold air pool study (PCAPS) in the Salt Lake Valley during January 2011 are used for an in-depth model performance evaluation (MPE) for that episode. Radiosondes, satellite imagery, ceilometers, and surface measurements are used to evaluate the remaining two cases in December 2013 and February 2016. The model validation highlights the importance of evaluating vertical profiles of temperature and wind speed within cold-air pools, as well as the heightened sensitivity of cold-air pools to snow cover, cloud cover, and lake surface conditions in the various Utah basins.

The meteorological simulations all capture the strong vertical static stability (or capping inversion) and the onset, intensity, and decay of the cold-air pools. Previous modeling of cold-pools in many cases was unable to simulate these key aspects. However, the vertical mixing depth in the numerical simulations of the cold-air pools appears to be systematically biased 100+ m too shallow compared to available observations.

The weak 10-m wind speeds (generally below 2.5 m s⁻¹) that are a common observed feature during cold-air pools are well-simulated in all basins for all three of the simulations. Previous cold-air pool simulations have struggled with premature strong winds and resulting early pollutant mix-out.

The 2-m temperature evolution is simulated well in the Salt Lake Valley in all simulations, for which the model surface state was modified based on PCAPS observations to correctly represent the urban and surrounding Great Salt Lake surface state. However, model over- and under-estimation of both cloud cover and snow cover negatively impacted in some cases the surface temperature in the Cache Valley, Utah Valley, and Uintah Basin.. It is unknown how much of an impact these performance characteristics have on the overall dispersion and transport within the cold-air pools.

Table of Contents

1.	Introduction	5
1.1	Overview.....	5
1.2	<i>Cold-Air Pool Modeling Challenges</i>	6
1.3	<i>Cold-Air Pool Episode Selection</i>	8
2.	WRF Meteorological Modeling Configuration	9
2.1	Overview.....	9
2.2	<i>Modeling Domain and Resolution</i>	9
2.3	<i>Land Use and Topographic Data</i>	12
2.4	<i>Atmospheric Initial and Boundary-Conditions</i>	13
2.5	<i>Surface and Snow Cover Initialization</i>	13
2.6	<i>Modifications to Snow and Vegetation Parameters</i>	17
2.7	<i>Data Assimilation and Nudging</i>	20
2.8	<i>WRF Physics Options</i>	20
3.	WRF Meteorological Modeling Performance Evaluation (MPE).....	20
3.1	Overview.....	20
3.2	<i>Performance Evaluation Observational Datasets</i>	20
3.3	<i>1-11 January 2011 Vertical Cold-Air Pool Structure Model Evaluation</i>	23
3.3.1	<i>PCAPS 1-11 January 2011 Vertical Cold-Air Pool Structure Model Evaluation</i>	23
3.3.2	<i>PCAPS 1-11 January 2011 Case Surface Cold-Air Pool Model Evaluation</i>	28
3.3.3	<i>1-11 January 2011 Surface Cold-Air Pool Model Evaluation Using Standard Obs</i>	37
3.4	<i>7-21 December 2013 Cold-Air Pool Model Performance Evaluation</i>	42
3.4.1	<i>7-21 December 2013 Vertical Cold-Air Pool Structure Model Evaluation</i>	46
3.4.2	<i>7-21 December 2013 Case Surface Cold-Air Pool Model Evaluation</i>	51
3.5	<i>1-17 February 2016 Cold-Air Pool Model Performance Evaluation</i>	54
3.5.1	<i>1-17 February 2016 Vertical Cold-Air Pool Structure Model Evaluation</i>	57
3.5.2	<i>1-17 February 2016 Case Surface Cold-Air Pool Model Evaluation</i>	57
4.	Summary	69
5.	References	70

1. Introduction

1.1 Overview

The Weather Research and Forecasting (WRF), Advanced Research WRF (WRF-ARW) model version 3.7 was used in this study. WRF meteorological model development of cold-air pool simulations has been conducted by the University of Utah over the past 4 years in both the Uintah Basin and in the Salt Lake Valley through research partially supported by both the Utah Division of Air Quality (UDAQ) and the National Science Foundation. In this technical support document, we present scientific support of the final configuration of the WRF meteorological model simulations provided to UDAQ and model performance evaluation (MPE) of three cold-air pools simulated for use in the UDAQ PM_{2.5} state implementation plan (SIP).

Meteorological modeling of cold-air pools remains difficult. In particular, the following aspects of cold-air pools are important for meteorological modeling as they all impact pollutant transport and mixing heights:

- Vertical profiles of temperature, humidity, and winds
- Clouds
- Land surface characterization
- Model initialization

Historically, air quality model performance evaluation has not included all of these characteristics, because the importance of the vertical profiles had not been demonstrated and the validation data sets did not typically exist for a vertical evaluation beyond basic surface weather station and infrequent weather balloon data. However, the Persistent Cold-Air Pool Study (PCAPS) in Utah's Salt Lake Valley in January 2011 provided unprecedented data to better understand cold-air pool evolution and numerical weather prediction of cold-air pools. Using PCAPS data, model performance evaluation of these 4 key areas will be used in this document to validate the meteorological simulation during the January 1-11 2011 cold-air pool in the Salt Lake Valley.

This document describes the meteorological modeling component of the Technical Support Document. The document is comprised of four main sections:

- Section 1). Overview of difficulties in modeling cold-air pools and what modeling techniques used to overcome these limitations.
- Section 2). WRF basic configuration details: domain, resolution, initial and boundary-conditions, physics options. WRF land use and snow cover modifications implemented to improve simulations discussed. Comparison of default and improved WRF configurations.
- Section 3). WRF model performance, with an emphasis on the vertical evolution of the cold-air pool evolution which is critical for modeling boundary-layer mixing during these

shallow pollution episodes. Also a brief discussion of improvements obtained through the modifications for the January 2011 cold-air pool will be discussed.

1.2 Cold-Air Pool Modeling Challenges

The episodic wintertime conditions that lead to air stagnation during cold-air pools have been the topic of significant study during the Persistent Cold-Air Pool Study (PCAPS) and the Uinta Basin Winter Ozone Study (UBWOS) (Lareau et al. 2013; Lyman et al. 2014). These studies identified the various weather patterns and meteorological conditions associated with highly stable boundary-layers and significant air-stagnation leading to elevated wintertime $PM_{2.5}$ in the Salt Lake Valley and elevated wintertime O_3 in the Uinta Basin. Figure 1 summarizes the key processes that must be properly simulated for meteorological simulations of cold-air pool pollutant transport. The default WRF model settings are often insufficient for cold-pool modeling, and modifications to the model were implemented as a result of extensive research and testing. As discussed by Neemann et al (2015) and Foster et al. (2017), surface state conditions in western U.S. cold pools are often poorly represented in standard operational weather forecast models. In addition, planetary boundary-layer parameterization schemes often struggle to properly simulate turbulent mixing within stable-boundary-layers as well as clouds.

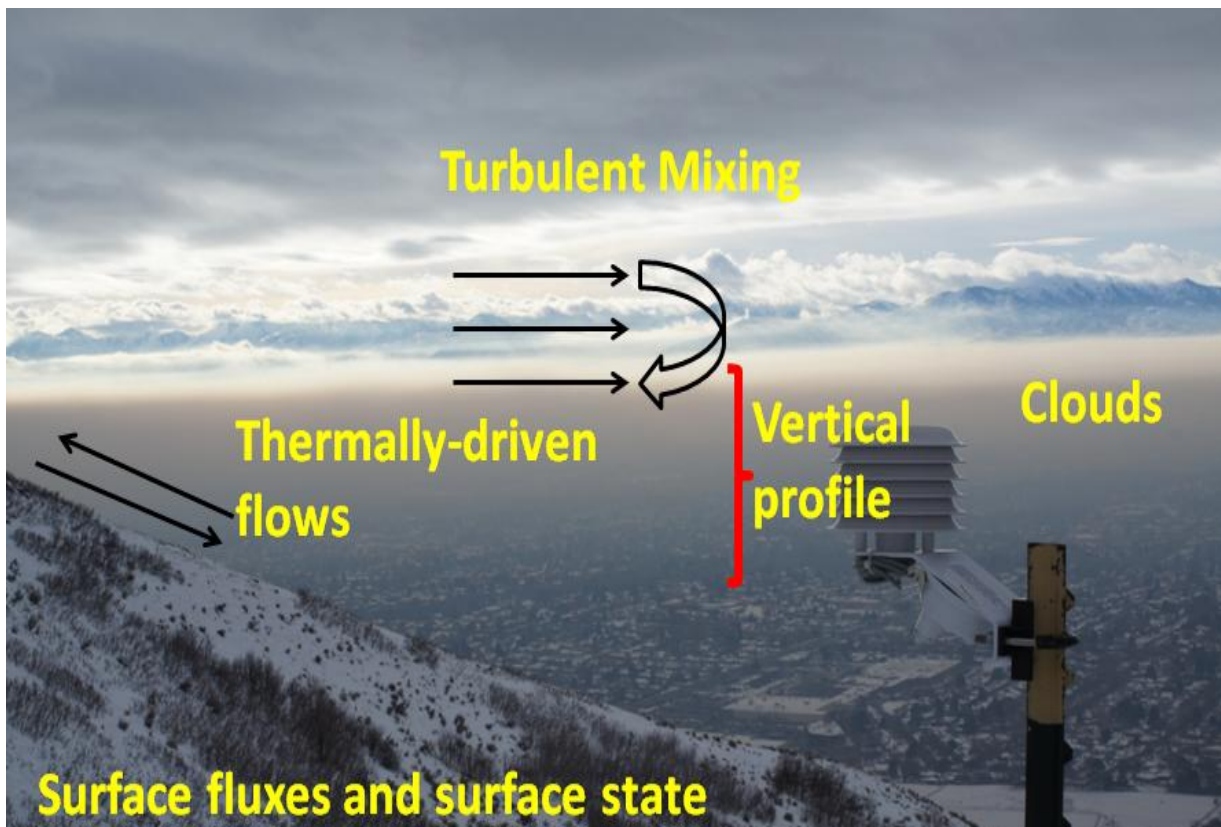


Figure 1. Several key processes that impact cold-pool meteorological simulations.

As discussed by Foster et al. (2017), the default land use characterization and snow cover fields (and thus surface flux and initial snow cover) are also often poorly represented in northern Utah. Across northern Utah, each of the three key basins have different modeling challenges that need to be addressed (Figure 2). In the Great Salt Lake Basin, complex flow patterns and exchange of air masses between the Utah Valley, Salt Lake Valley, and the Great Salt Lake are observed. In the Uintah Basin, the deep and bowl-shaped topography results in much longer-lived and more intense cold-pool structures than in the other Valleys. In the smaller Cache Valley, very intense and shallow inversions are observed, although a lack of vertical profiles exists in the Cache Valley.

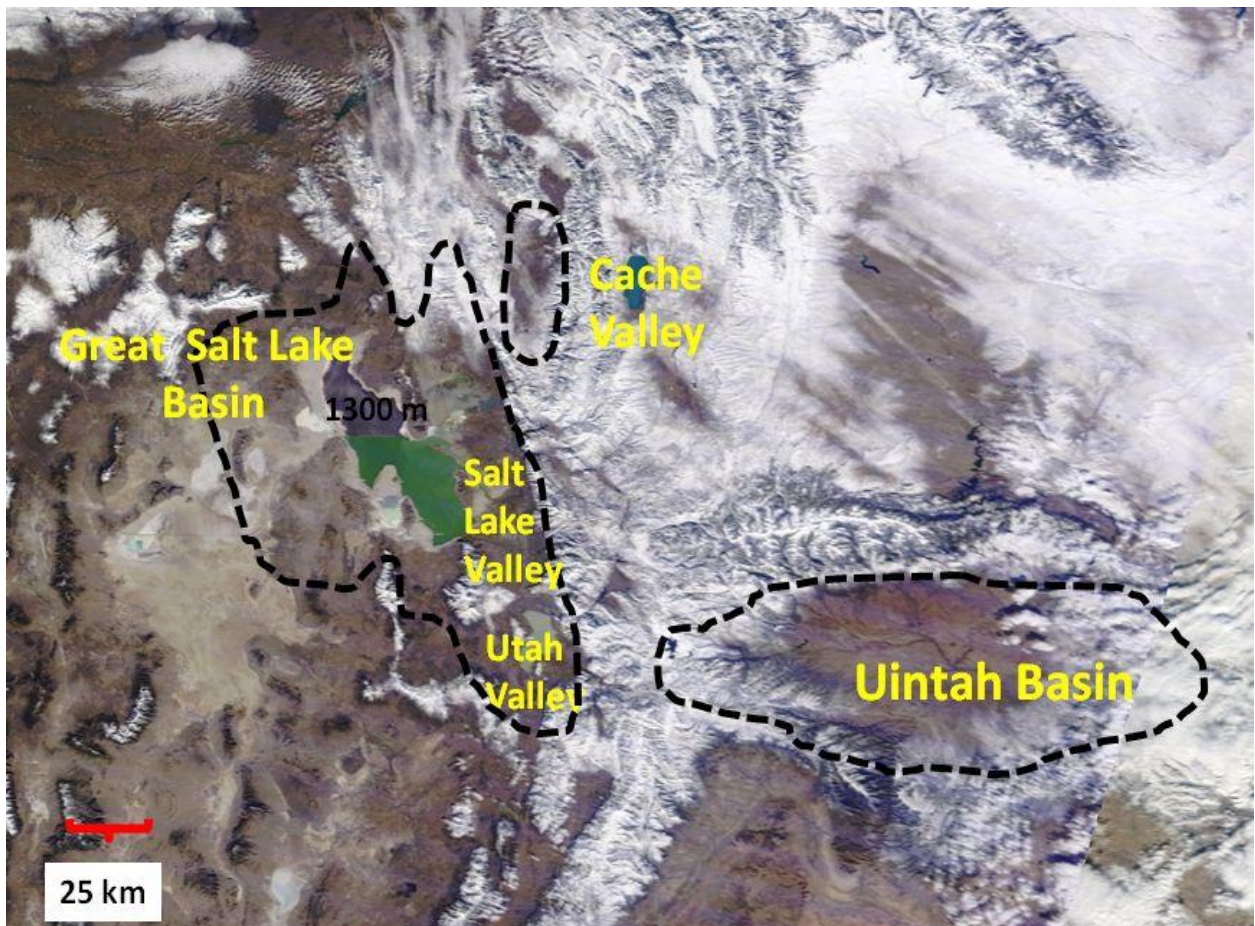


Figure 2. MODIS true color image of the three primary northern Utah basins and associated sub-basins that observe elevated wintertime pollutant concentrations during wintertime cold-air pools.

1.3 Cold-Air Pool Episode Selection

Three persistent cold-air pool episodes were selected. All of the cold-air pools were high impact episodes in terms of observed pollutant concentrations and long duration. Table 1 outlines the cold-pool episode duration as observed in the Salt Lake Valley. The January 2011 cold-air pool was studied in depth by Foster (2015) and Foster et al. (2017) as part of the initial work for this project, and was selected because of the rich validation data set available during the PCAPS field campaign that occurred in the winter of 2010-2011 (Lareau et al. 2013). There were significant differences between the evolution of the three cold-air pools, although all three were selected with light to moderate winds aloft, due to the fact that cold-air pools have been found to be very difficult to model accurately when wind speeds at mountaintop level are higher than $10\text{-}15\text{ m s}^{-1}$. All three episodes were snow covered at the beginning of the episode with greater than 4 cm of snow cover in the Salt Lake Valley, Cache Valley, and Uinta Basin. For the December 2013 and January 2011 cases, the cold-air pools remained snow covered for the duration of the episode (Figure 3). For the February 2016 episode, the snow had mostly melted during the last 3 days of the episode. Similarly, variations in cloud cover and wind speeds aloft were noted during the three episodes.

Table 1. Cold-air pool episodes modeled.

Cold-air pool start date (approximate)	Cold-air pool end date (approximate)	Duration of clouds(% of cold-air pool)	Duration of snow cover (% of cold-air pool)	Snow depth in valleys (m)
January 1 st 2011	January 11 th 2011	20%	100%	5-15 cm
December 7 th 2013	December 21 st 2013	40%	100%	10-20 cm
February 1 st 2016	February 17 th 2016	50%	75%	0-8 cm

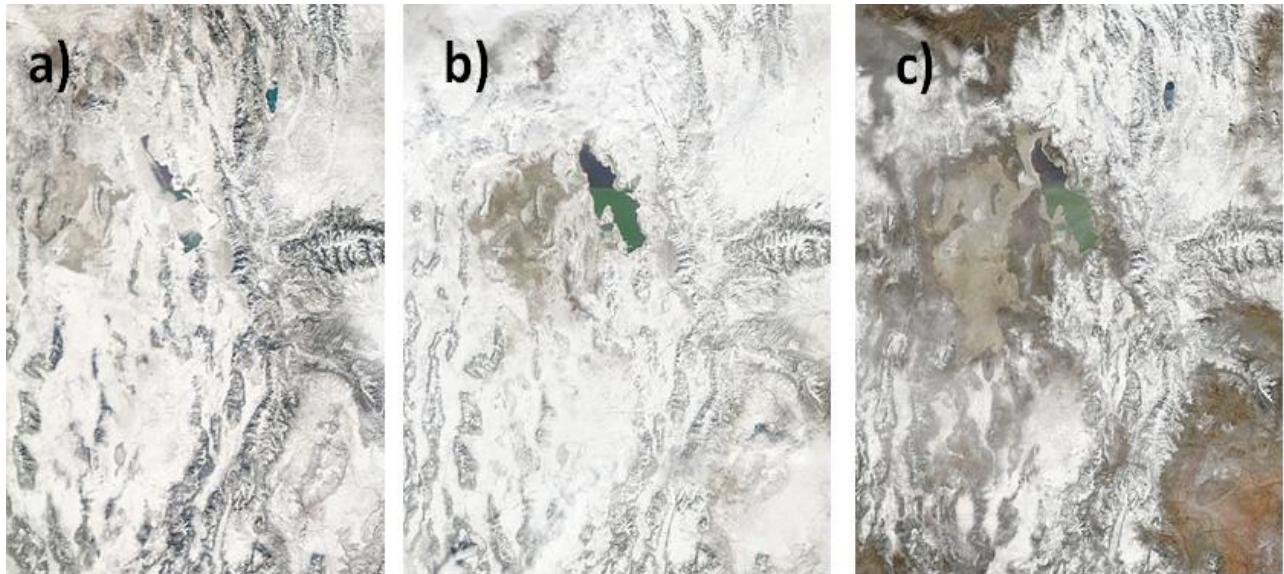


Figure 3. MODIS true color images over northern Utah and surroundings. a) 10 December 2013. B). 2 February 2016. C) 15 February 2016. See Figure 8 for snow cover for the January 2011 cold-air pool episode

2. WRF Meteorological Modeling Configuration

2.1 Overview

This section will describe UDAQ's configuration of the WRF model used for northern Utah. Additional details on the choice of the model configuration options, and several detailed sensitivity studies on the impacts of model improvements on cold-air pool structure can be found in Neemann (2014), Foster (2015), Neemann et al. (2015), and Foster et al. (2017).

2.2 Modeling Domain and Resolution

The modeling domain followed the general set-up used successfully for a number of cold-pool simulations over northern Utah (Foster (2015), Foster et al. 2017). The model uses a Lambert Conformal projection with a number of specific WRF WPS parameters needed to eliminate any grid overlap issues with the photochemistry model (Table 2). Three one-way nested simulations with horizontal grid spacing of 12 km, 4 km, and 1.33 km for the outer, middle, and innermost domains, respectively (Figure 4). The inner next was made large enough to easily cover the key basins of interest in northern Utah, namely the Great Salt Lake Basin, the Cache Valley, and the Uintah Basin.

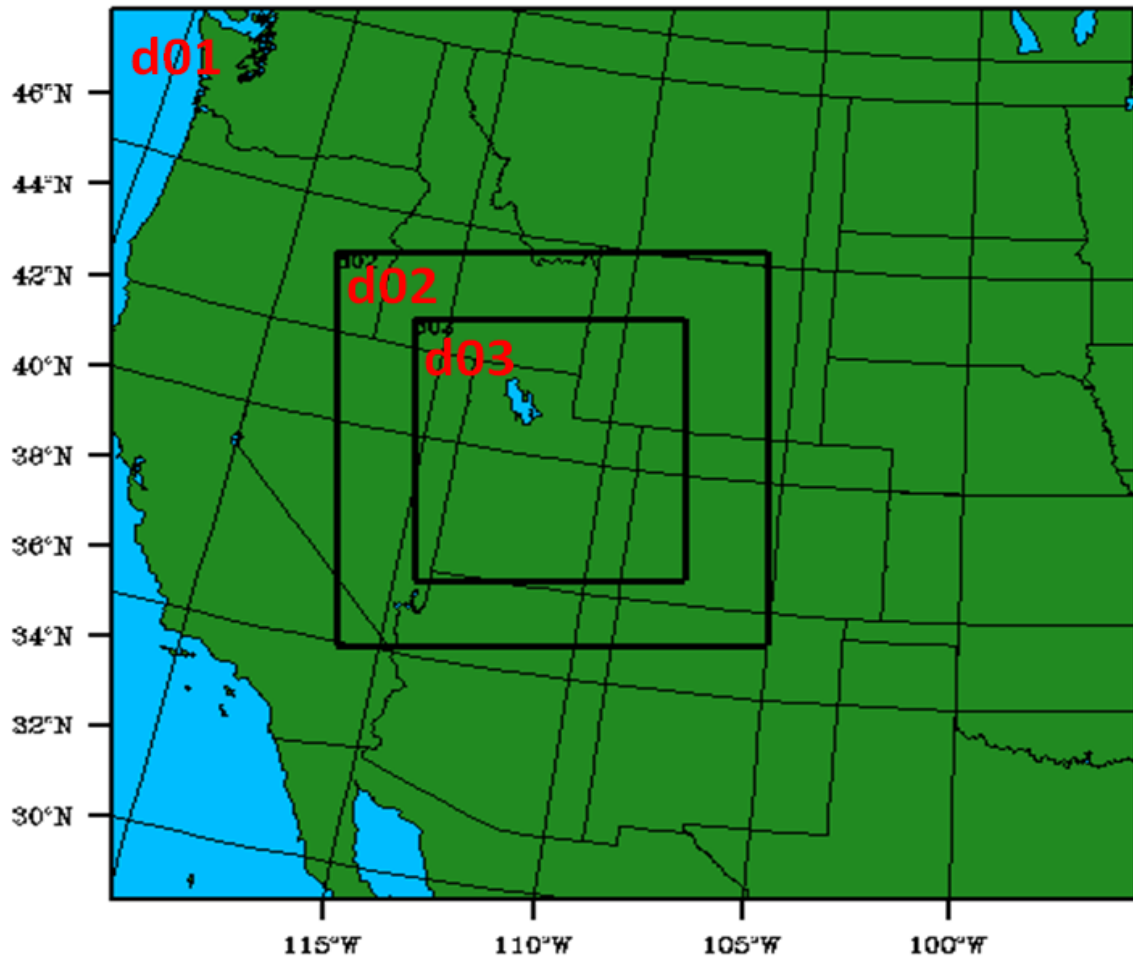


Figure 4. The WRF meteorological modeling domains (Outer d01=12 km, middle d02=4 km, and inner d03=1.33 km).

Previous UDAQ meteorological simulations did not include such high resolution inner nests (1.33 km), in part because they are very computationally expensive. However, Neemann et al. (2015) found that some local improvements in the cold-pool simulations were likely achieved by the higher-resolution model simulations. The higher-resolution simulations also allow for improved surface land use characterization and topography. A total of 42 vertical levels were used, with variable stretched spacing such that grid spacing increases from approximately 10 m near the surface > 500 m above 5,000 m AGL (Table 3). Increasing the number of vertical levels to as high as 109 did not have significant impacts on the on the cold-pool simulations. However, fewer than 30 levels began to degrade the cold-pool simulations near the surface (Neemann et al. 2015). For this study, we used the same number of vertical levels (41) found to be appropriate by Neemann et al. (2015).

Table 2. Grid definitions for WRF Preprocessor System (WPS).

Parameter name	Parameter value
Projection	Lambert conformal
Reference latitude	40 N
Reference longitude	-97 W
ref_y parameter	90.5
ref_x parameter	190.5
truelat1	33
truelat2 =	45
stand_lon =	-97

Table 3. WRF model grid configuration and topographical, land use and boundary and initial conditions.

	Domain 1	Doman 2	Domain 3
Grid Size (x,y)	200 x 190	250 x 250	475 x 499
Vertical levels	42	42	42
Vertica grid spacing	20-40 m in boundary-layer	20-40 m in boundary-layer	20-40 m in boundary-layer
Horizontal resolution (km)	12	4	1.33
Model time step (s)	45	15	5
Topographic dataset	USGS GTOPO30	USGS GTOPO30	USGS GTOPO30
Land use data set	NLCD2011 modified 9s	NLCD2011 modified 9s	NLCD2011 modified 9s
Veg parm table variables modified in BASE simulation	SNUP, MAXALB	SNUP, MAXALB	SNUP, MAXALB
Snow cover initialization in BASE (improved) simulation	Linear UofU obs analysis	Linear UofU obs analysis	Linear UofU obs analysis
Snow cover initialization in DFLT simulation	NAM	NAM	NAM
Initial and boundary-layer meteorology	NAM	NAM	NAM

2.3 Land Use and Topographic Data

The standard WRF USGS topography data (GTOPO30) was used in all three domains (Figure 5). However, the available default land use (UGSG) data was found to be insufficient. In this study, both the USGS and National Land Cover Database (NLCD) 2011 updated land use datasets were used.

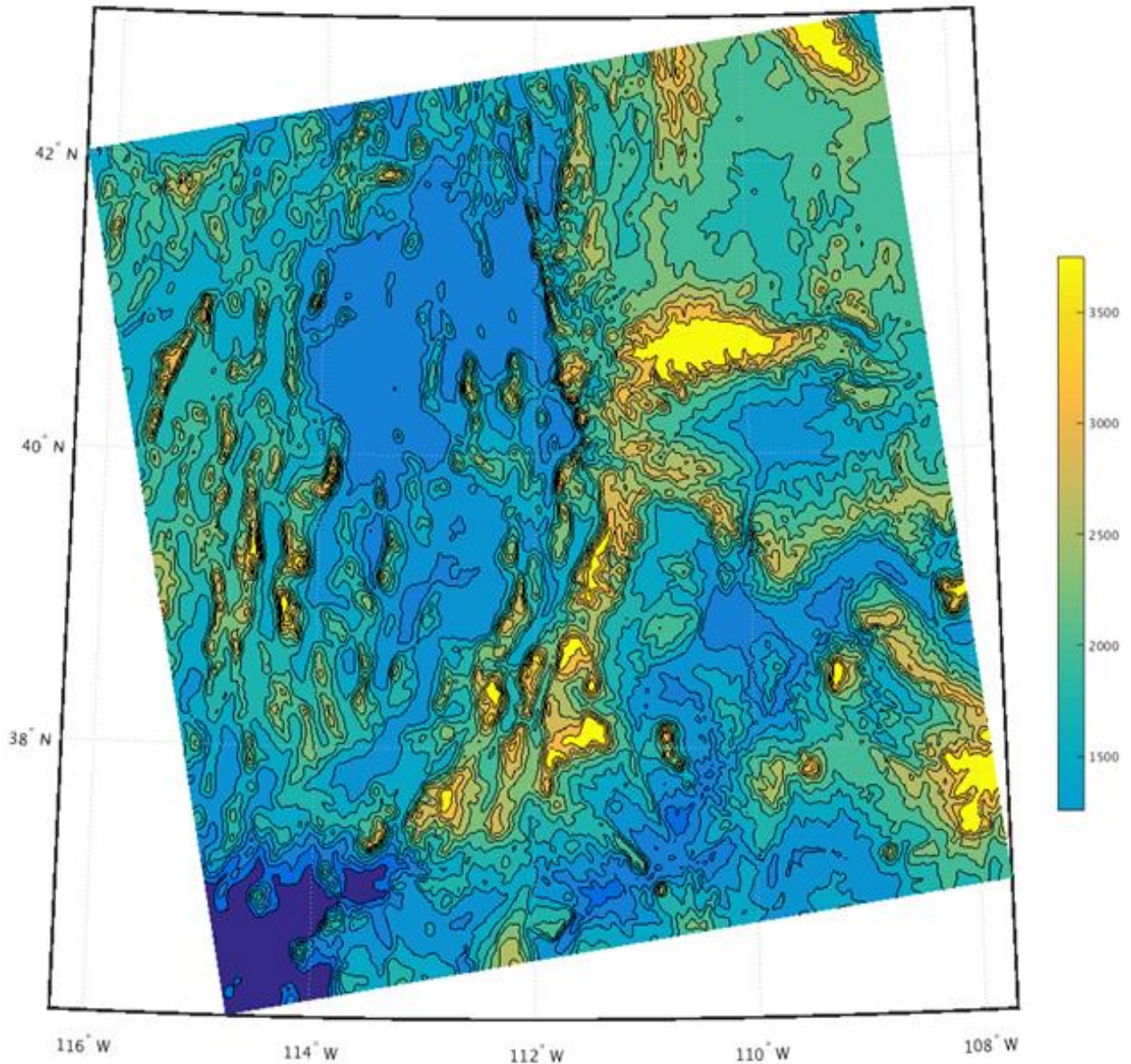


Figure 5. The WRF meteorological modeling topography for the inner d03=1.33 km nest. Blue colors range between 1000-2000 m ASL. Orange colors are between 2000-3000 m ASL, and yellow colors delineate high terrain > 3000 m ASL.

As seen in Figure 6 and 7, large differences are noted between the default WRF USGS land use characterization and the improved WRF NLCD updated land use in northern Utah and the Salt Lake Valley. In particular, the urban footprint and Great Salt Lake surface area were much improved by the updated NLCD2011 data set implemented for this study.

Satellite data from the National Aeronautics and Space Administration (NASA) was used in conjunction with the NLCD2011 data to provide the land use that was implemented in this study, which still overestimated the Great Salt Lake extent before the manual fixes were implemented. More details on the procedures employed to get the modified NLCD data set are given in Foster (2015) and Foster et al. (2017). For this study, the BASE simulation uses the best available land use (NLCD 2011 that was updated visually to improve Great Salt Lake surface area) and the improvements to the snow and vegetation parameters discussed in sections 2.5 and 2.6. The DFLT simulation used older land use (UGSG) and did not incorporate the improvements used in BASE. The DFLT simulation was not used by UDAQ for modeling. We show results for the DFLT simulation only to illustrate the improvements gained in the BASE meteorological simulation used by UDAQ in this study.

2.4 Atmospheric Initial and Boundary-Conditions

The initial and lateral atmospheric boundary-conditions for the simulations were provided by the National Center for Environmental Prediction (NCEP) North American Model (NAM) operational reanalysis data. Foster (2015) did testing to determine if the simulations were sensitive to the start time of the simulation and the quality of the initial analyses (as cold-air pools are often poorly represented in the analyses). Sensitivity to initiation time was found by Foster (2015), with improved simulations resulting from simulations that are not initialized in the center of an inversion period. Thus, for the simulations conducted for this study were all initialized *prior to the onset* of a cold-air pool by at least 12 hours.

2.5 Surface and Snow Cover Initialization

The initial soil moisture and soil temperature for the simulations were provided by the NAM operational reanalysis data. The available snow cover analyses in the NAM model analyses did not agree well with snow depth observations at a number of mesonet stations across northern Utah. Different research groups have taken different approaches to gain improved snow cover initialization, which was shown by Neemann et al. (2015) to have large impacts on the cold-pool temperature and vertical profiles. For the Utah DAQ WRF meteorological modeling, we employed a basic fit similar to that of Neemann (2015) by utilizing all available snow depth and water equivalent observations from the following reporting stations:

- SNOTEL
- CoCORAHs
- National Weather Service
- Cooperative Weather Observer Co-Op and sites
- PCAPS volunteer station

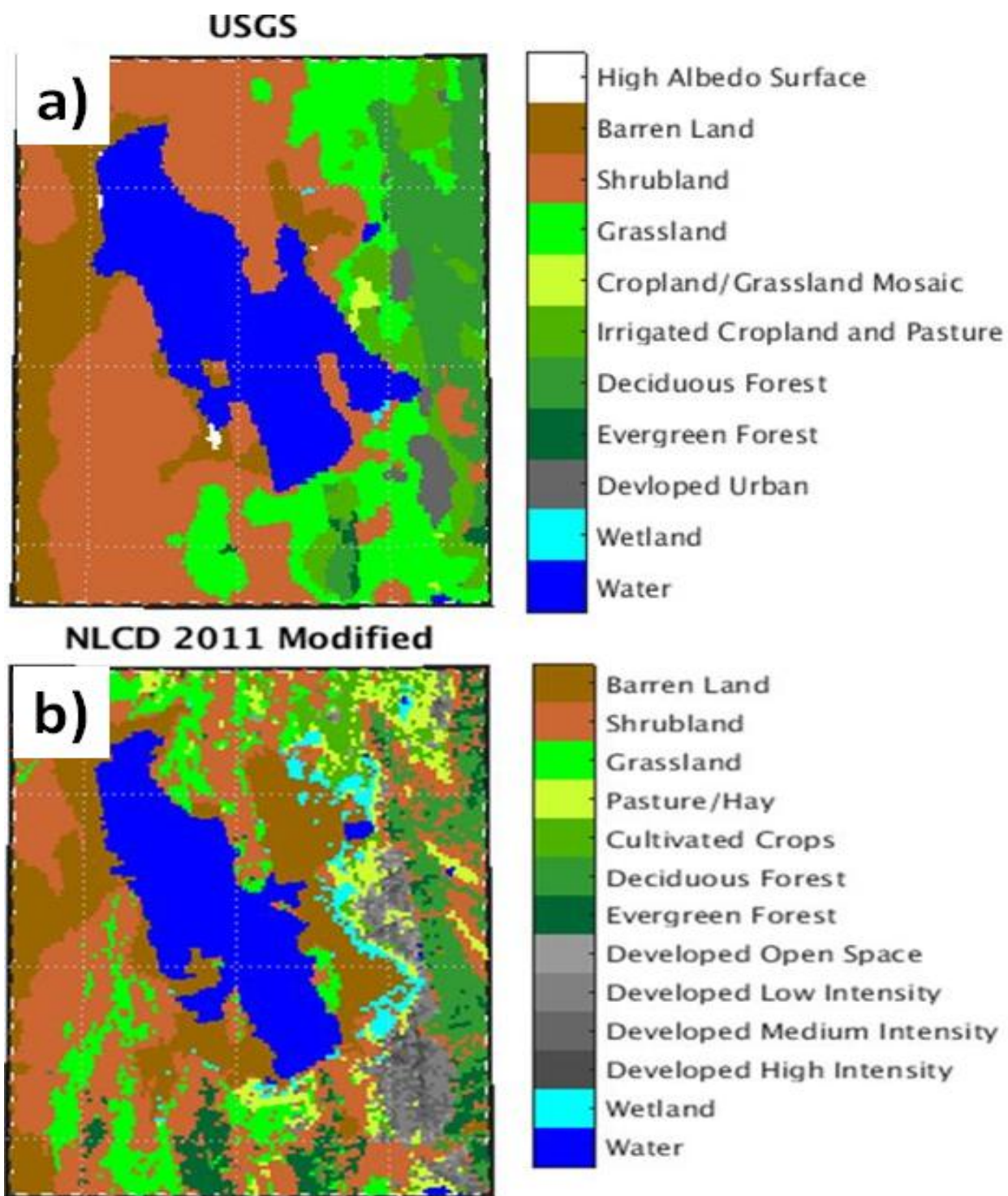


Figure 6. (a) Default WRF land use in the Salt Lake Valley (USGS circa 1993) and (b) the modified 2011 NLCD land use applied in this study.

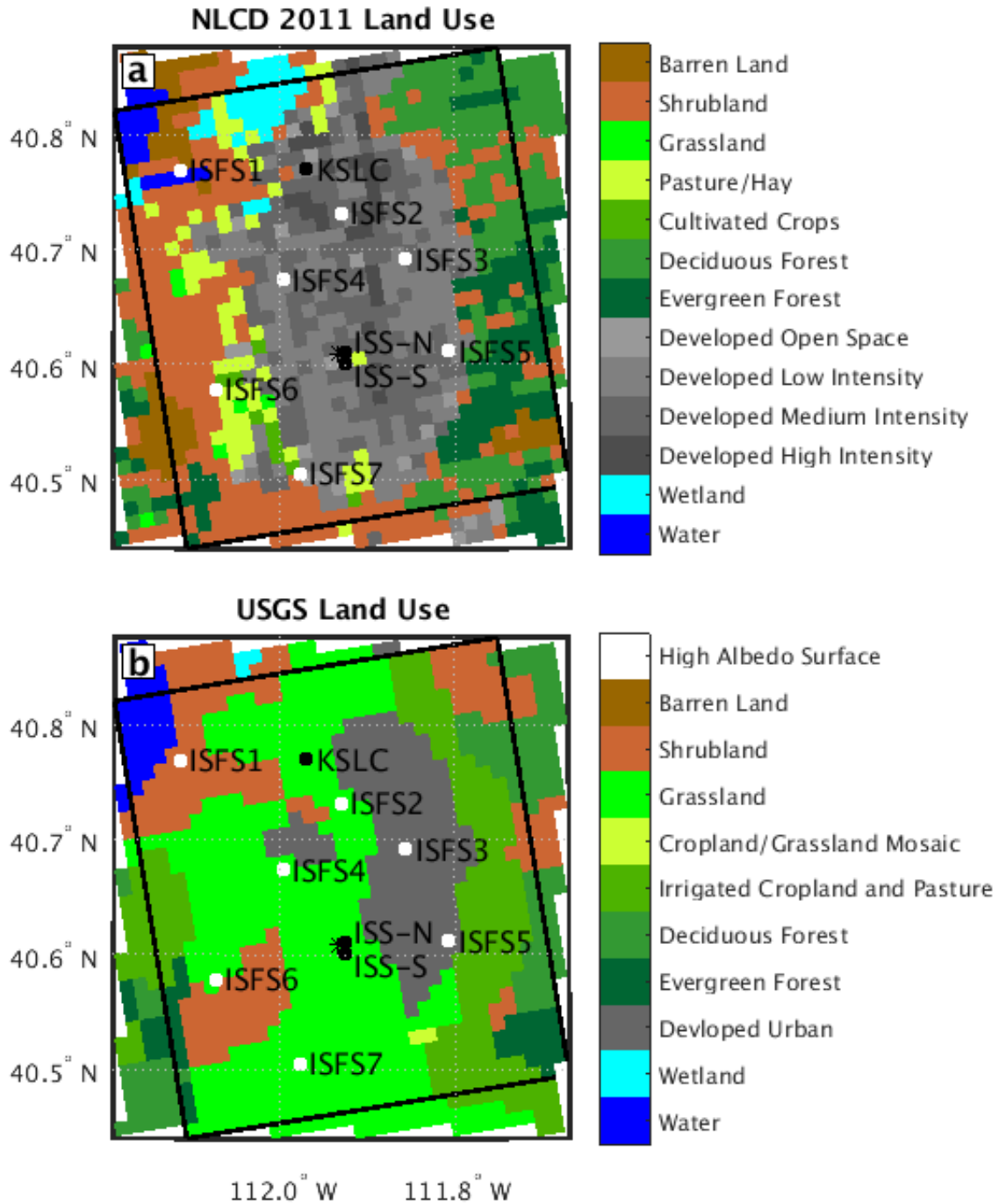


Figure 7. ISFS (white dots) and ISS (black dots) station locations deployed during the PCAPS field campaign of the 2010-2011 winter period, as well as the Salt Lake Airport station (KSLC) plotted at grid point they represent. The black star indicates the grid point closest to the two ISS locations where model time heights within the Salt Lake Valley are later plotted. The boundary of the Valley Subdomain is plotted in solid black lines. **a** Station locations are plotted over the modified NLCD 2011 land use cover used in the BASE simulation. **b** Station locations are plotted over the USGS land use used in the DFLT simulation.

Snow depth data was obtained for the key basins in northern Utah (Cache, Salt Lake, and Uintah) with available snow measurements. In addition to using available in situ snow observations, visible satellite imagery was used to determine the extent of snow cover over unpopulated barren lands in northern Utah (Figure 8).

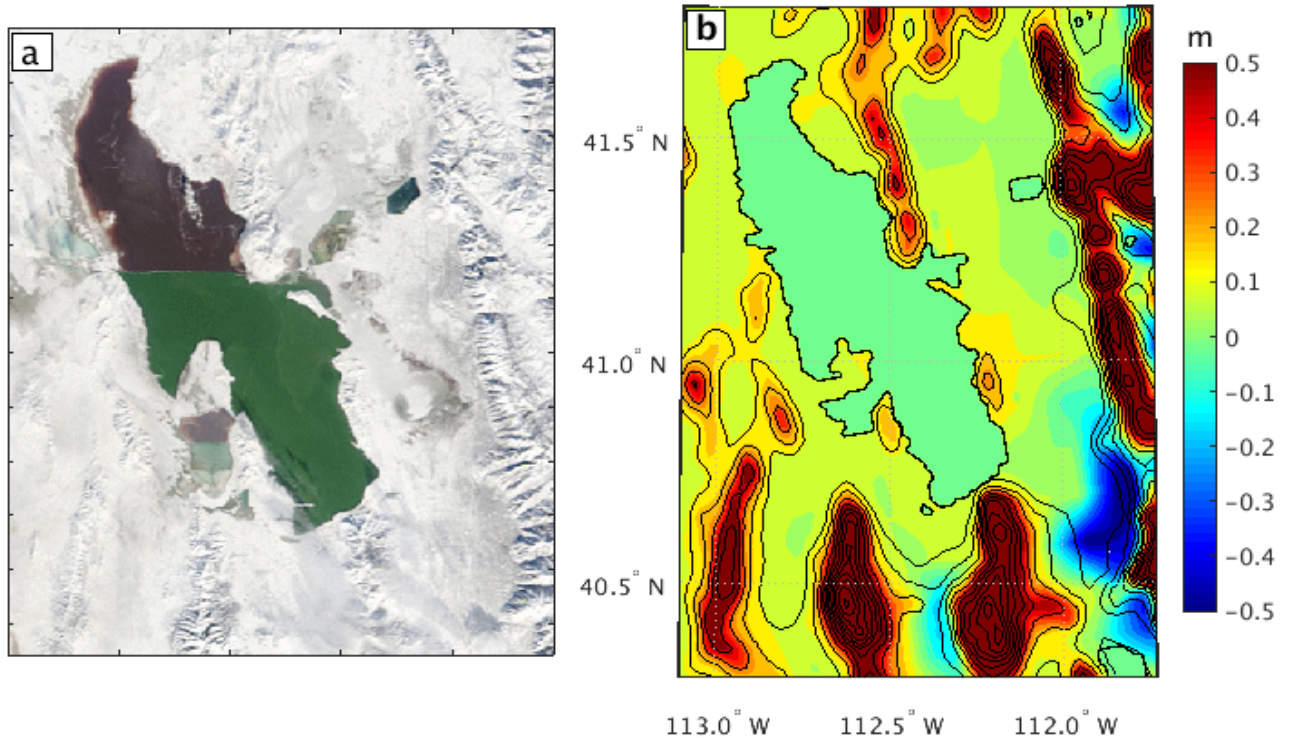


Figure 8. **a** MODIS satellite imagery from the Terra platform on 1 January 2011 centered over the Great Salt Lake and the Salt Lake Valley. **b** Difference in initial snow depth (m, shaded) at 0000 UTC 1 January 2011 between NAM analyses and the prescribed snow depth. Reproduced from Foster et al. 2016

The satellite imagery confirmed that the NAM analyses did not capture the shallow snow cover that existed over the entire Great Salt Lake Basin during the January 2011 case. Following Alcott et al. (2013), a linear function was fit to the observed snow depth and snow water equivalent values as a function of elevation. For the January 2011 cold-air pool, the linear function employed is shown in Figure 9, with a slowing increasing snow cover depth below 1500 m ASL, and an increasing snow cover depth with elevation between 1600 and 2600 m ASL. Above 2700 m ASL, a constant snow depth was assumed, given limited observations in the highest elevations of the various mountain ranges. The difference between the snow depth in the NAM analyses and the snow depth employed for the January 2011 cold-air pool is shown in Figure 8b.

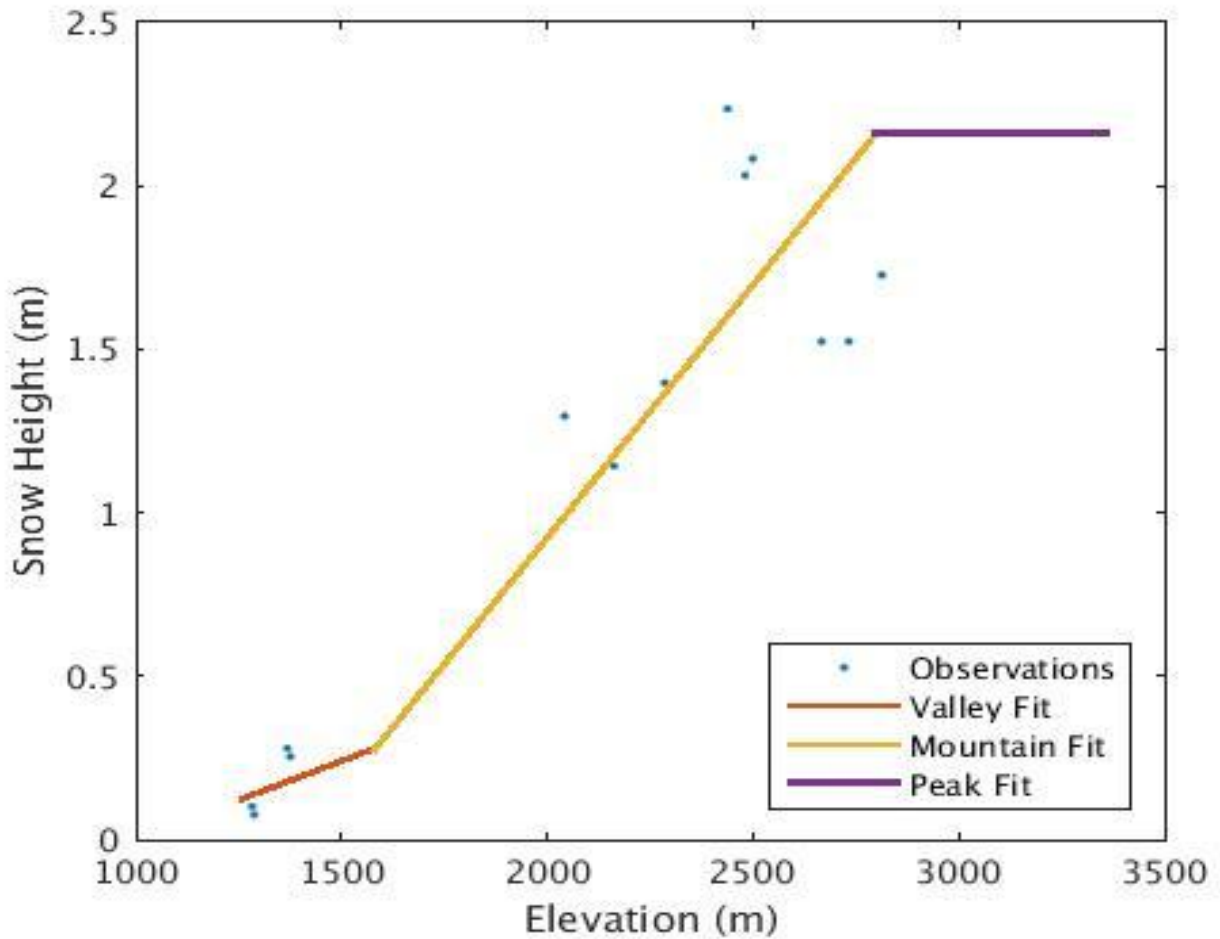


Figure 9. Idealized snow depth fit versus elevation for valley (red), mountain (yellow), and peak (purple) elevations for the initialization of the January 2011 cold-air pool. Observations are represented by blue dots. Reproduced from Foster (2016).

In the eastern portions of the Salt Lake Valley, the NAM analyses overestimated snow depth by up to 50 cm, while over the desert regions of western Utah, the NAM analyses had no snow cover, whereas in the DAQ WRF modeling run a depth of around 10 cm of snow was initialized.

2.6 Modifications to Snow and Vegetation Parameters

Following the work of Neemann et al. (2015), the default vegetation parameters for scrub vegetation in the typical default WRF set-up were found to be unrepresentative over northern Utah. In essence, the scrubland in the default WRF configuration for barren land types is too deep (Neemann et al. 2015). Consequently, the amount of snow needed to cover the scrub and allow for an increased surface albedo is less in reality than the default WRF parameters. To correct for this issue, the following changes were made to the WRF snow and vegetation parameters:

- The amount of snow required to cover the ground (WRF parameter SNUP in the Vegparm table) was decreased over barren land from 0.03 m to 0.01 m, and over shrubland from 0.03 m to 0.02 m, and over cropland from 0.04 m to 0.02 m (Table 4)
- The maximum albedo (which occurs after fresh snow has reached a depth greater than the specified SNUP for the given land use type) was increased by 5-25% over most land use types, allowing for higher albedos in many urban and surrounding areas. These changes were made due to the observed higher albedos at 7 PCAPS observation locations.

Figure 10 shows the resulting WRF modeled and observed evolution of snow now albedo during the 1-9 January 2011 cold-air pool in the Salt Lake Valley. The seven locations shown (ISFS1-7) were scattered across the Salt Lake Valley. Please refer to Foster (2015) for more detailed description of the land use types and location of the ISFS locations.

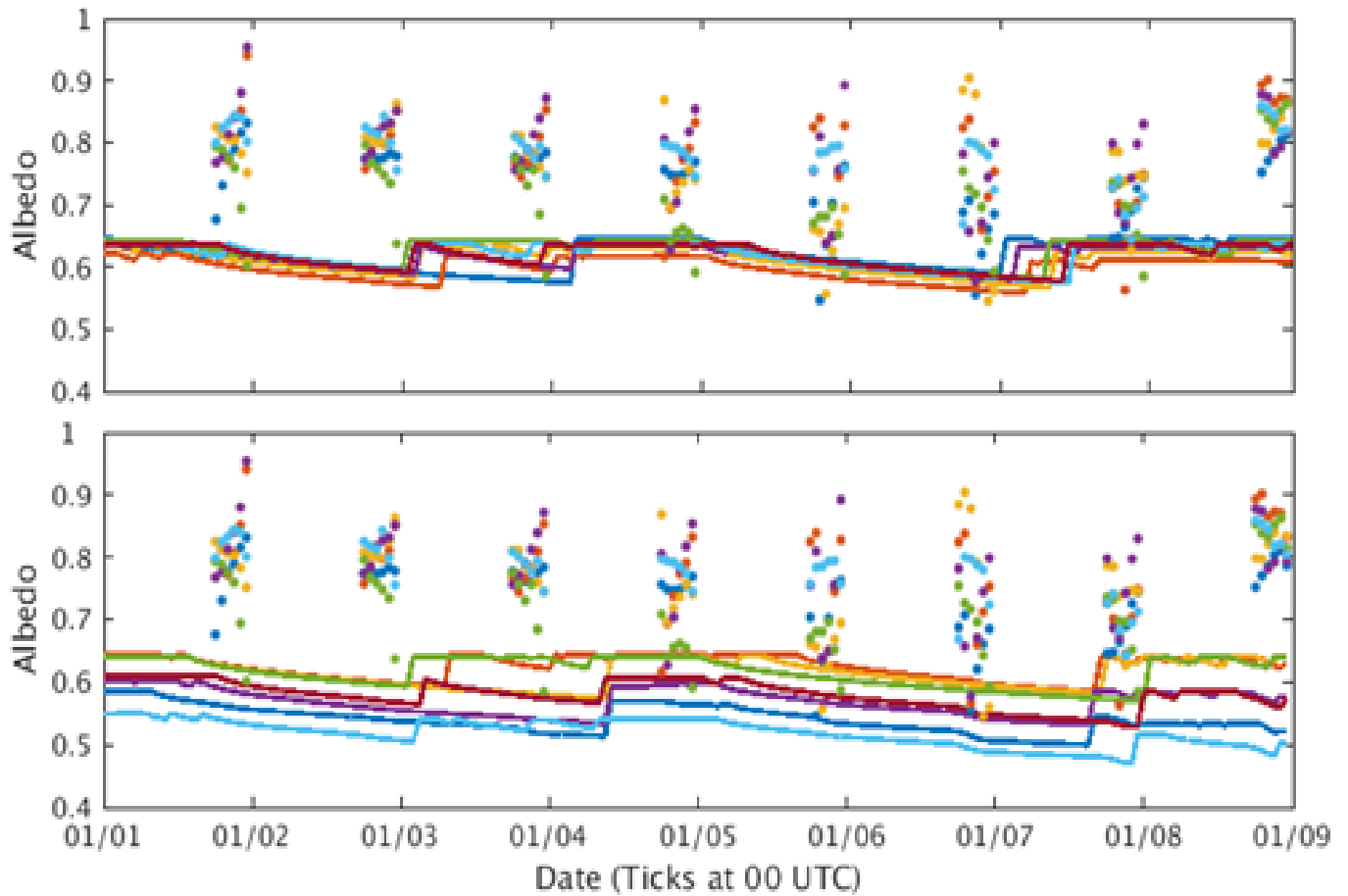


Figure 10. Comparison of albedo between the WRF model (solid lines) and PCAPS observations (dots) in the Salt Lake Valley for the DFLT WRF simulation (top panel) and BASE WRF simulation (bottom panel) during PCAPS cold-air pool in January 2011.

Table 4. Summary of modifications to the WRF model SNUP and MAXALB parameterizations incorporated into the BASE simulation based on PCAPS observations. For more details see Foster (2015).

Land use type	SNUP original	MAXALB original	SNUP modified	MAXALB modified
Barren Land	0.03 m	75%	0.01 m	80%
Scrubland	0.03 m	60%	0.02 m	80%
Urban	0.04 m	46%	0.04 m	70-75%

2.7 Data Assimilation and Nudging

Numerical modeling of cold-pools in the Uintah Basin showed that nudging numerical simulations of cold-air pools toward surface observations are highly detrimental to the simulations, as the surface observations can be very unrepresentative of actual conditions just 10's of meters above the stable surface (Trang and Huy Tran, personnel communication). Thus, nudging was not employed for any of the simulations in this study. In addition, no data assimilation was conducted in the simulations, using the same arguments as in the nudging case. Inadequate spatial and vertical profile data exists in the observations, even during most of PCAPS period to allow for notable improvements to simulations using this technique, and as seen in the Uintah Basin, data assimilation and nudging may negatively impact cold-air pool simulations.

2.8 WRF Physics Options

The WRF physics options that were used are given in Table 5. The Mellor-Yamada-Janic (MYJ) planetary boundary layer (PBL) scheme was used given the improved results found in previous tests conducted at the University of Utah and because it performed best in the Uintah Basin for a cold-air pool simulation there (Neemann et al. 2015). A study conducted by Lu and Zhong (2014) did not find significant performance differences between the various PBL schemes. This is consistent with the findings of the Utah DAQ in the 2013 SIP PM2.5 report, which also found that no PBL schemes tested provided improved results (Avey, 2013). Our experience is that all PBL schemes fail in the presence of strong winds aloft. However, for this study only cold-air pools with light to moderate synoptic-scales winds were chosen because of this reason. This is a change from the last Utah DAQ SIP which used the Pleim-Xlu (ACM2) PBL scheme. Other physics options used included the RRTMG longwave and shortwave radiation scheme, which includes new options to include for slope shading which could be important in wintertime situations, as well as the NOAA land surface model, which incorporates parameterization of snow and snow albedo aging.

Table 5. WRF Model Physics Options used

Physics Option	Option Selected
Microphysics	Thompson
Longwave Radiation	RRTMG
Shortwave Radiation	RRTMG
Land Surface Model (LSM)	Noah
Planetary Boundary Layer (PBL)	Mellor-Yamada-Janic (MYJ)
Surface layer	ETA similarity
Cumulus Scheme	None in d02, d03, Kain-Fritz (d01 12 km domain only)

3. WRF Meteorological Modeling Performance Evaluation (MPE)

3.1 Overview

As discussed in the introduction, three cold-air pool episodes were simulated in northern Utah Basins that are discussed in this modeling performance evaluation (MPE) document. Extensive research on cold-air pools has shown that validation of vertical profiles of temperature, wind, and moisture are needed to accurately validate model simulations of persistent cold-air pools. Fortunately, the Persistent Cold Air Pool (PCAPS) field study allowed for an unprecedented observational data set to validate the WRF meteorological model during the January 2011 cold-air pool in the Salt Lake Valley. For the other two episodes, in 2013 and 2016, and in the other basins (Utah Valley, Uintah Basin and Cache Valley) we primarily use standard available surface observations in combination with satellite data to validate the model.

Both qualitative and quantitative evaluation of the simulations was conducted. The following performance metrics were used in the WRF MPE:

- **Bias**
- **Root mean squared error (RMSE)**

3.2 Performance Evaluation Observational Datasets

A wide array of meteorological observations were used for model validation (Figure. 11 and Table 6). As discussed in the introduction, three cold-air pool episodes were simulated:

- January 1-11 2011
- December 7-21 2013
- February 1-17 2016

Extensive research on cold-air pool meteorology was conducted during the PCAP study in January 2011. Consequently, weather data from seven National Center for Atmospheric Research (NCAR) ISFS (Figure 7) was used in addition to an hourly vertical profile of temperature, wind and humidity that was available at the ISS location (Figure 11 upper right inset).

In addition, surface weather station data from the National Weather Service or UDAQ stations in Salt Lake City, Provo, Vernal, and Logan was used to evaluate the cold-air pool in the Salt Lake Valley, Utah Valley, Uintah Basin, and Cache Valley, respectively. Daily morning (nominally 5 MST) and late afternoon (nominally 1700 MST) weather balloon soundings from the Salt Lake City airport were also used to validate the vertical temperature and wind profiles for all three cold-air pool episodes (Table 6).

3.3 1-11 January 2011 Cold-Air Pool Model Performance Evaluation

The strongest cold-air pool during the 2010-2011 winter occurred within the period from 1-9 January 2011 with potential temperature deficits as large as negative 30 K between the surface and 700 hPa. The passage of an upper level trough and associated cold front (700 hPa temperatures dropped to as low as $-23.5\text{ }^{\circ}\text{C}$) across the western United States during 30-31 December 2010 resulted in widespread fresh snowfall across the Salt Lake Basin (e.g., roughly 0.05 m at the Salt Lake International Airport, KSLC). Following this, ridging aloft dominated the western United States from 1-8 January with 700 hPa temperatures increasing to as high as $0\text{ }^{\circ}\text{C}$. The cold air left behind in the basin combined with fresh, high-albedo snow cover helped maintain the cold-air pool in the Salt Lake Valley until 9 January, when a cold front rapidly cooled the atmosphere aloft, resulting in destabilization of the vertical temperature profile, enhanced vertical mixing, and an end to the cold-air pool and associated poor air quality by 12:00 UTC (Lareau et al. 2013). Hourly $\text{PM}_{2.5}$ concentrations in the Salt Lake Valley at the height of the cold-air pool episode exceeded $80\text{ }\mu\text{g m}^{-3}$ while the 24-h average $\text{PM}_{2.5}$ concentrations exceeded the National Ambient Air Quality Standard of $35\text{ }\mu\text{g m}^{-3}$ between 4-8 January.

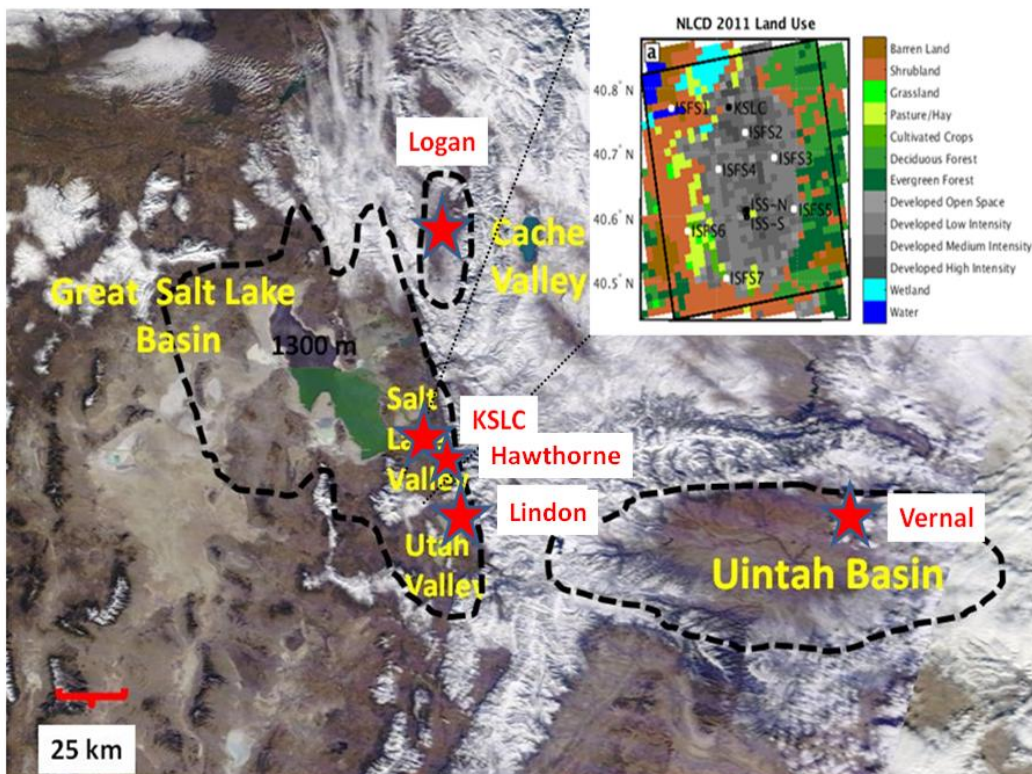


Figure 11. Location of key meteorological sites used in model performance evaluation. Refer to inset in upper right for location of enhanced PCAPS Integrated Surface Flux Stations (ISFS) station data within the Salt Lake Valley for the January 2011 cold-air pool episode (Table 6).

Table 6. Meteorological observational datasets used for modeling evaluation. See Figure 11 for the locations of the various stations.

Observation Type	Station Name	Location	Cold-pool episode available
Surface station	ISFS1	SL Valley	January 2011
Surface station	ISFS2	SL Valley	January 2011
Surface station	ISFS3	SL Valley	January 2011
Surface station	ISFS4	SL Valley	January 2011
Surface station	ISFS5	SL Valley	January 2011
Surface station	ISFS6	SL Valley	January 2011
Surface station	ISFS7	SL Valley	January 2011
Surface station	Hawthorne	SL Valley	January 2011, December 2013, February 2016
Surface station	Logan	Cache Valley	January 2011, December 2013, February 2016
Surface station	Lindon	Utah Valley	January 2011, December 2013, February 2016
Surface station	Vernal	Uintah Basin	January 2011, December 2013, February 2016
Rawindonde	Salt Lake City International Airport	Salt Lake Valley	January 2011, December 2013, February 2016
ISFS Rawindonsde, lidar(s), radiometer	NCAR ISS	South Jordan, Salt Lake Valley	January 2011
Laser Ceilometer	various	SL Valley	January 2011, December 2013, February 2016
Laser Ceilometer	various	Cache Valley Uintah Basin	February 2016

3.3.1 PCAPS 1-11 January 2011 Vertical Cold-Air Pool Structure Model Evaluation

Numerous studies over the past 10 years have shown that the vertical structure and mixing height of the cold-air pool and the winds therein are critical for obtaining an adequate cold-air pool numerical meteorological simulation.

In this section we present validation results from both the DFLT and BASE simulations (Section 2.3, Figures 6 and 7). The DFLT simulation used older land use (UGSG) and did not incorporate the improvements used in BASE. Only the BASE simulation was used by UDAQ in the final SIP modeling. We show results for the DFLT simulation only to illustrate the improvements gained in the BASE meteorological simulation used by UDAQ in this study.

The basic vertical evolution of the January 2011 persistent cold-air pool was well-simulated by the WRF model. Figure 12 shows the vertical profiles of temperature and relative humidity which can be compared against the modeled vertical profiles of temperature and cloud water mixing ratio. The model simulates well these key features of the observed January 2011 cold-air pool (examples of these features are labeled on Fig. 12 according to the numbers listed below):

- (1) Descending subsidence inversions 1-3 January and 5-8 January
- (2) Weak weather system passage 4-5 January
- (3) Nocturnal surface inversions
- (4) Daily convective daytime mixed layers
- (5) formation 7-9 January

However, careful analysis shows that not all meteorological features are captured, despite good overall agreement. For example, mid-level clouds resulted in decreased nocturnal cooling on 3 and 4 of January (Fig. 12a). However, this decreased nocturnal cooling was not observed in the simulation, which did not produce the thin mid-level clouds that resulted in the thermal impacts observed. In addition, a “notable band” of warm bias temperatures is noted aloft in both the DFLT and BASE simulations (Fig. 12c, e).

When comparing simulated vertical profiles at the ISS site with PCAPS observations, a notable band of warm model bias occurs between 1500-2000 m AGL (Figs. 12c and e in this document). The warm bias is strongest between mid-afternoon and sunset on 2 and 3 January, which may arise from a shallower afternoon mixed layer in the simulations compared to observation even though the absorbed radiation in the model is generally higher than observations. Thus, some other factor than surface heating (such as vertical diffusion by the PBL scheme) may be affecting the afternoon mixing heights. Other factors also likely contribute to the elevated model warm temperature bias including mid-level clouds aloft that were not captured well in the simulation on the 3rd of January and the underestimation of low clouds in the DFLT

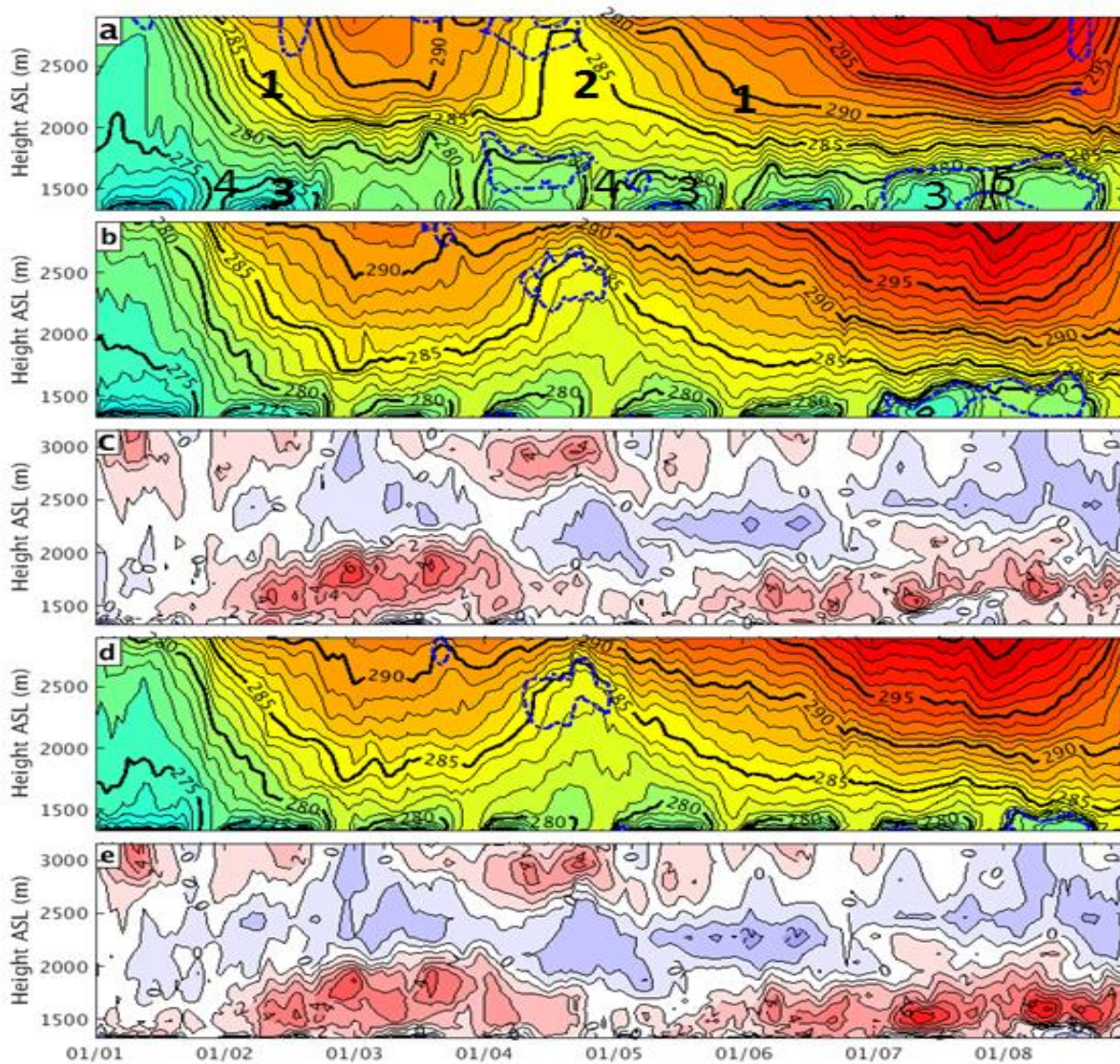


Figure 12. Comparison of PCAPS observations against WRF model vertical profiles of temperature and moisture during the core period of the cold-air pool between 1-9 January 2011. **a** Observed conditions at ISS near the center of the Salt Lake Valley from 0000 UTC 1 January 2011 to 0000 UTC 9 January 2011 of potential temperature (K, color shaded with bold contours every 5 K and light contours every 1 K) and relative humidity (90% threshold contoured in dashed blue line). **b** BASE modeled conditions in the Salt Lake Valley from 0000 UTC 1 January 2011 to 0000 UTC 9 January 2011 of potential temperature (K, color shaded with bold contours every 5 K and light contours every 1 K) and cloud water mixing ratio (0.1 g kg^{-1} threshold plotted in dashed blue line). **c** Difference in potential temperature between BASE and observations (K, color shaded with contours every 1 K and labels every 2 K, **a** – **b**). **d** as in B, except for DFLT. **e** as in c, except for difference between DFLT and observations.

simulation on the 7 and 8 January. The onset and duration of low clouds were also simulated more realistically in the BASE simulation than in the DFLT (compare Figs. 12a, b, and d). The onset of low cloud cover between 1300 and 1700 m a.s.l. occurs a day earlier (7 January) and is noted within a deeper layer in BASE (Fig. 12b and Fig. 12d). This results in several degrees more cooling in the boundary-layer 100-400 m a.g.l. in the BASE simulation (Fig. 11e), which agrees more closely with the PCAPS observations (Fig. 11c and Fig. 11e), with relative humidity > 90% (Fig. 12a).

The reasons for these relatively modest biases are unknown, but are possibly linked to the inability of the PBL scheme in the WRF model to generate adequate vertical mixing, resulting in a mixing height that is somewhat too low in the model. As shown in Figure 13, the depth of pollutants in the boundary-layer as observed by the backscatter from a laser ceilometers ranged from between 400-600 m above ground level. However, as can be seen in Figure 13, the pollutant depth is typically 100-200 m deeper than the mixing height (height of constant potential temperature, indicating neutral stability for dry parcels).

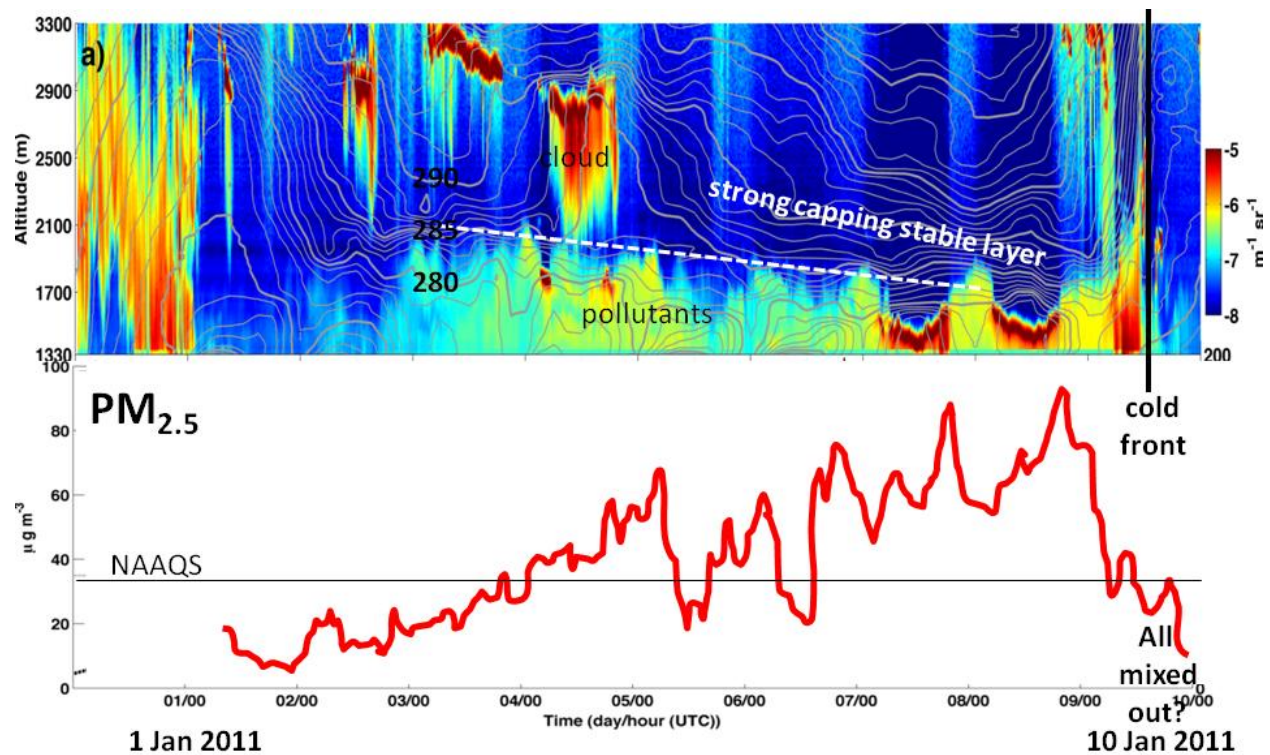


Figure 13. top: Laser ceilometer backscatter (color scale) and potential temperature (thin contours every 1 K, thick contours every 5 K). bottom: Time series of hourly $PM_{2.5}$ concentrations at Hawthorne Elementary UDAQ air quality site during the January 1-11 2011 persistent cold-air pool.

Figure 14. illustrates the time evolution of the vertical profile of winds at ISS (see Figure 7) in the south-central portion of the Salt Lake Valley. At this location, a commonly-observed flow feature is an elevated drainage flow that enters the Salt Lake Valley through the gap in the topography at the southern end of the Valley. The variations in the elevated southerly jet penetrating the Salt Lake Valley from the south in the DFLT versus BASE simulations at ISS are seen in the lowest 400 m of the boundary-layer. Figure 13b-c shows that jet wind speeds $> 5 \text{ m s}^{-1}$ do not reach as close to the surface in BASE, as opposed to DFLT, during the time periods when it was present, such as 1-2 and 5 January 2011. Near surface winds in BASE are shown to be weaker during these periods of elevated flow (blue shading in Fig. 14d). While the timing of the low-level jet is quite good compared to PCAPS observations, both the DFLT and BASE simulations overestimate the intensity and underestimate the height of the jet (Fig. 14a).

Summarizing the model performance evaluation of the boundary-layer wind speeds:

- The simulated boundary-layer flow timing is well-represented in model
- The overall depth and structure of the 'elevated jets' are well-represented
- The simulated wind speeds have a high bias
- The simulated jet wind speed maxima are located too close to the surface

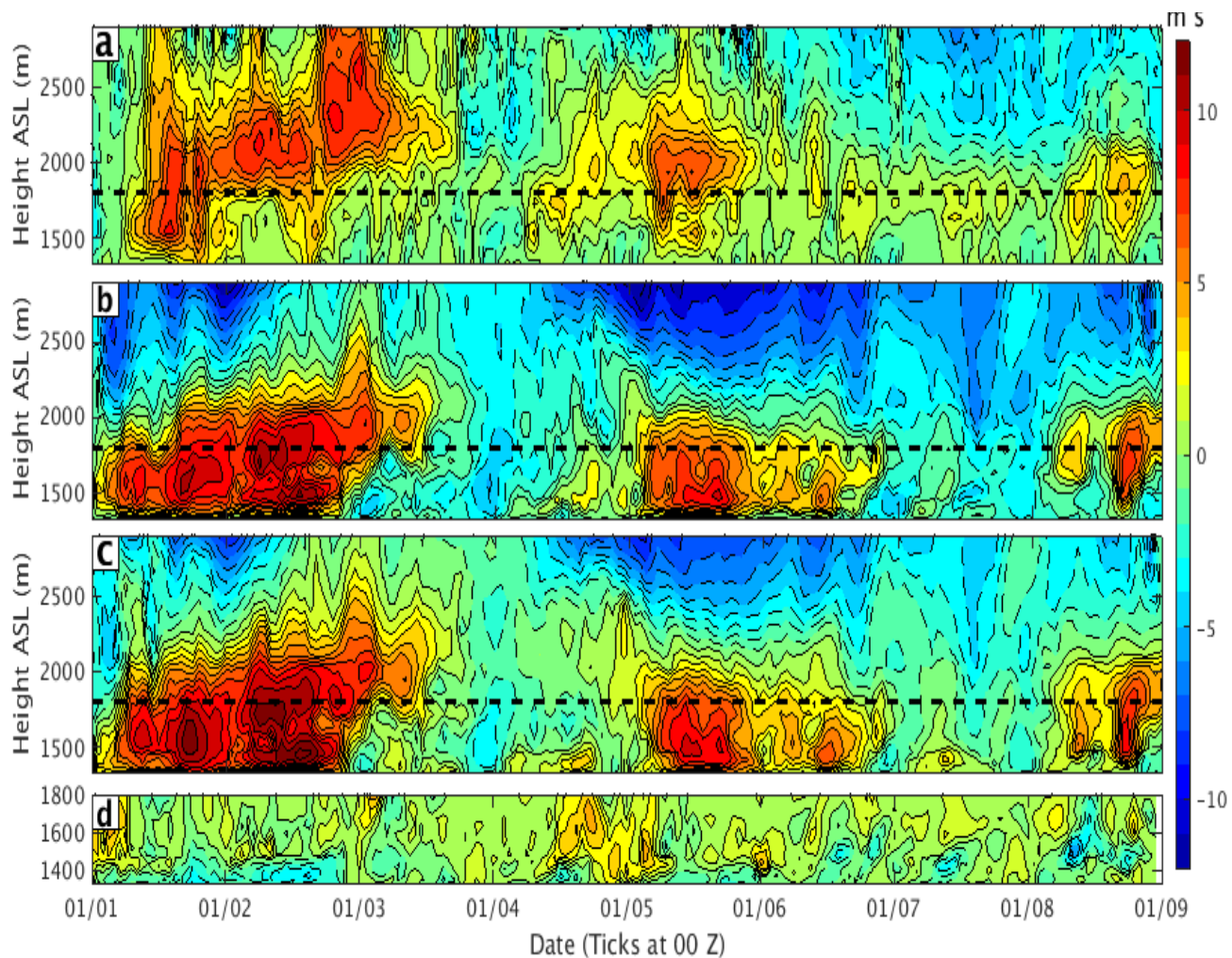


Figure 14. Meridional (v) wind component (m s^{-1} , contoured and shaded) in the central Salt Lake Valley from 0000 UTC 1 January 2011 to 0000 UTC 9 January 2011 for **a**, observation; **b**, BASE; **c**, DFLT; **d**, **b** - **c** below 1800 m ASL. Dashed line in **a** through **c** marked at 1800 m ASL.

3.3.2 PCAPS 1-11 January 2011 Case Surface Cold-Air Pool Model Evaluation

The BASE WRF simulation captured the basic evolution of near-surface boundary-layer temperature, low cloud cover, and flow features in the Salt Lake Valley well as compared to PCAPS observations. However, the WRF simulations overestimated the boundary-layer wind speeds in general.

In this section we present validation results from both the DFLT and BASE simulations (Section 2.3, Figures 6 and 7). The DFLT simulation used older land use (UGSG) and did not incorporate the improvements used in BASE. Only the BASE simulation was used by UDAQ in the final SIP modeling. We show results for the DFLT simulation only to illustrate the improvements gained in the BASE meteorological simulation used by UDAQ in this study.

Improvements in 2-m temperature were gained through the model modifications employed as part of this study. Figure 15 shows the difference in 2-m temperature between DFLT and BASE between 1-8 January 2011. The average differences are calculated separately for day and night hours (1800 – 0000 UTC for daytime and 0600 – 1200 UTC for nighttime). Many of the temperature differences between the two simulations are influenced by the changes made to the land surface (e.g., cold and snow covered, barren surface in BASE compared to the relatively warm lake surface in DFLT). Snow covered land is also unable to absorb as much solar radiation during the daytime, and snow's high emissivity enhances nighttime radiative cooling. Over the Great Salt Lake, the warm lake surface temperature relative to the surrounding land surfaces (the water temperature is held constant in WRF), extending over a larger surface area in DFLT compared to BASE results in substantive increases in the 2-m temperature in DFLT.

Over the lower elevation areas of the Great Salt Lake Basin outside of portions of the Salt Lake Valley, the average 2-m temperature was lower in the BASE simulation than the DFLT (Fig. 15a-b). The 2-m temperature difference between simulations is more pronounced at night (3-4 °C) (Fig. 15b). The areas to the east and west of the lake where snow cover was increased the most in BASE leads to increased reflectance of incoming solar radiation and widespread cooling > 2 °C compared to the DFLT simulation. In addition, the higher heat capacity of the larger surface areas associated with the Great Salt Lake in the DFLT simulation may offset the nighttime cooling in those areas surrounding the lake, keeping temperatures higher. In much of the Salt Lake Valley, however, BASE is 0.5-2.0 °C warmer than DFLT during the nighttime for the duration of the model run (positive differences/red shading in Fig. 15b). On average, higher 2-m temperatures were simulated in the eastern half of the Salt Lake Valley in BASE, an area where snow depth was lower (Fig. 15b) and changes to land cover included increasing the urban extent of the valley by more than half (Fig. 7).

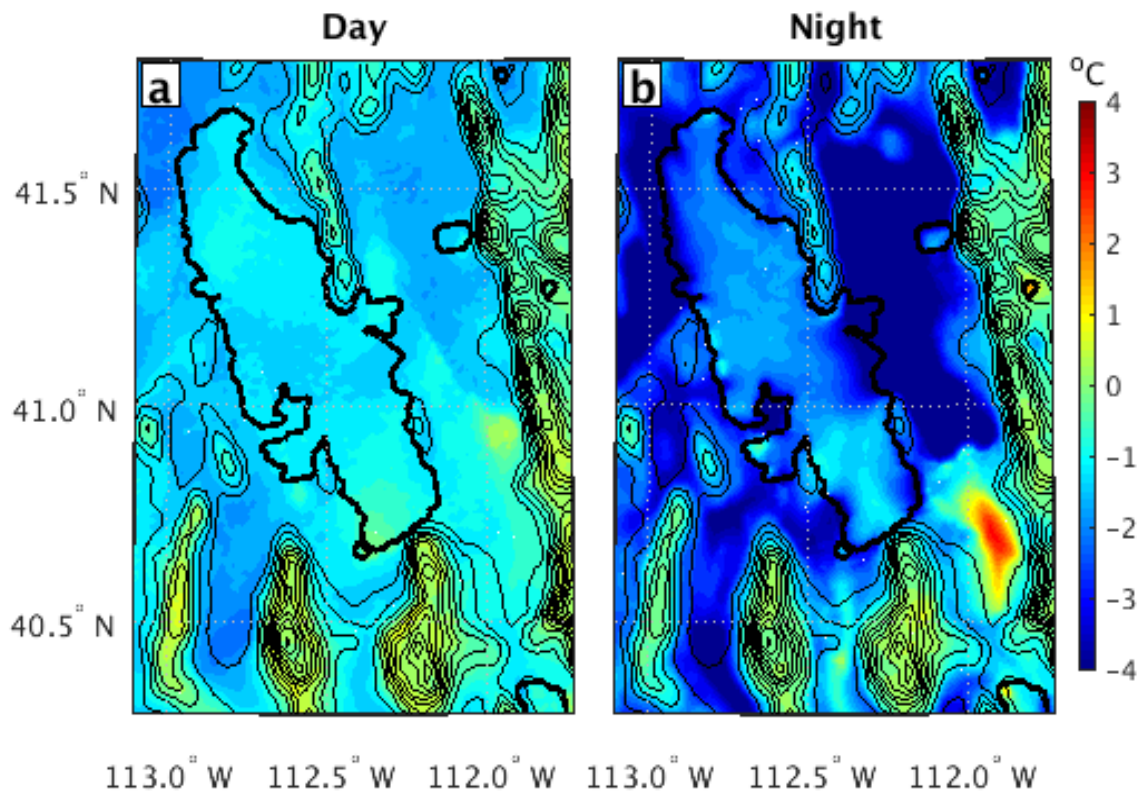


Figure 15. Difference in average 2 m temperature ($^{\circ}\text{C}$, shaded) between BASE and DFLT simulations (BASE minus DFLT) over the period from 0000 UTC 1 January 2011 to 0000 UTC 9 January 2011 during **a**, day, 1800 – 0000 UTC; **b**, night, 0600 – 1200 UTC. Elevation contoured as solid black lines at an interval of 150 m.

Quantitative model performance of 2-m temperatures at the 7 PCAPS ISFS stations is shown in Figures 16 and 17 and Table 9. The improvements to the modeling framework improved the overall performance of 2-m temperature. Areas in the western and northern portions of the Salt Lake Valley near the Great Salt Lake observed much lower 2-m temperatures and much larger diurnal cycles in 2-m temperature in BASE ($> 12^{\circ}\text{C}$ in BASE compared to $< 3^{\circ}\text{C}$ in DFLT) due to the effects of replacing the unrealistic water surface in DFLT with the more realistic land and snow cover in BASE (Fig. 16a). The ISFS 1 (Fig. 16) site was sited to be representative of the playa regions surrounding the Great Salt Lake, which is generally sparsely vegetated by scrub. It is classified as barren land with snow cover by BASE and shrub/scrub with minimal snow cover by DFLT. In BASE, small improvements were noted overall in the nighttime temperature

simulations compared to DFLT, with an average RMSE in 2-m temperature between BASE (DFLT) and observations of 3.49 °C (4.49 °C).

While the changes in land use and snow depth did not affect as much the albedo within the central and southern portions of the urbanized Salt Lake Valley in BASE compared to DFLT (albedo decreased by 0.05-0.10 in southern two thirds of the Salt Lake Valley, see Figs. 6 and 7), the net impacts of these changes on the 2-m temperature in the urban environment were nonetheless notable. At the downtown urban site (ISFS2, Fig. 16), DFLT temperatures (red) remain lower than BASE temperatures (blue), especially during the night, with an average RMSE in temperature between BASE (DFLT) and observations of 1.73 °C (3.61 °C). At the ISFS 6 site located on the western slope of the Salt Lake Valley, a smaller diurnal temperature range was observed due to the slope location (250 m above the valley floor) and weaker diurnal cold-air pool formation and deeper snow cover (0.25-0.30 m) at this site (Figs. 7a). Despite the 10-25% decrease in net solar radiation due to higher albedo at this site in the BASE simulation (Fig. 16), only minor differences in the simulated 2-m temperatures were noted during 1-6 January. We suspect that differences in winds and vertical stability between the simulations compensated at ISFS 6 for the differences in the local energy budget during this period. A more substantive difference in temperature between the BASE and DFLT simulations appears at the end of the time period, when BASE temperature remained lower than DFLT and closer to observations. The average RMSE of 2-m temperature between BASE (DFLT) and observations at ISFS 6 was 3.32 °C (4.61 °C). All the changes discussed previously are summarized in Table 9, which shows the RMSE between observation and each of the two simulations at each of the 7 ISFS site and Syracuse. Overall, the changes made to the BASE simulation represent an average improvement of 1.30 °C in the modeled 2-m temperature at the seven ISFS locations.

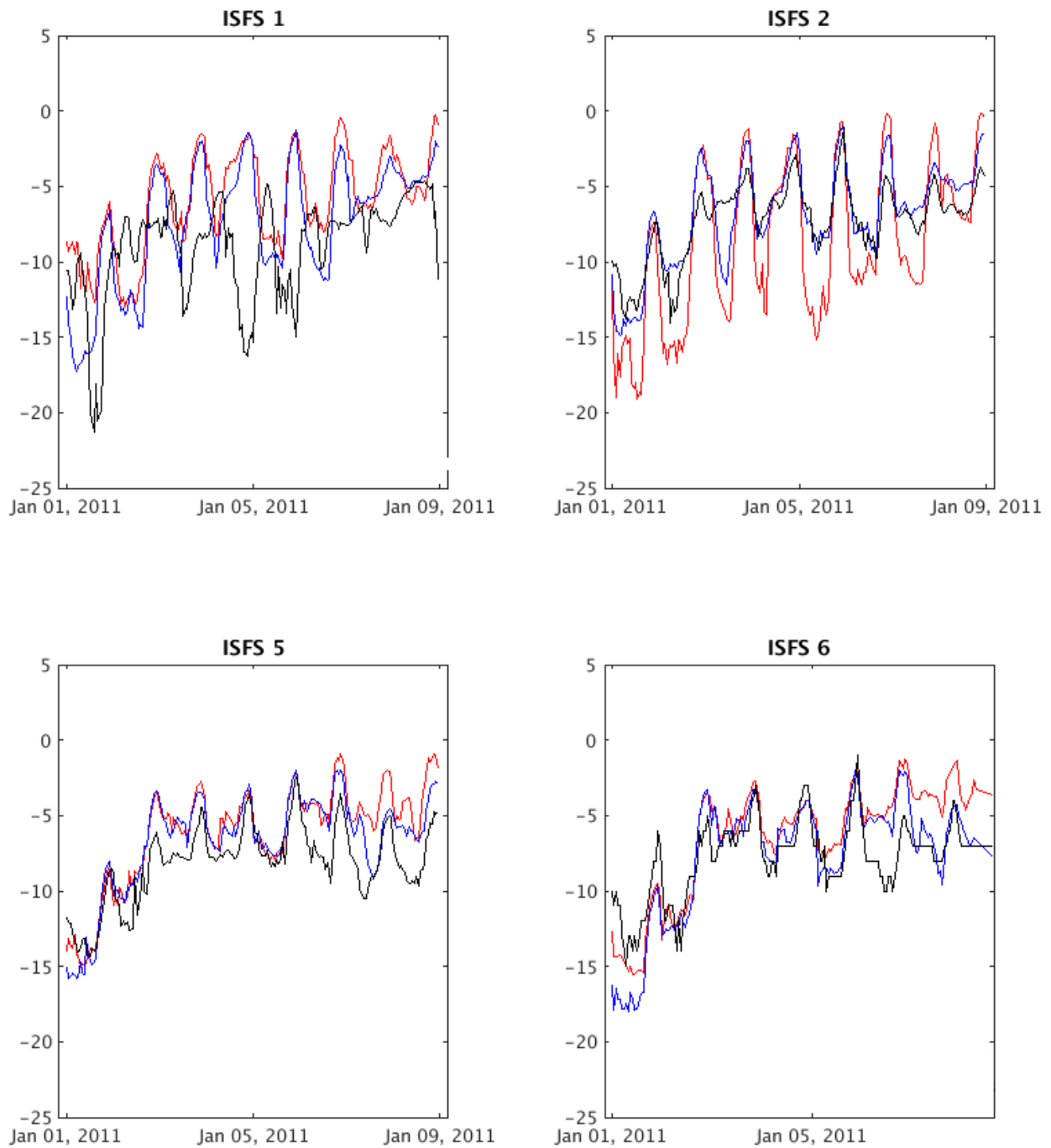


Figure 16. Temperature ($^{\circ}\text{C}$, solid lines) from 0000 UTC 1 January 2011 to 0000 UTC 9 January 2011 at ISFS 1 (upper left), ISFS 2 (upper right), ISFS5 (lower left) and ISFS 6 (lower right). Black lines are observed temperature, blue lines are BASE simulation temperature, and red lines are DFLT simulation temperature.

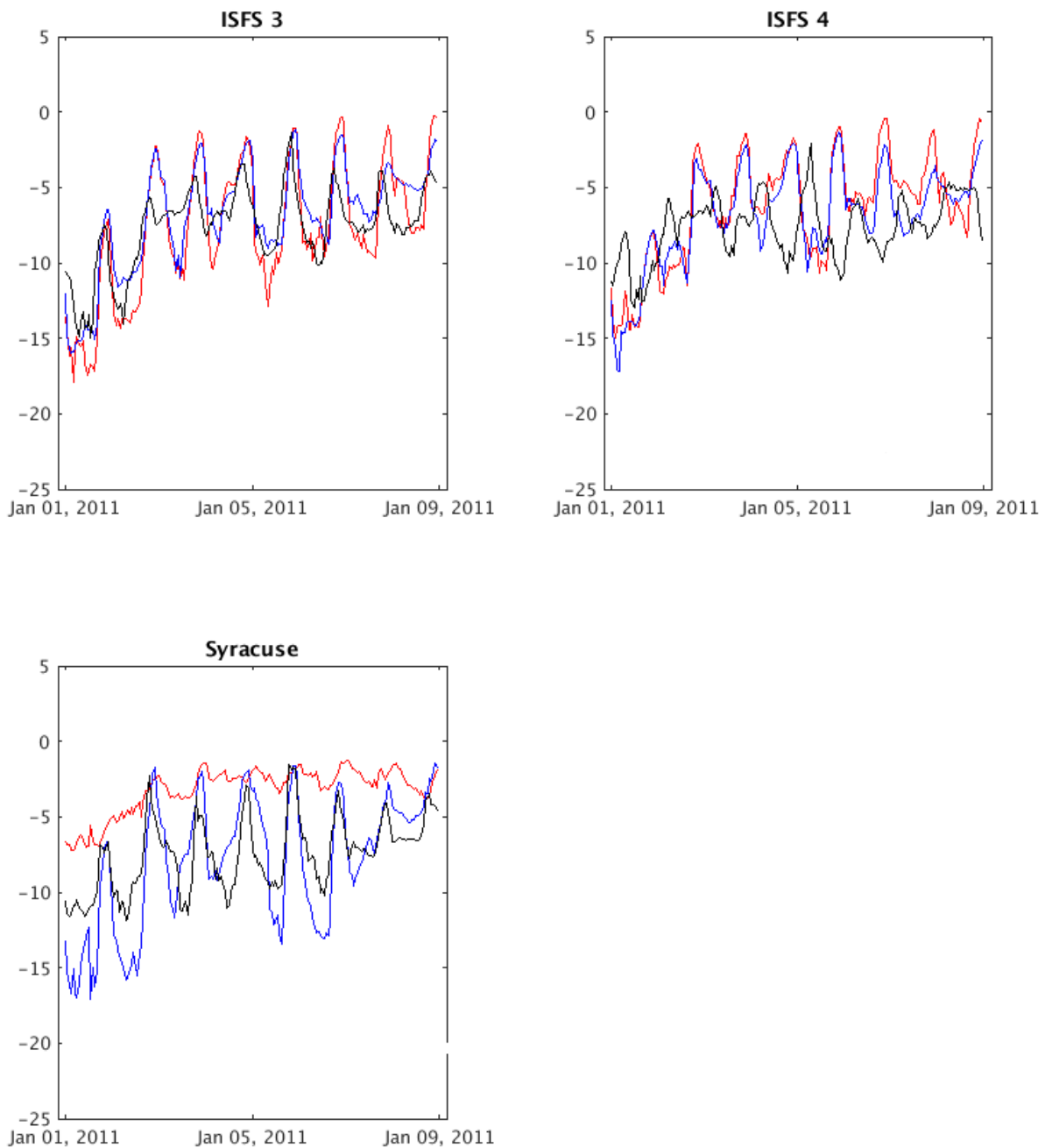


Figure 17. Temperature ($^{\circ}\text{C}$, solid lines) from 0000 UTC 1 January 2011 to 0000 UTC 9 January 2011 at ISFS3 (upper left), ISFS 4 (upper right), and Syracuse (lower left). Black lines are observed temperature, blue lines are BASE simulation temperature, and red lines are DFLT simulation temperature.

Table 9. WRF performance for 2-m temperature for core period of the January 2011 cold-air pool

Station	DFLT RMS Error (°C)	BASE RMS Error (°C)	RMS Error Improvement in BASE versus DFLT
ISFS1	4.49	3.49	1.00
ISFS2	3.61	1.73	1.88
ISFS3	2.21	1.78	0.43
ISFS4	2.89	2.12	0.77
ISFS5	2.63	2.11	0.52
ISFS6	4.61	3.32	1.29
ISFS7	2.71	1.88	0.83
Syracuse	4.85	2.59	2.26

The ability of the WRF simulations to model the surface energy balance during the cold-air pool can be explored further in Fig. 18 by comparing time series of the simulated and observed net longwave and shortwave radiation (available only at the ISFS sites, see Fig. 7 for site locations).

The following general conclusions can be made regarding the WRF model capabilities to simulate the observed net short and long wave radiation:

- The diurnal cycle of net longwave and shortwave radiation is well-represented.
- The WRF model on some days and locations overestimates the net shortwave and longwave radiation.
- Surface albedo plays a significant role in the modeled net radiation
- The improvements implemented in the UDAQ WRF modeling simulations as compared to the 'default' WRF run improved the simulated net radiation.

We now elaborate on the improvements to the net radiation in the BASE simulation used by UDAQ. In general, BASE provides improved simulations of net shortwave and longwave radiation compared to DFLT. At ISFS 1, simulated net shortwave during the day tends to be higher than that observed, while that simulated in BASE shows improvement, but remains too high compared to observations (Fig. 18a). The decrease in the BASE simulated net shortwave at ISFS 1 between 1-6 January is primarily due to the increase in albedo (Fig. 7b-c), which resulted in

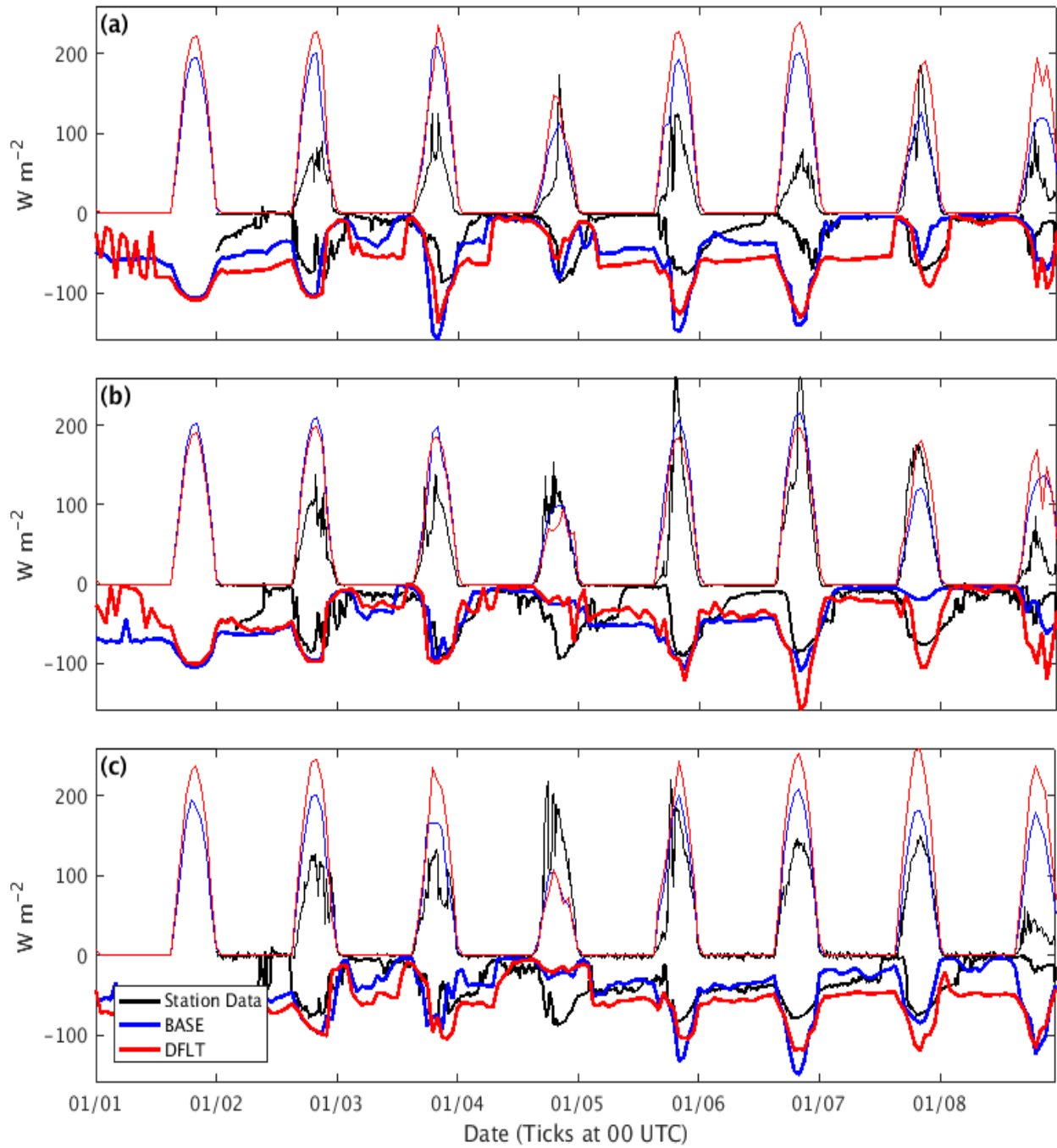


Fig. 18 Net shortwave radiation ($W m^{-2}$), thin lines) and net longwave radiation ($W m^{-2}$), thick lines) from 0000 UTC 1 January 2011 to 0000 UTC 9 January 2011 at **a**, ISFS 1; **b**, ISFS 2; **c**, ISFS 6. Black lines are observed radiation, blue lines are BASE simulation radiation, and red lines are DFLT simulation radiation.

less shortwave being absorbed by the surface. On 7 and 8 January, increased cloud cover resulted in less incoming solar radiation in BASE compared to DFLT (Fig. 18a). For net longwave radiation, both simulations generally overestimate the nocturnal longwave cooling compared to observations. During the day at ISFS 1, net longwave radiational cooling of the surface tends to be greater in BASE (for reasons that are unclear) but still less than observations. The opposite tends to be true during the night, with greater radiational cooling generally observed in DFLT until the last two days of the simulation when clouds are present.

At ISFS 2 (the downtown, urban site), the differences in simulated shortwave radiation between the simulations are of opposite sign and smaller than at ISFS 1 (Fig. 18b). At this location, the urban classification was modified in BASE (which allowed for a higher maximum albedo under deep snow conditions), but the actual snow depth decreased after removal of the inaccurate snow analysis used in DFLT. Consequently, the net shortwave radiation was generally increased in the BASE simulation compared to DFLT, allowing the cold bias of DFLT in the urban core to be somewhat overcome in that region in BASE (see Figs. 8 and 10). At ISFS 6 (a barren rangeland site on the western slope of the Salt Lake Valley at an elevation 250 m above valley floor), we see a situation similar to that seen at ISFS 1, although on some days such as January 3rd and 7th the improvements in the simulated net shortwave radiation in the BASE simulation relative to DFLT are greater than at ISFS 1 (Fig. 18c). Net shortwave is higher than observation in both simulations, but BASE remains lower than DFLT each day except 4 January, when both are similarly less than that observed. This site saw the highest increase in albedo in the BASE simulation (Fig. 8), where snow cover increased approximately 0.1 m and the pasture/hay land use classification was modified to allow for higher albedo. As will be shown in the following two Sections, these relatively subtle changes in land use and snow cover and the resulting modifications to the energy balance across the Salt Lake Valley impacted the low-level stability, katabatic flows, and cloud cover during the cold-air pool.

3.3.3 1-11 January 2011 Surface Cold-Air Pool Model Evaluation in Salt Lake Valley, Utah Valley, Cache Valley, and Uintah Basin Using Standard Observations

The previous sections elaborated on the performance of the January 2011 cold-air pool for both the DFLT and improved BASE configuration of the WRF model with respect to the detailed and unprecedented PCAPS observations obtained in the Salt Lake Valley during the field campaign that winter.

In this section, we use the typical limited available observations in the Salt Lake Valley, Cache Valley, Utah Valley, and Uintah Basin to validate the 2-m temperature and 10-m wind speeds at locations in each of these basins to discuss model performance more broadly and to provide a baseline comparison to the model performance for the other two episodes for which no PCAPS data exists (December 2013 and February 2016) (See Figure 11 and Table 6 for validation station metadata).

Table 10. WRF performance for **2-m temperature (°C)** for 1-11 January 2011 cold-air pool

Station	Bias (°C)	RMS Error (°C)
Hawthorne	-1.969	2.141
Salt Lake City	0.756	2.051
Lindon	-2.365	1.722
Vernal	2.237	4.743
Logan	6.372	6.824

The 2-m temperatures were simulated well in the Salt Lake Valley at the Hawthorne and Salt Lake Airport locations, which are expected given the good performance noted in Section 3.3.2 at the ISFS sites (Tables 9-10 and Figure 19). In the Utah Valley, the model performance for 2-m temperature was similar to the Salt Lake Valley, with a cool bias and RMS error of ~2 °C (Table 10 and Figure 20).

2-m temperature biases and RMS errors were similar to those observed during the more highly validated PCAPS observations in the Salt Lake Valley and Utah Valleys. As discussed above, the biases were similar to the PCAPS January 2011 case, some of the RMS error in the Salt Lake Valley resulted from the model not properly capturing the cold overnight low temperatures observed.

The 2-m temperatures showed higher biases and RME errors compared to observations in the Cache and Uintah basins. While the exact reasons for these errors in these basins are unknown, as only limited surface observations and no vertical profiles are available during this cold-air pool with which to validate the models in these basins for the episodes of interest, the impact of clouds does appear to be a factor in these cases as discussed below.

In the Uintah Basin and Cache Valleys between 3 and 9 of January 2011, the model handled the 2-m temperature evolution poorly at nighttime compared to in the Salt Lake and Utah Valleys. The reason for this poor handling of the nighttime model temperature in the Uintah Basin may be related to model problems with cloud cover, which limits nocturnal cooling in the model, effectively ‘insulating’ the basin from radiative cooling during this time. Between the 5th and 9th of January, the WRF model produced extensive cloud cover in the Uintah Basin, whereas in reality there was no cloud cover observed on satellite during this period. This is a common problem with numerical weather prediction in the Uintah Basin. In the Cache Valley, a similar model warm bias was observed. While the model did at times produce spurious nocturnal fog that may have impacted the warm model temperature bias, other unknown factors are at play as well in creating the warm temperature bias in the Cache Valley. One possible factor is that the local slope flows are too strong in the model, resulting in too much mixing and not allowing the extreme surface inversions to remain intact at Logan during the night (Figure 22).

10-m wind speeds biases and errors were generally low for all basins (Table 11), as the model captured will the light winds associated with cold-air pool conditions. Wind speeds in the model and observed generally remained below 3 m s⁻¹ at all observation locations during the duration of the cold-air pool. The weakest winds were observed and simulated at Vernal, with the strongest winds, presumably because of lake breezes and drainage flows, were observed at the Salt Lake International Airport (Figures 21 and 22). While the numerical simulations in general captured the very light wind speeds, the numerical simulations were unable to simulate winds below around 0.75 m s⁻¹. At extremely light or calm (0 m s⁻¹) wind speeds, the model continued to simulate a 0.5-1 m s⁻¹ flow. Also at Logan, the WRF model simulated too strong of drainage flows on certain days (Figure 22).

Wind directions were also analyzed but are not shown here as they were not deemed important. Wind directions are highly irregular, sporadic, and controlled by small unrepresentative terrain and building features during such light speeds.

Table 11. WRF performance for 10-m wind speed for 1-11 January 2011 cold-air pool

Station	Bias (m s ⁻¹)	RMS Error (m s ⁻¹)
Hawthorne	-0.221	0.834
Salt Lake City	-0.045	1.464
Lindon	-0.082	0.805
Vernal	-0.339	1.153
Logan	0.988	1.724

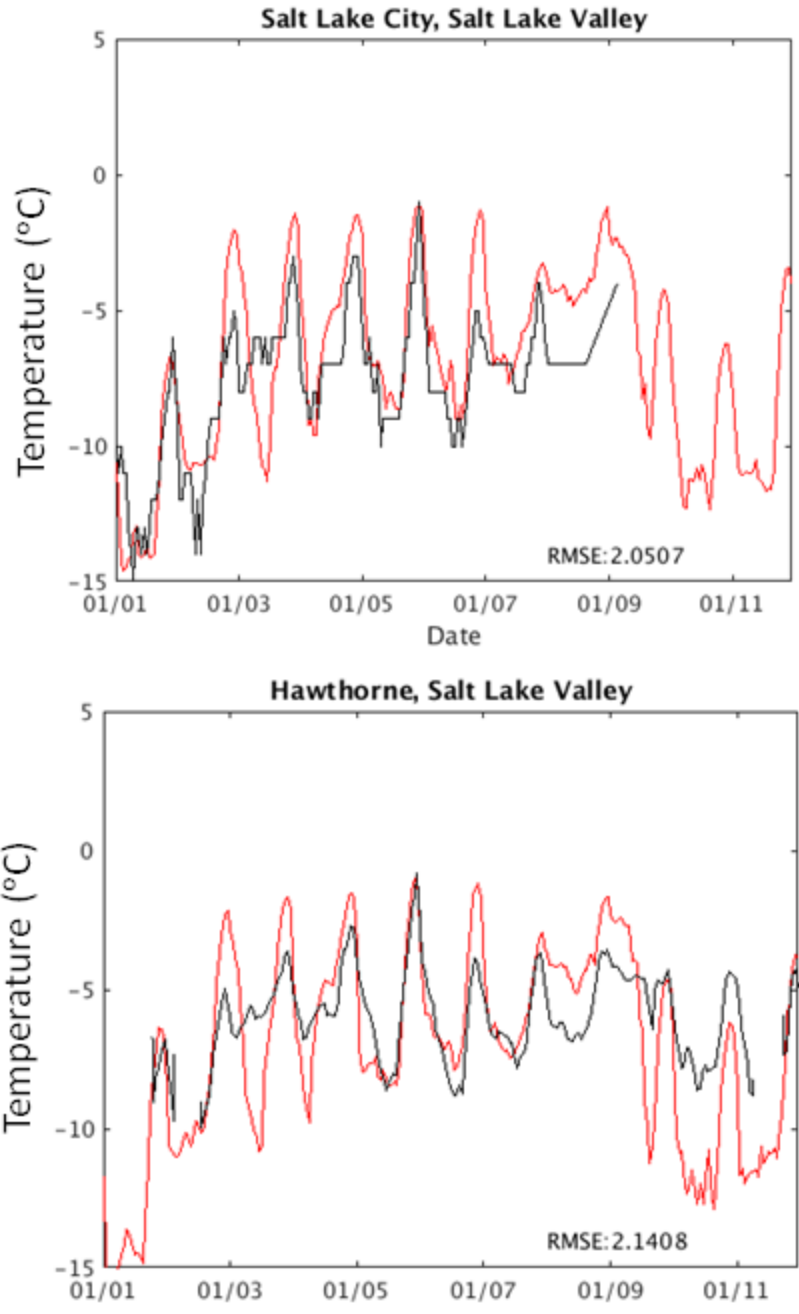


Figure 19. Comparison of model (red line) and observed (black line) 2-m temperature (°C) in the Salt Lake Valley at the Salt Lake City International Airport (top) and the UDAQ Hawthorne Elementary (bottom) between 1-11 January 2011.

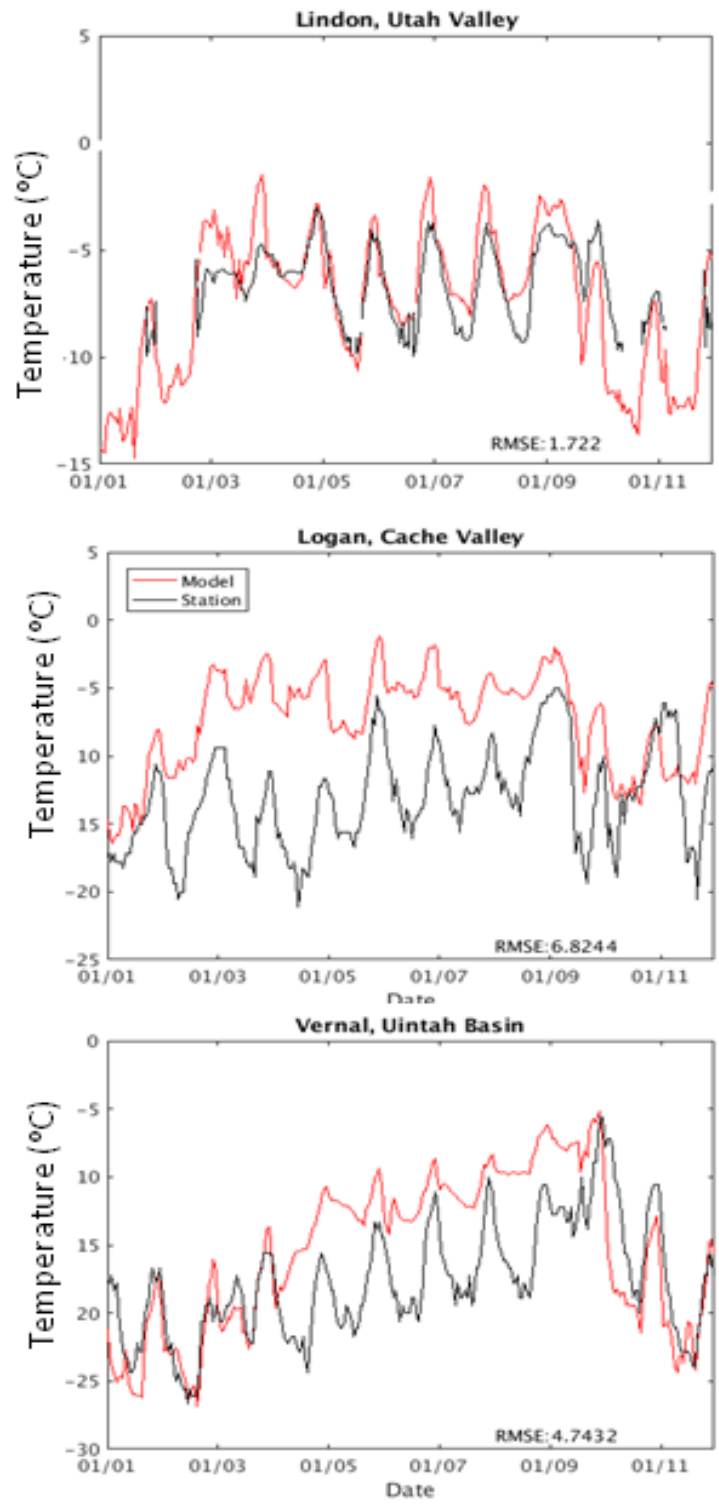


Figure 20. Comparison of model (red line) and observed (black line) 2-m temperature (°C) in the Utah Valley (top panel), Cache Valley (middle panel), and Uintah Basin (bottom panel) for 1-11 January 2016.

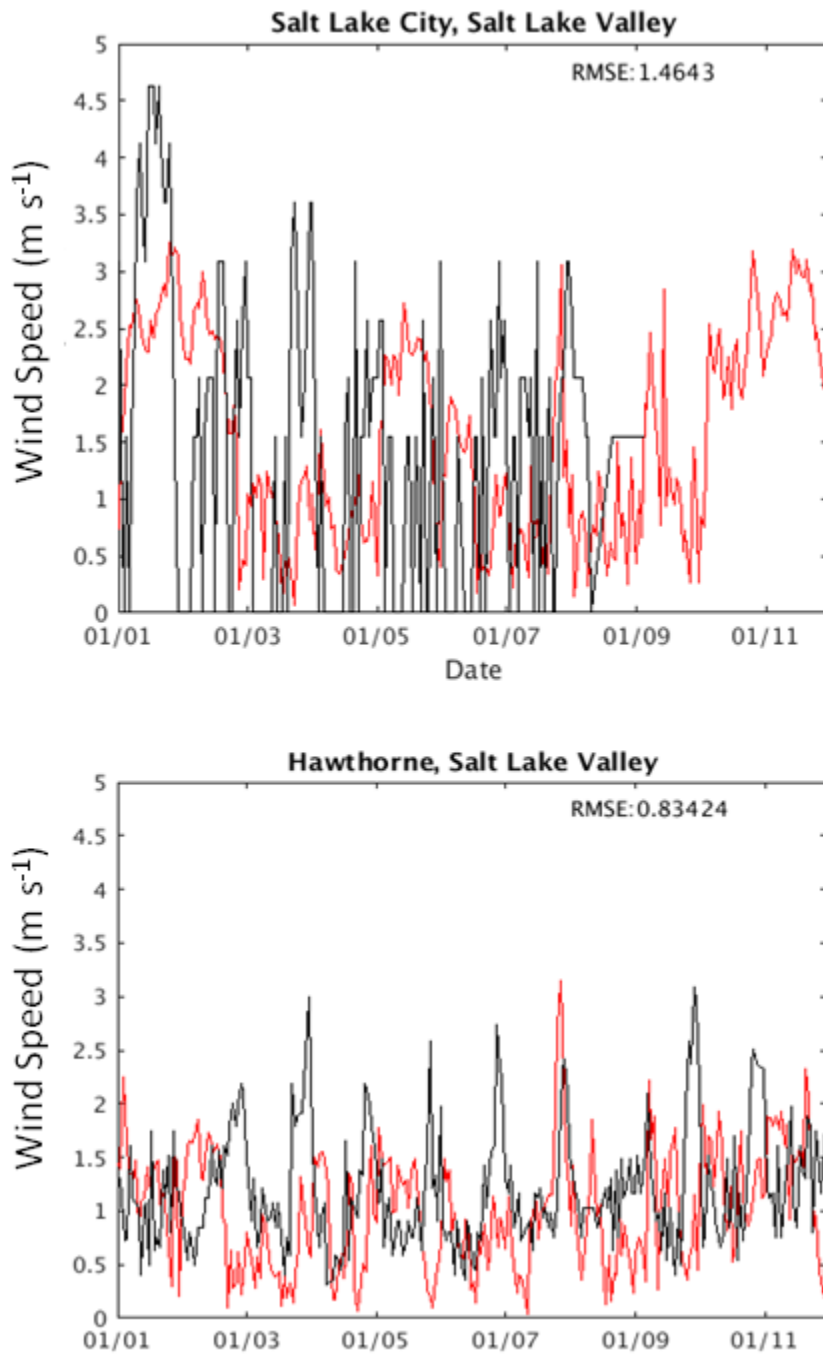


Figure 21. Comparison of model (red line) and observed (black line) 10-m wind speed (m s^{-1}) in the Salt Lake Valley at the Salt Lake City International Airport (top) and the UDAQ Hawthorne Elementary (bottom) between 1-11 January 2011.

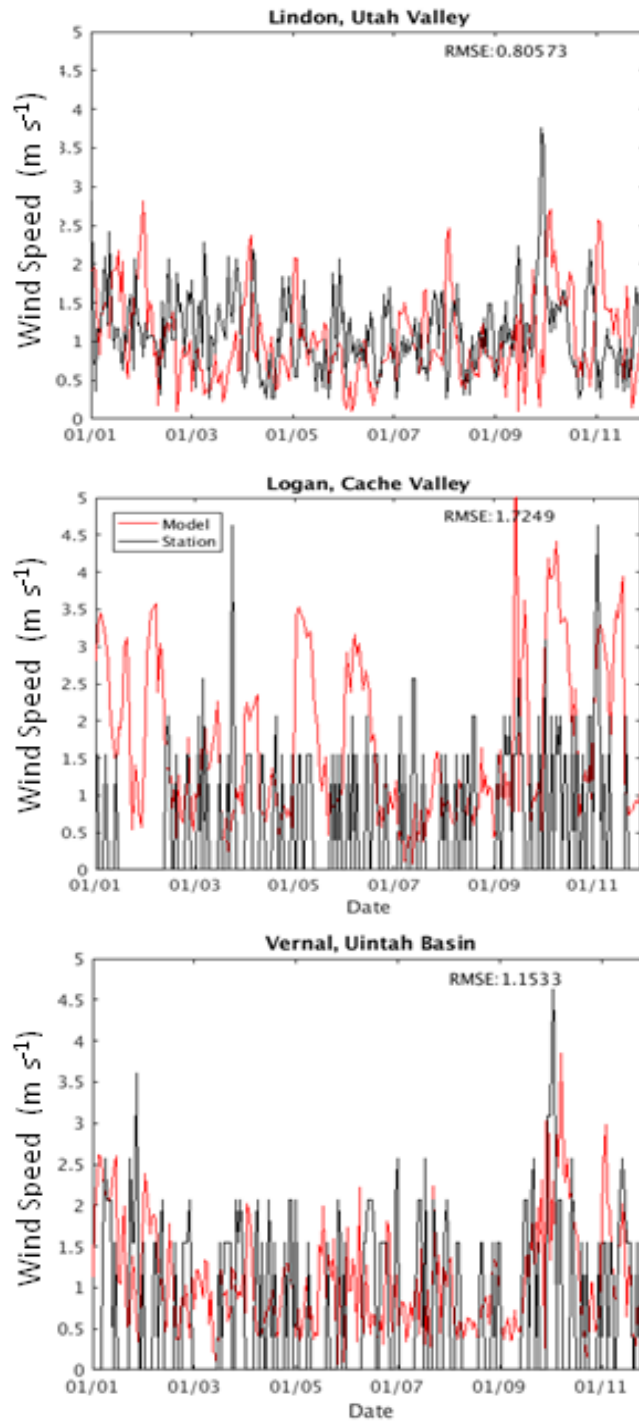


Figure 22. Comparison of model (red line) and observed (black line) 10-m wind speed (m s^{-1}) in the Utah Valley (top panel), Cache Valley (middle panel), and Uintah Basin (bottom panel) for 1-11 January 2011.

3.3.4 Supplemental: Expanded Discussion on Cache Valley Cold-Air Pool Model Performance Errors 1-11 January 2011

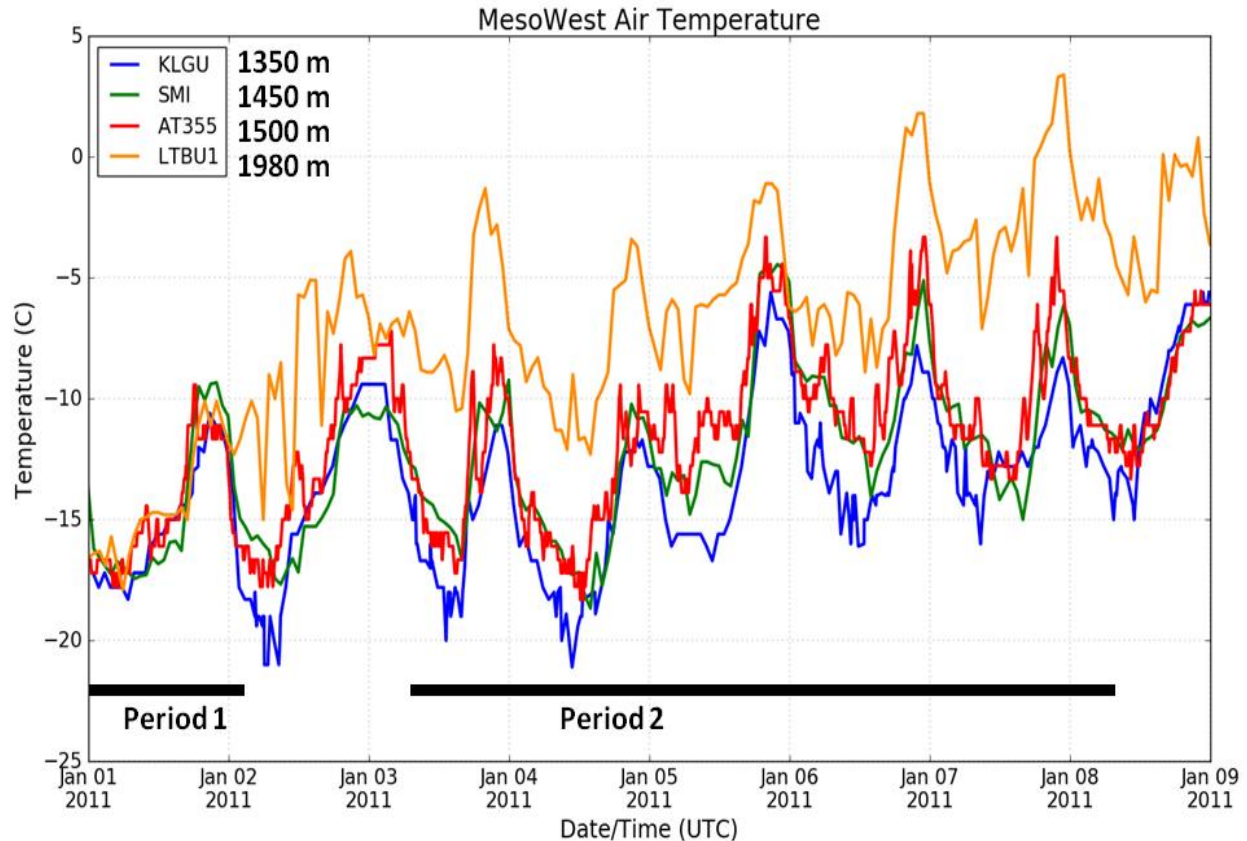
As discussed in the previous section, while surface wind speeds were well-simulated (Figure 22) in the Cache Valley, significant errors in the WRF model simulated 2-m temperature were observed during January 1-11 2011 (Figure 20). Additional analysis of satellite data, modeled time-height profiles of clouds and temperature in the Cache Valley, and all available Mesowest surface observations indicate that the 1-11 January 2011 simulated cold-air pool had the following errors (and potential sources of errors in the model listed):

- Too strong of radiation inversion noted on 1-2 January, *underestimating the mixing height by ~100 m*. Potential WRF model error source: strong surface cooling in the presence of light winds. Similar issue (but less pronounced) is noted during Salt Lake Valley during this episode (See Supplemental Figures 1 and 2).
- Too weak of low-level capping inversion above the surface on 3-5 January, *overestimating the mixing height by ~200-350 m*. Likely WRF model error source. Extensive simulated low cloud cover that resulted in too deep of mixed layers in the Cache during this time (See Supplemental Figures 1 and 2).
- More realistic mixing heights in the model 4-9 January based on ceilometers observations that indicate mixing heights should be in the 200 m range in Cache.

As seen in Supplemental Figure 1, the low-level temperatures in the Cache Valley below 1600 m ASL elevation remained between -5 and -20 °C during the 1-9 January period.

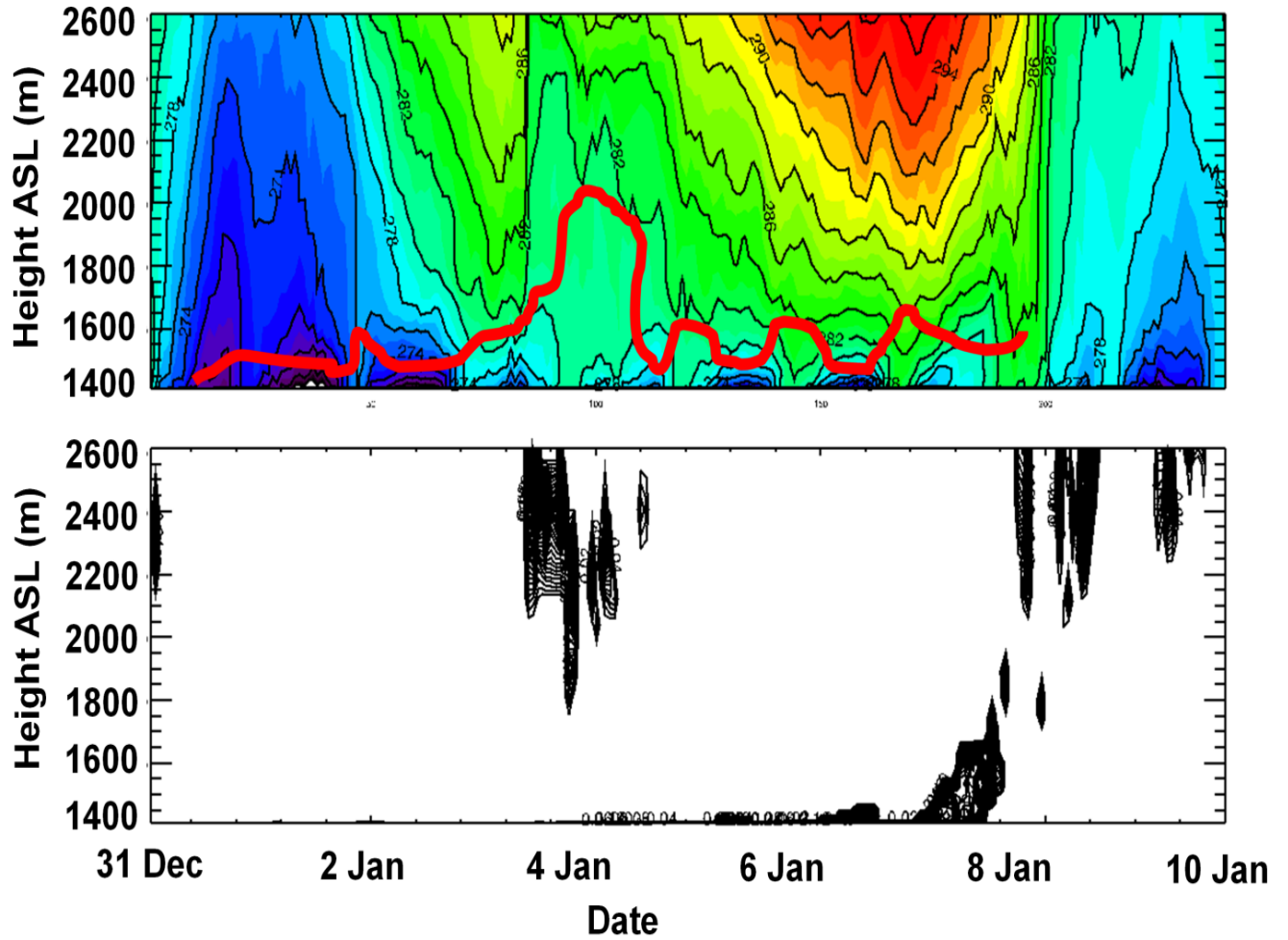
However, part-way up the valley slope at an elevation of 1980 m, temperatures climbed during the cold-air pool as high pressure and a descending inversion set in. The difference between the valley sites and the 1980 m elevation site can be used as a proxy for the overall inversion strength.

In addition, the stability of the lowest 200 m is critical for pollutant dispersion and how high pollution levels climb during an inversion. Comparing the observed temperature profiles at the lowest elevation site (KLGU) to sites 100-150 m (SMI and AT355) above the elevation of KLGU gives insight into the evolution of how strongly stably stratified the lowest portions of the cold-air pool was during this episode in the Cache Valley. The temperature difference between KLGU and SMI/AT355 is small on January 1, indicating that the inversion was weak at that time. Between January 4th and January 7th this difference is maximized, indicating that during this time less vertical mixing and a shallower layer of pollution would be expected. Ceilometer observations during other cold-air pools in 2015 and 2016 indicate that snow-covered cold-air pools in the Cache often see pollution remaining trapped below 250 m above ground level (see Figures 34-35).

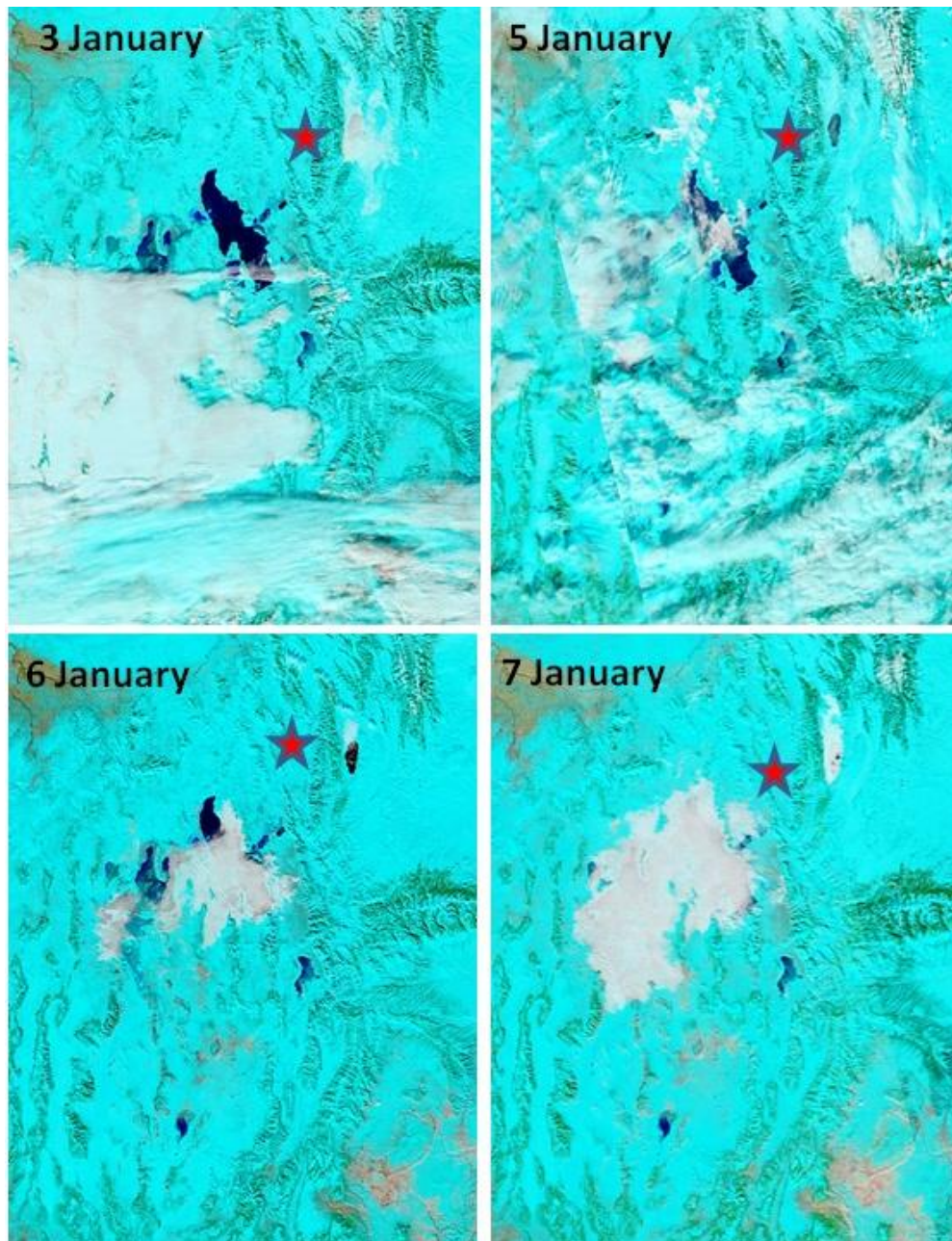


Supplemental Figure 1. Time series of observed Mesowest observations in the Cache Valley during the 1-9 January cold-air pool episode. The 4 stations are located at different elevations. KLGU = 1350 m ASL; SMI at 1450 m ASL; AT355 at 1500 m ASL; LTBU1 at 1980 m ASL. Period 1 represents the weaker cold-air pool onset period. Period 2 indicates the when the vertical temperature profile was most stable.

Unfortunately, the WRF model did not capture to capture the observed vertical temperature evolution, which would have impacts on the simulated mixing heights. As seen in Figure 20, the WRF model simulated temperature at Logan had a 5-15 °C warm biases during the period when the cold-air pool was strongest (Period 2 in Supplemental Figure 1). Analysis of the WRF model vertical temperature profiles (Supplemental Figure 2, upper panel) shows that the WRF model produced too stable of mixed layers between 31 December and 2 January. After that time, spurious clouds (that did not form in reality) resulted in a deep sub-cloud mixed layer in the Cache Valley between 3 and 5 January. In reality, these clouds did not form and the temperature inversion was much stronger (as shown in Supplemental Figure 1). As seen in Supplemental Figure 3, thick low clouds were not observed over the Cache Valley during this time.



Supplemental Figure 2. Time-height of potential temperature (top panel, according to labels) and cloud water (bottom panel, g kg^{-1}) at Logan, Utah between 1-9 January 2011. The estimated mixing height based on visual inspection of the vertical potential temperature gradient is annotated with a red line in (a).



Supplemental Figure 3. MODIS satellite images from early afternoon on 3, 5, 6 and 7 January 2016. Note that while low clouds formed over the Great Salt Lake, the Cache Valley remained clear throughout the episode.

3.4 7-21 December 2013 Cold-Air Pool Model Performance Evaluation

The 7-21 December 2013 cold-air pool was a significant pollution episode over northern Utah. The modeling framework for the December 2013 meteorological simulation was identical as used in the BASE WRF simulation for January 2011. The surface snow cover initialization also used the linear analysis fit to observations methodology described in Section 2.5. See Section 3.2 for more details on the observations used for MPE.

3.4.1 7-21 December 2013 Vertical Cold-Air Pool Structure Model Evaluation

The basic vertical evolution of the February 2016 persistent cold-air pool was well-simulated by the WRF model. Figure 23 shows the WRF model simulated vertical profiles of temperature and relative humidity in the Salt Lake Valley. A strong descending capping inversion was noted between 9-11 December (Fig. 23). Strong surface-based radiation inversions (the blue ‘domes’ in Figure 23) existed each night, except on 13 December when fog limited surface radiational cooling. A weak weather system brought a ‘partial mix-out’ on 14-15 December, with a reinforcing subsidence inversion that descended toward the surface between 16-19 December. The cold-air pool ‘mixed out’ between 19-21 December. The simulated mixing depth during the cold-air pool ranged from 200-300 m above ground level in the afternoon. Similar to the more extensively studied January 2011 PCAPS cold-air pool, these simulated mixing heights appear to be somewhat underestimated (Figs. 23-26).

Comparisons of vertical profiles of temperature and wind speeds in the Salt Lake Valley at the Salt Lake City International Airport show reasonable agreement with the model simulations throughout the lifecycle of the cold-air pool (Figures 24-26).

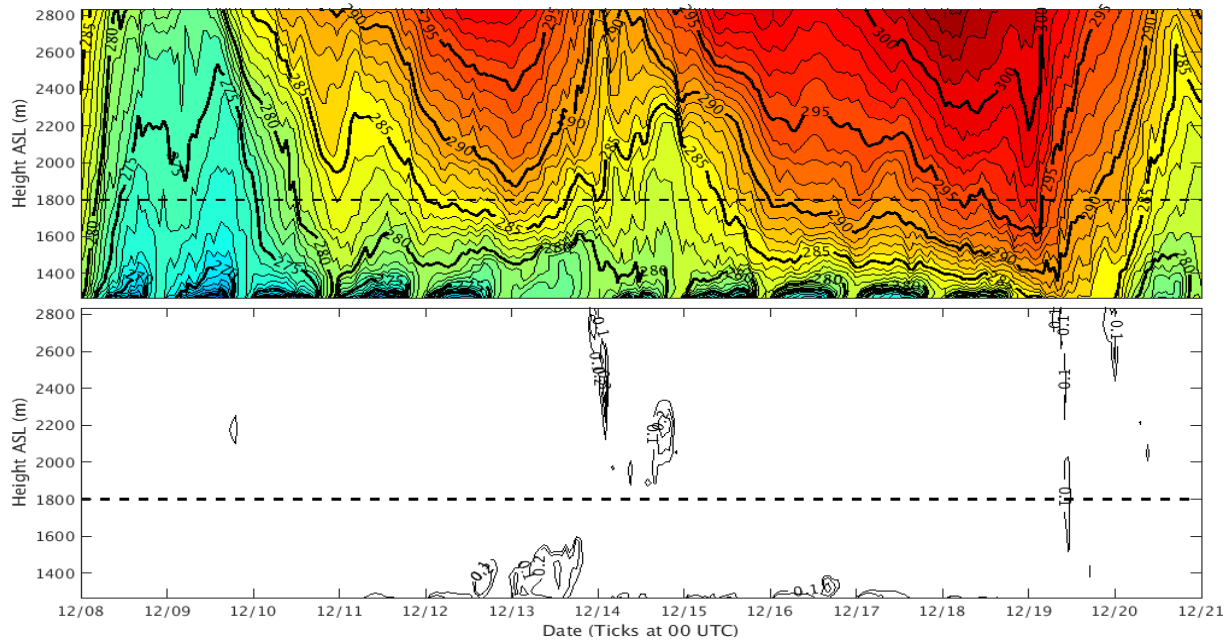
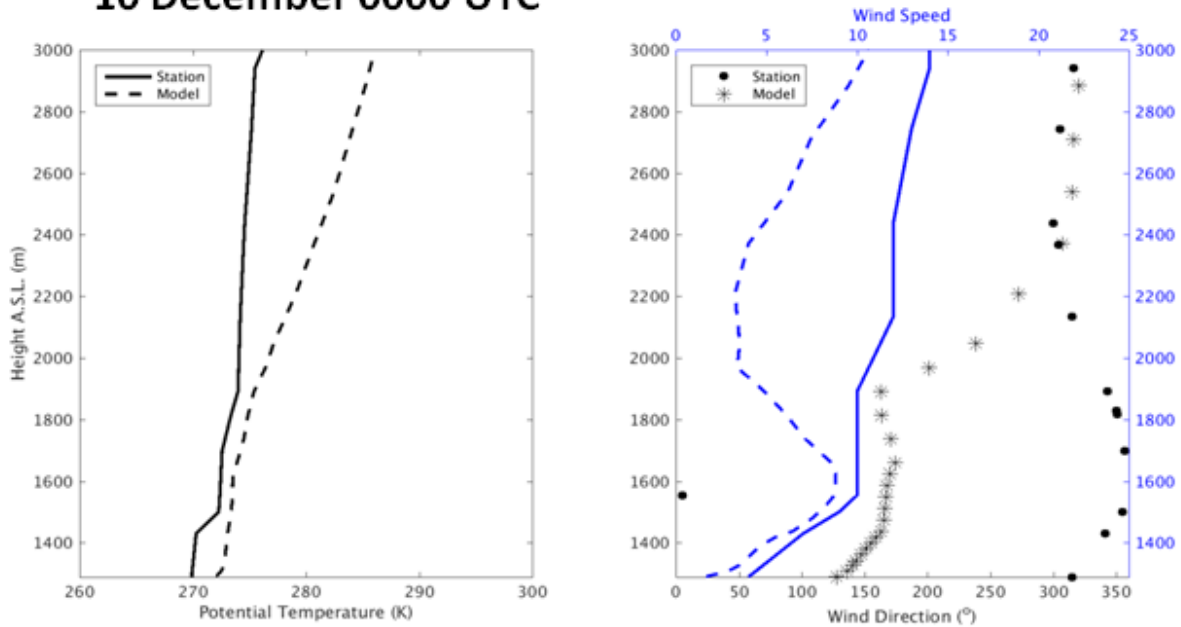


Figure 23. WRF simulation modeled vertical profiles time-height diagram at ISS near the center of the Salt Lake Valley 8-21 December 2013 for **top** potential temperature (K, color shaded with bold contours every 5 K and light contours every 1 k) and **bottom** cloud water (g/kg, contoured).

10 December 0000 UTC



12 December 1200 UTC

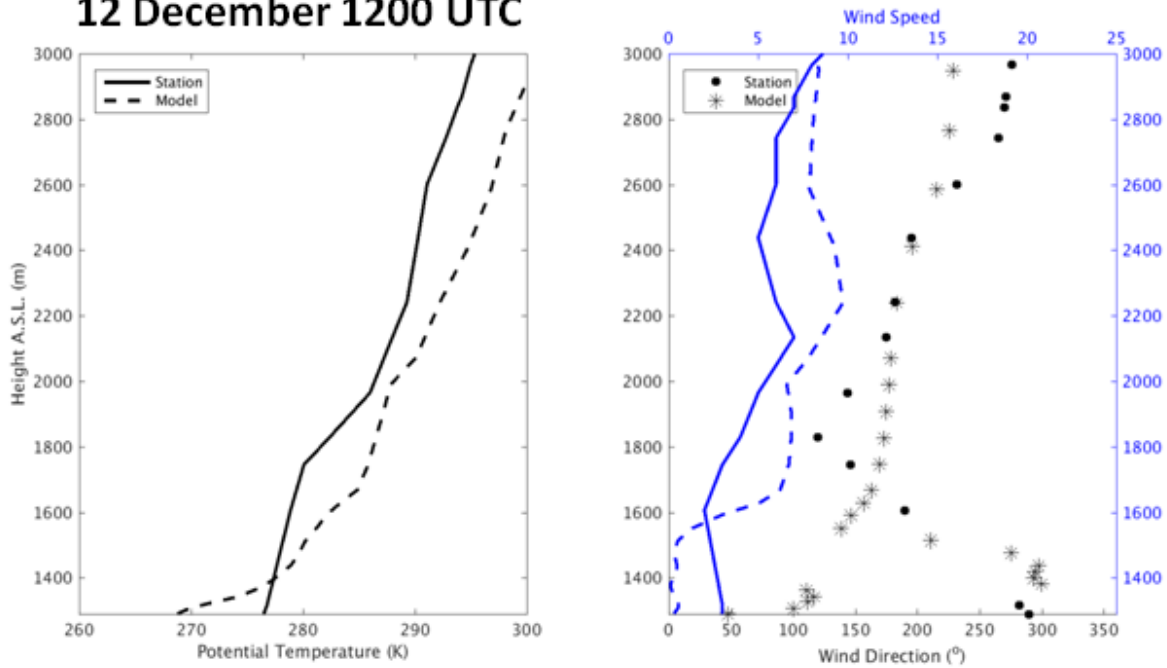
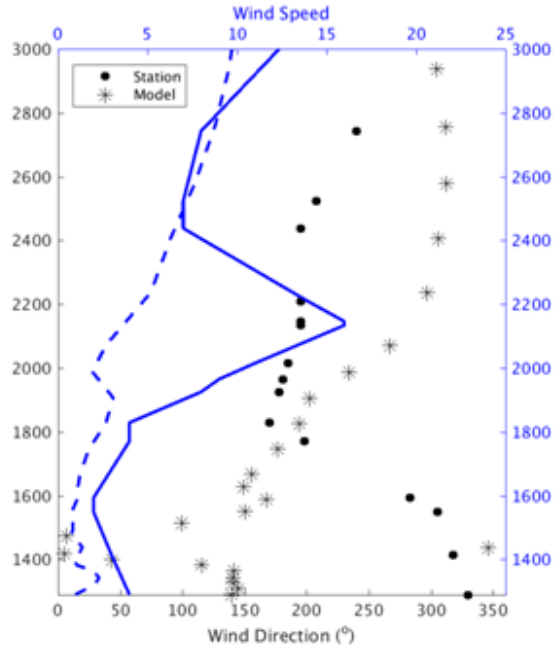
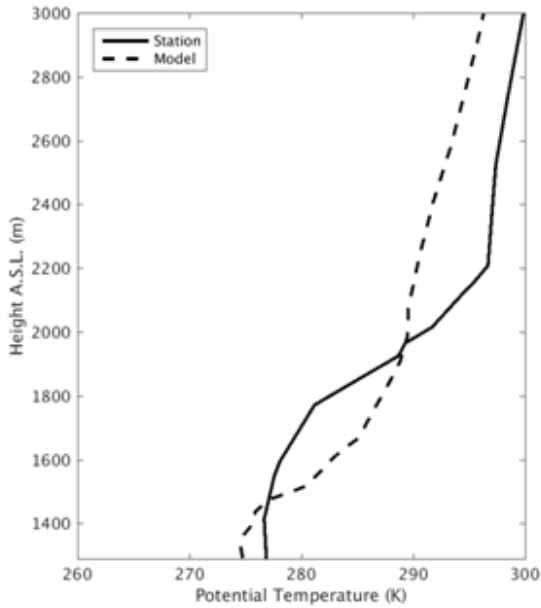


Figure 24. Comparison of WRF simulation modeled vertical profiles (dashed lines) against Salt Lake City Airport Radiosondes (solid lines) for potential temperature (black colors, K); wind speed (blue colors, $m s^{-1}$); and wind direction (in degrees, observations are black circles, model represented by *). Top panel is for 10 December 2013 at 0000 UTC. Bottom panel is for 12 December 2013 at 1200 UTC.

13 December 1200 UTC



15 December 1200 UTC

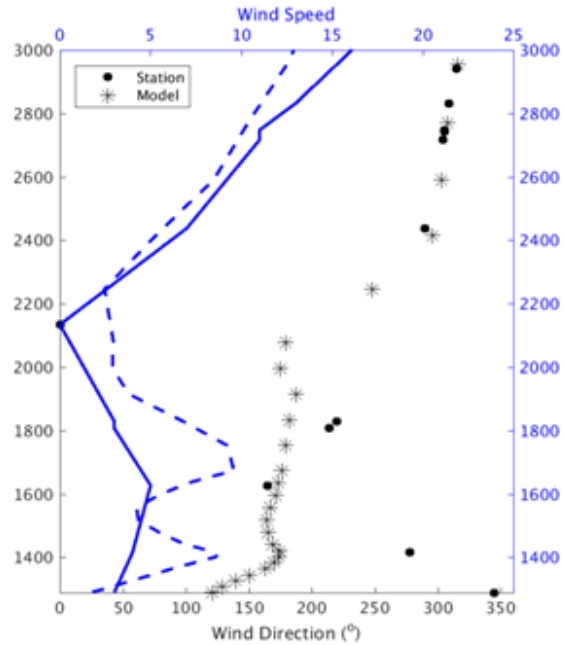
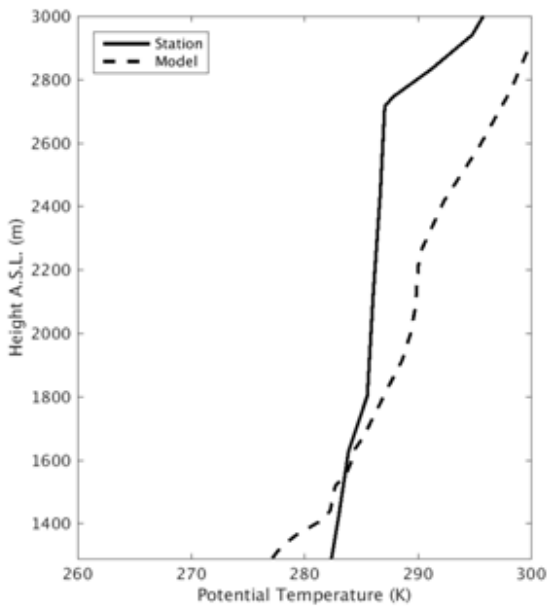


Figure 25. Comparison of WRF simulation modeled vertical profiles (dashed lines) against Salt Lake City Airport Radiosondes (solid lines) for potential temperature (black colors, K); wind speed (blue colors, m s⁻¹); and wind direction (in degrees, observations are black circles, model represented by *). Top panel is for 13 December 2013 at 1200 UTC. Bottom panel is for 15 December 2013 at 1200 UTC.

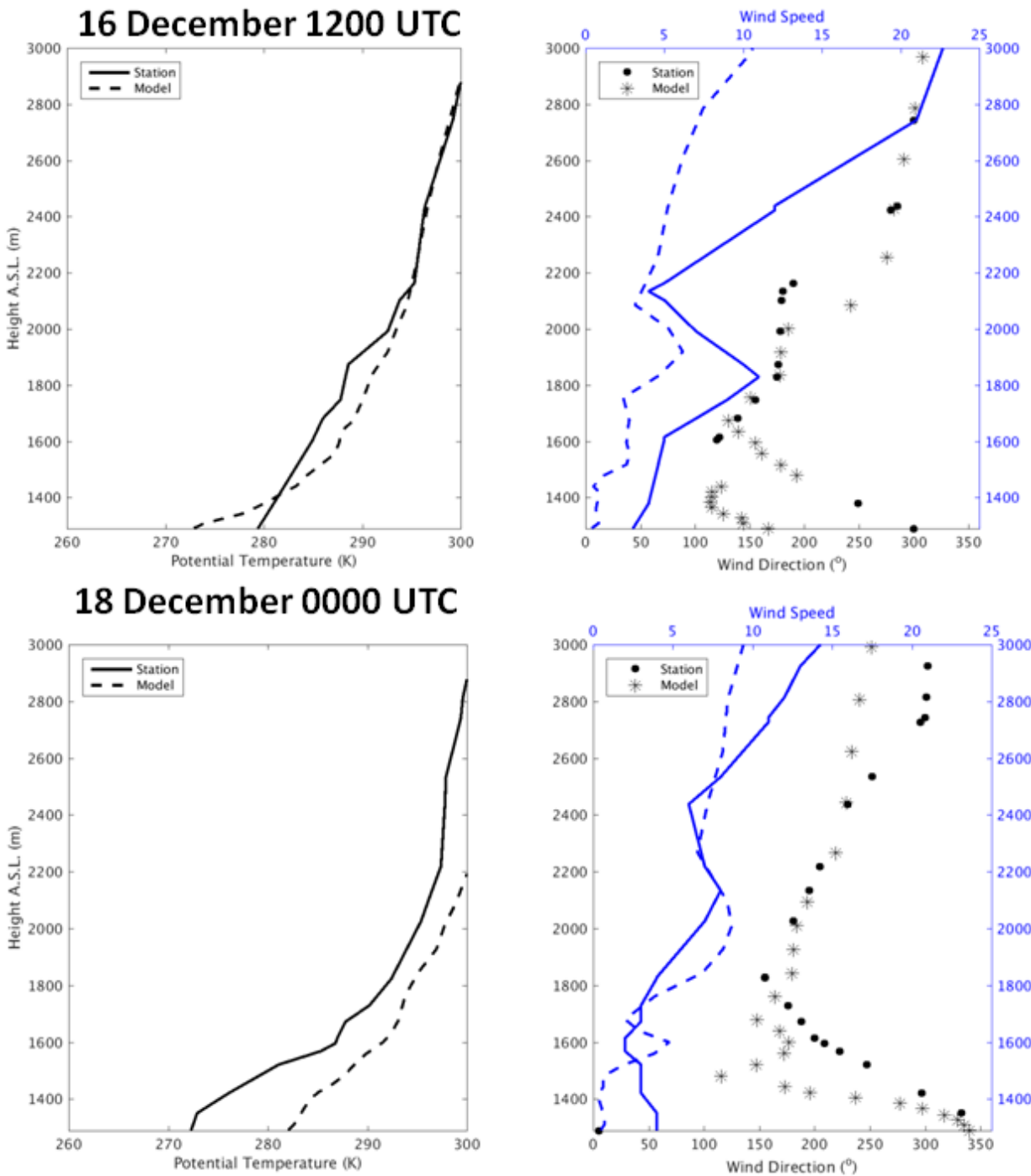


Figure 26. Comparison of WRF simulation modeled vertical profiles (dashed lines) against Salt Lake City Airport Radiosondes (solid lines) for potential temperature (black colors, K); wind speed (blue colors, m s^{-1}); and wind direction (in degrees, observations are black circles, model represented by *). Top panel is for 16 December 2013 at 1200 UTC. Bottom panel is for 18 December 2013 at 0000 UTC.

3.4.2 7-21 December 2013 Case Surface and Near-Surface Cold-Air Pool Model Evaluation

The 2-m temperatures were simulated relatively well in the Salt Lake Valley (Table 12 and Figure 27). Biases and RMS errors were relatively small and similar to those observed during the more highly validated case in January 2011. Similar to the PCAPS January 2011 case, some of the RMS error in the Salt Lake Valley resulted from the model not properly capturing the cold overnight low temperatures observed.

As with the other simulations, the 2-m temperatures showed somewhat higher RME errors compared to observations in the other Utah basins (Table 12 and Figure 28). The exact reasons for these errors in these basins are unknown, as only limited surface observations are available with which to validate the models in these basins for the episodes of interest, however, we present some probable hypotheses below.

Careful analysis of the model output compared to satellite observations of cloud cover points to model issues with too much cloud cover in the simulations in the Uintah Basin and Cache Valley. In the Utah Valley, model issues with not enough cloud cover and not freezing the lake may also play a role in the errors there.

The warm model temperature bias in Utah valley between 10-14 December appears at least partially related to inadequate stratus cloud formation in the model between 12-14 December, which resulted in greater incoming solar insolation and warmer temperatures in the simulations. In addition, the surface of Utah lake was not represented as frozen in the model, which could have played a large role in the warm nighttime model temperature bias, as the Utah Lake was frozen in reality. In contrast the warm model temperature bias in the Uintah Basin during nighttime between 13-17 December (Fig 28) is potentially related to the model creating extensive cloud cover when in reality there was none observed on satellite (not shown). In the Cache Valley, the reason for the persistent warm model bias is unknown, but may be due to the WRF model inability to reproduce extremely shallow surface inversions in the lowest 10s of meters of the boundary-layer. It is unknown how important these biases are for the overall ability to properly simulate mixing and transport in the Cache Valley cold-air pool.

Table 12. WRF performance for **2-m temperature (°C)** for 7-21 December 2013 cold-air pool

Station	Bias (°C)	RMS Error (°C)
Hawthorne	-0.942	2.420
Salt Lake City	0.046	2.414
Lindon	2.342	4.0258
Vernal	2.237	2.516
Logan	4.519	5.937

The 10-m wind speeds, both observed and modeled were exceptionally low during the December 2013 cold-air pool. The wind speed biases and RMS errors were generally low for all basins (Table 13), as the WRF model captured will the light winds associated with cold-air pool conditions. Wind speeds in the model and observed generally remained below 2 m s^{-1} at all observation locations during the duration of the cold-air pool. The weakest winds were observed and simulated at Vernal and Logan, with the strongest winds, presumably because of lake breezes and drainage flows, were observed at the Salt Lake International Airport (Figures 29 and 30). While the numerical simulations in general captured the very light wind speeds, the numerical simulations were unable to simulate winds below around 0.75 m s^{-1} . At extremely light or calm (0 m s^{-1}) wind speeds, the model continued to simulate a $0.5\text{-}1 \text{ m s}^{-1}$ flow (Fig. 30).

Wind directions were also analyzed but are not shown here as they were not deemed important. Wind directions are highly irregular, sporadic, and controlled by small unrepresentative terrain and building features during such light speeds.

Table 13. WRF performance for 10-m wind speed for 7-21 December 2013 cold-air pool

Station	Bias (m s^{-1})	RMS Error (m s^{-1})
Hawthorne	-0.197	0.770
Salt Lake City	-0.30	1.401
Lindon	0.093	0.868
Vernal	0.027	1.136
Logan	0.988	1.217

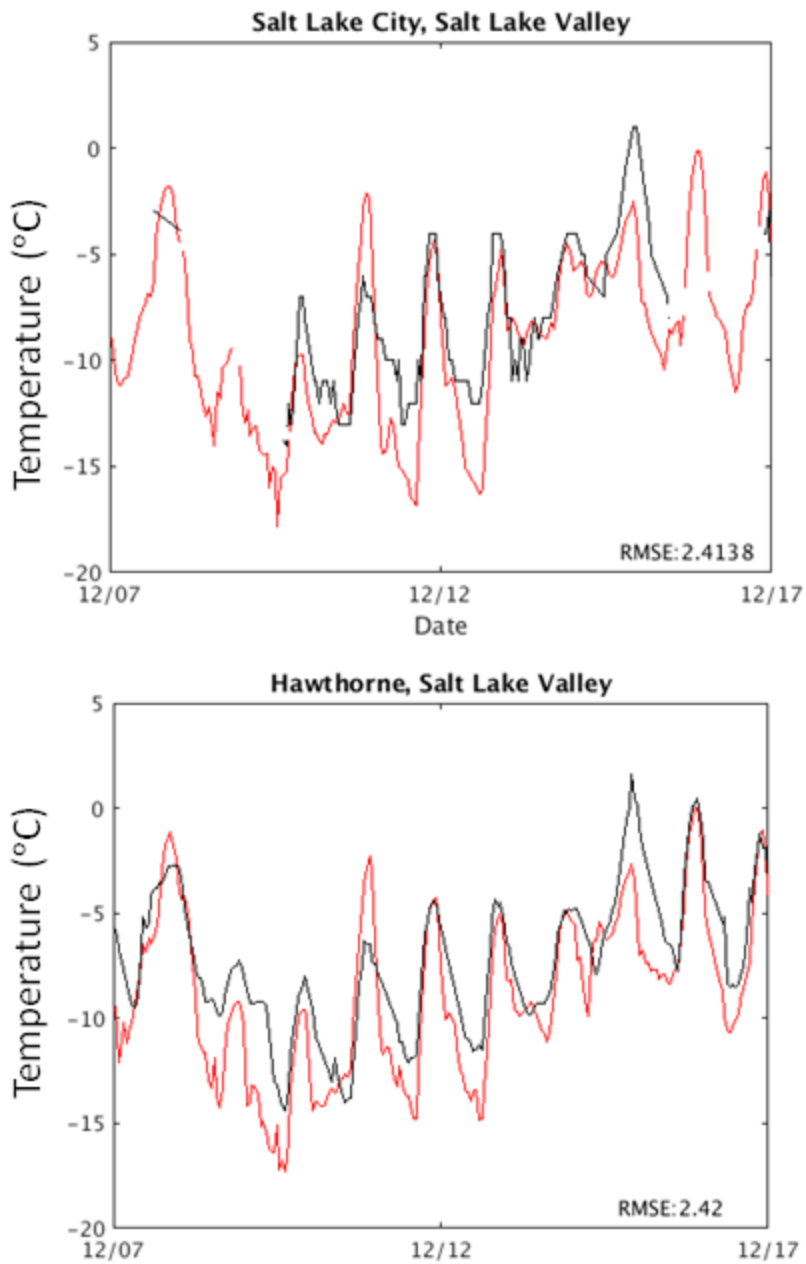


Figure 27. Comparison of model (red line) and observed (black line) 2-m temperature (°C) in the Salt Lake Valley at the Salt Lake City International Airport (top) and the UDAQ Hawthorne Elementary (bottom) between 7-17 December 2013.

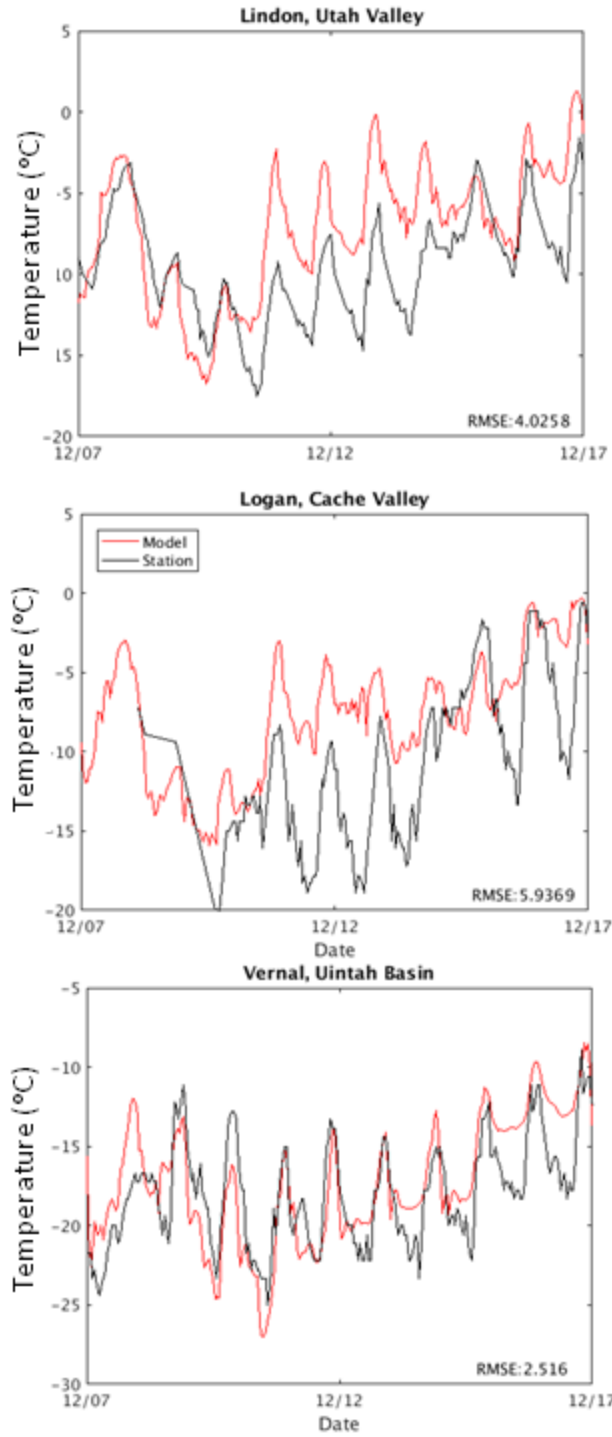


Figure 28. Comparison of model (red line) and observed (black line) 2-m temperature (°C) in the Utah Valley (top panel), Cache Valley (middle panel), and Uintah Basin (bottom panel) for 7-17 December 2013.

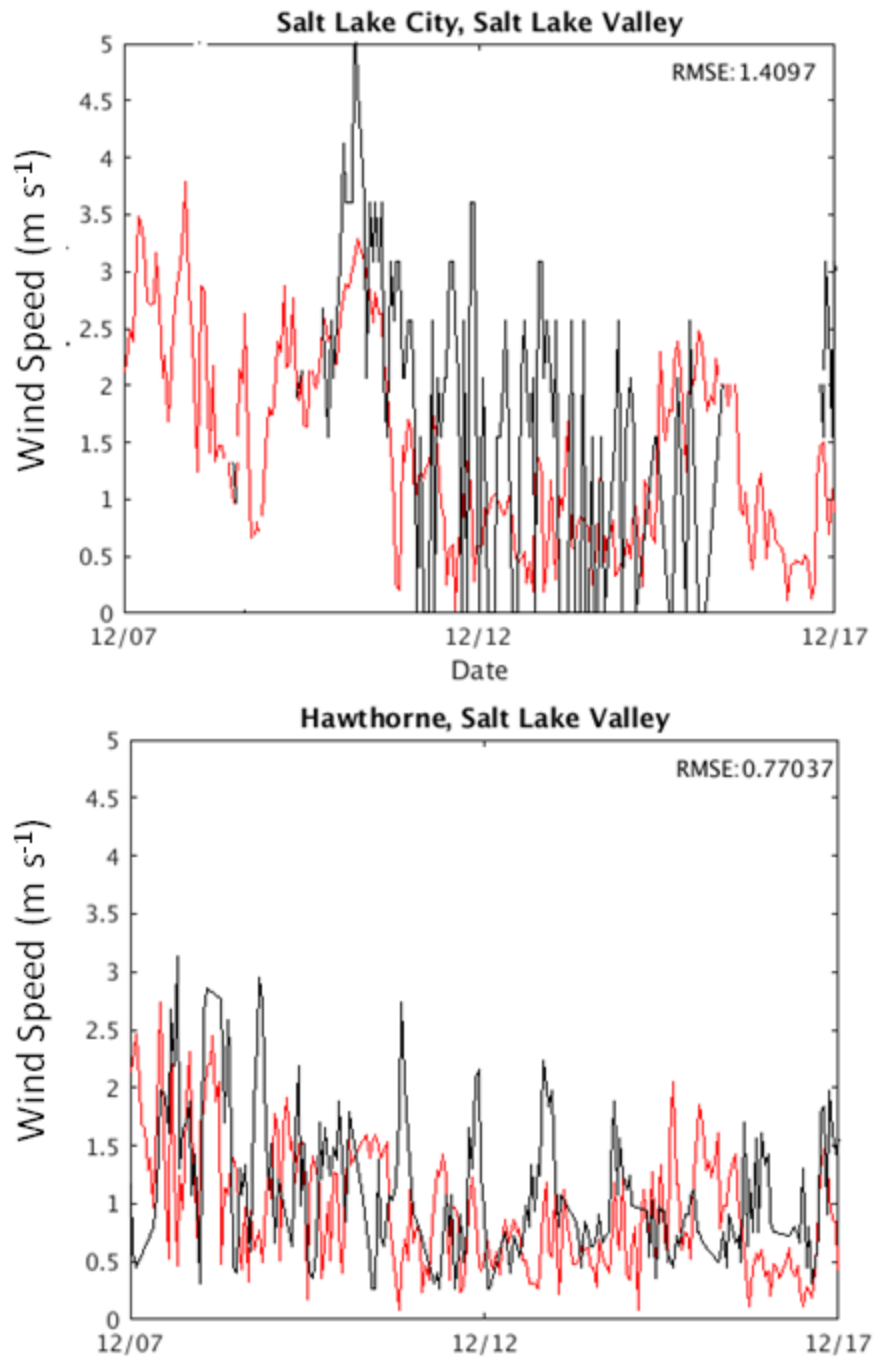


Figure 29. Comparison of model (red line) and observed (black line) 10-m wind speed (m s^{-1}) in the Salt Lake Valley at the Salt Lake City International Airport (top) and the UDAQ Hawthorne Elementary (bottom) between 7-17 December 2013.

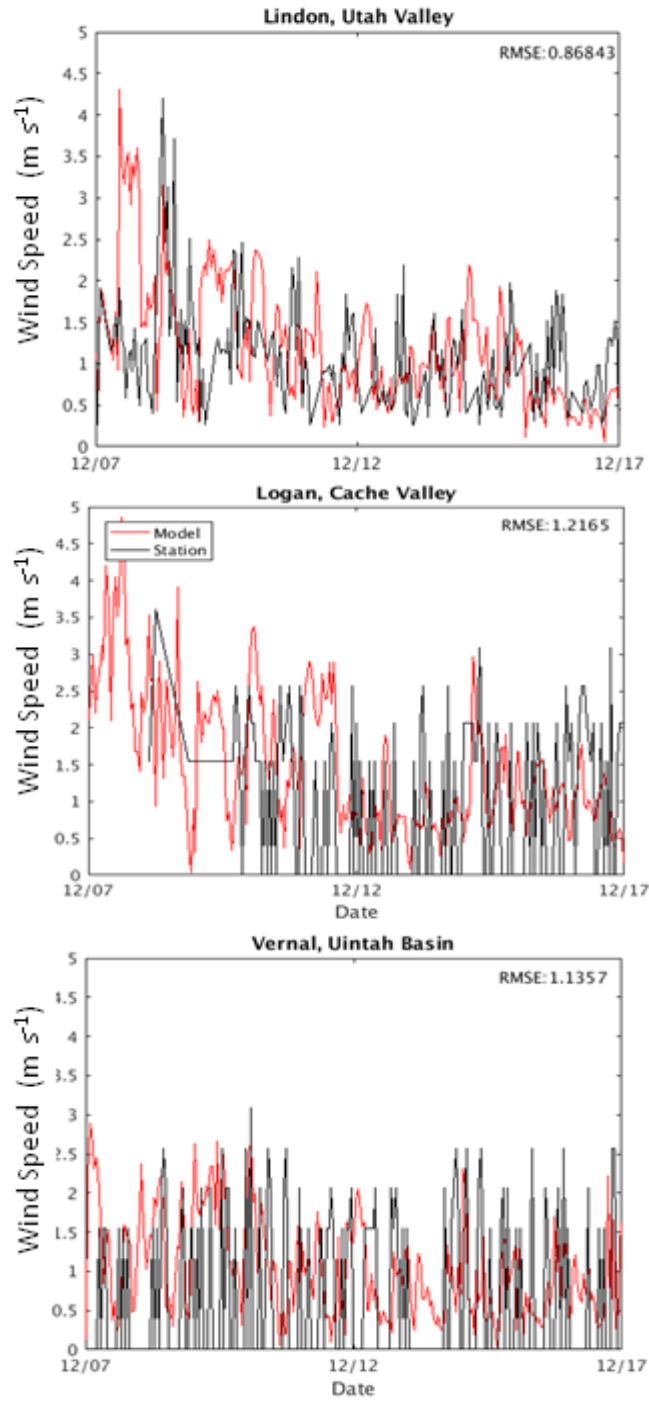


Figure 30. Comparison of model (red line) and observed (black line) 10-m wind speed (m s^{-1}) in the Utah Valley (top panel), Cache Valley (middle panel), and Uintah Basin (bottom panel) for 1-11 January 2011.

3.5 1-17 February 2016 Cold-Air Pool Model Performance Evaluation

The February 2016 cold-air pool was an unusually late season and long-duration episode with large heat deficits for early February (Dave Whiteman, personnel communication). The modeling framework for the February 2016 meteorological simulation was identical as used in the BASE WRF simulation for January 2011. The surface snow cover initialization also used the linear analysis fit to observations methodology described in Section 2.5. See Section 3.2 for more details on the observations used for MPE.

3.5.1 1-17 February 2016 Vertical Cold-Air Pool Structure Model Evaluation

The basic vertical evolution of the February 2016 persistent cold-air pool was well-simulated by the WRF model. Figure 31a shows the simulated vertical profiles of temperature and relative humidity which can be compared against the observed vertical profiles of temperature shown in Figure 31b (courtesy of Sebastian Hoch). The overall onset formation of low clouds during the second half of the cold-air pool was also well-handled by the WRF simulation, although the clouds did not persist in the model as many days as was observed (not shown). The model simulates well these key features of the observed February 2016 cold-air pool:

- (1) Descending subsidence inversion
- (2) Strong capping inversion
- (4) Sub-cloud mixed layers on 9-10 Feb
- (5) Mix-out

Similar to the December 2013 and January 2011 cases, the WRF meteorological simulations have a low bias of 50-150 m in general with respect to vertical mixing depth beneath the capping inversion (see ceilometers Figures 33 and 34 in Section 3.5.2). A more detailed evolution of the simulated potential temperature and cloud water are shown in Figure 32.

With respect to wind, the simulated vertical profiles captured the general evolution of synoptic wind speeds above the cold-air pool (not shown). A weather system with moderate winds on 15 February ended the cold-air pool episode.

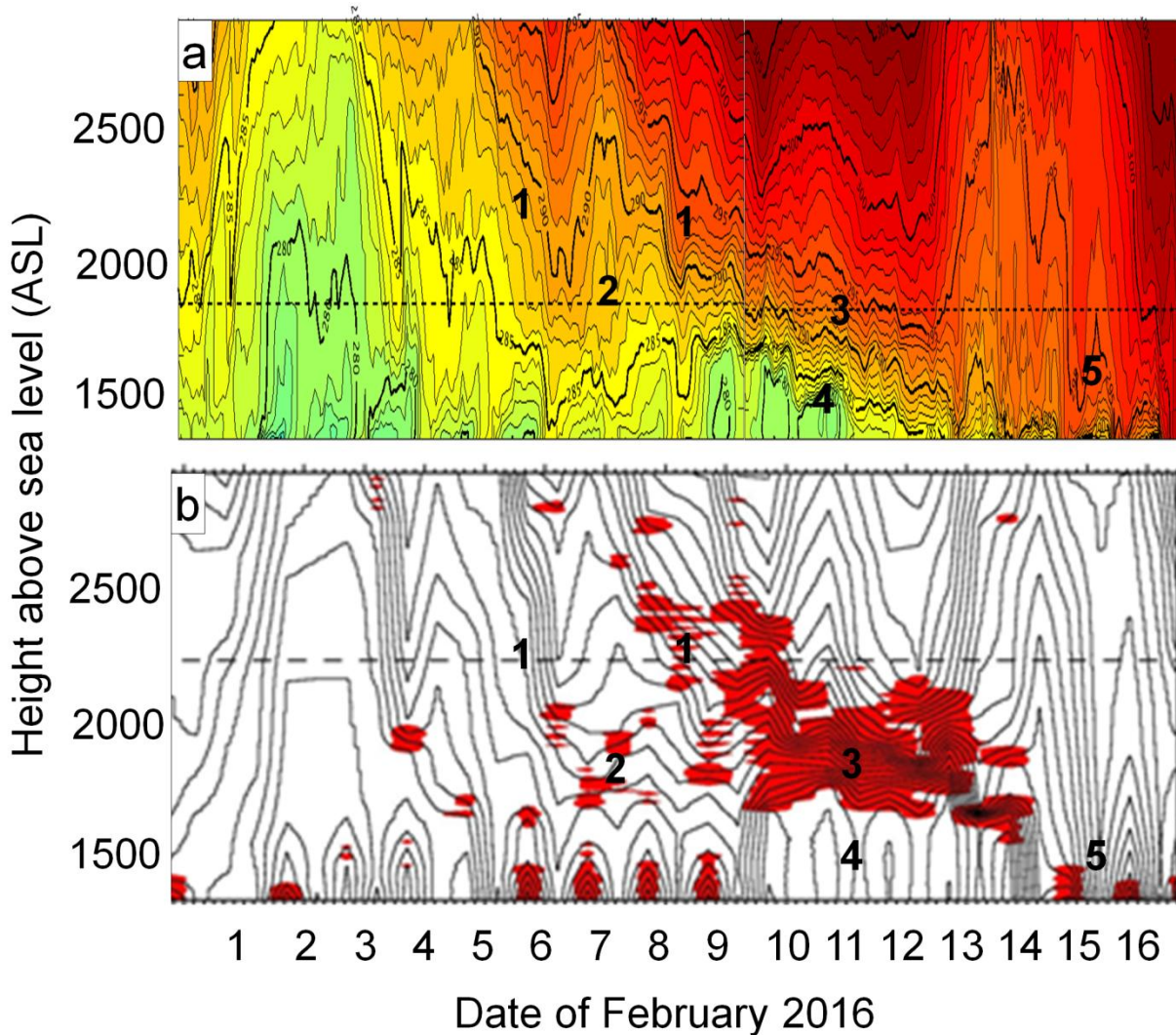


Figure 31. a. WRF model simulations of time-height cross-section of *isentropes* (isolines of constant potential temperature θ) in the Salt Lake Valley in February 2016 for b Observed time-height cross-section of *isentropes* (isolines of constant potential temperature θ) as recorded by twice-daily radiosondes at KSLC during the experimental winter season. Regions with elevated atmospheric stability ($d\theta/dz > 0.016 \text{ K m}^{-1}$) are highlighted in red. Figure b Courtesy of Sebastian Hoch for the UDAQ winter 2016 pollution study.

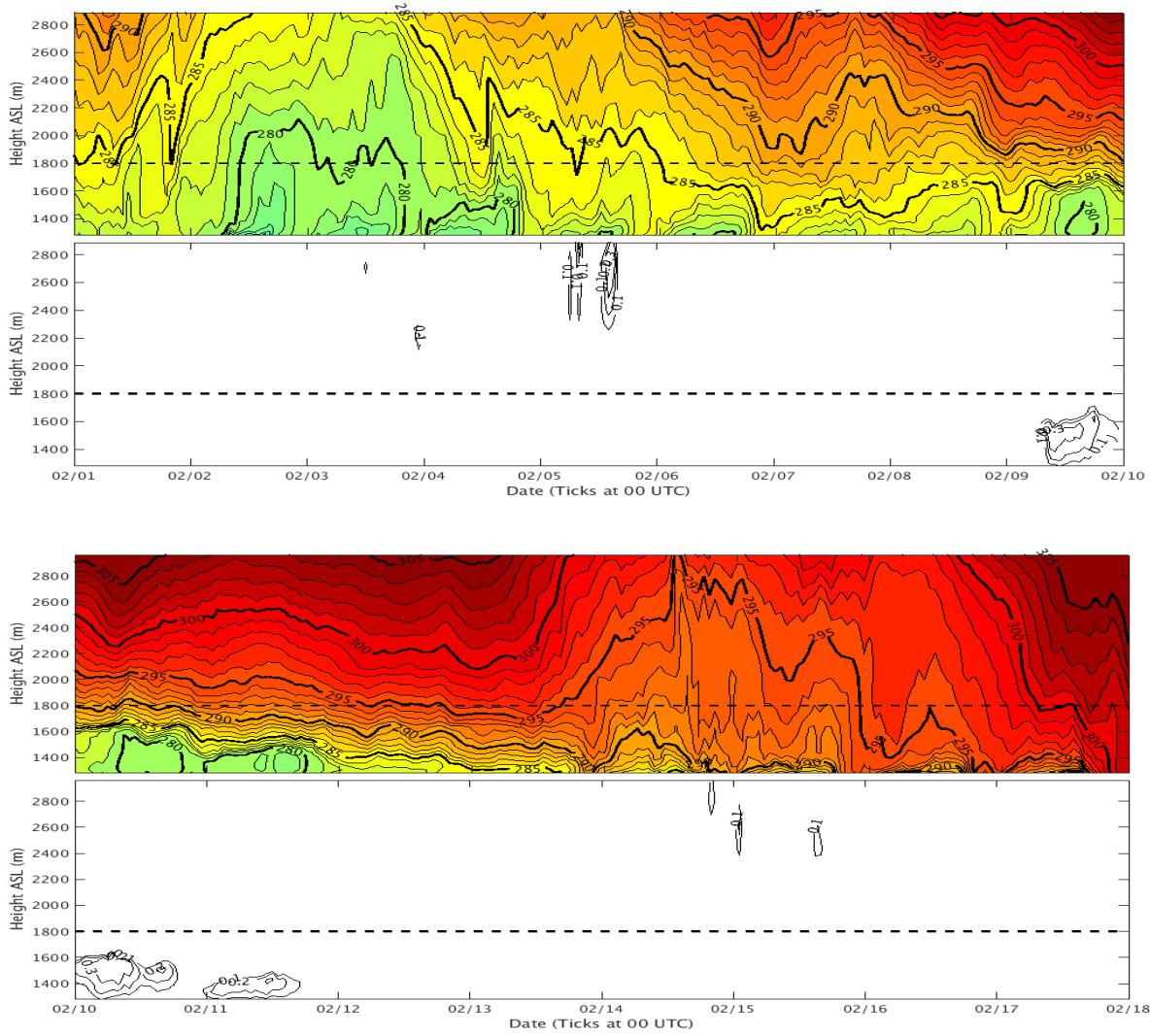


Figure 32. Modeled vertical profiles time-height diagram at ISS near the center of the Salt Lake Valley in February 2016 for **a** potential temperature (K, color shaded with bold contours every 5 K and light contours every 1 k) and **b** cloud water (g/kg, contoured).

3.5.2 1-17 February 2016 Surface Cold-Air Pool Model Evaluation in Salt Lake Valley, Utah Valley, Cache Valley, and Uintah Basin Using Standard Observations

As discussed in Section 3.5.1, the overall synoptic weather pattern and temperature and wind speeds aloft were well-captured by the WRF meteorological set-up. However, as was shown by Neemann et al. (2015), it is very difficult to correctly model low clouds and fog in the numerical models. These cases are no exception. In reality, during this intense late-season cold-air pool, low clouds formed first over the south-central basins of Utah, while all of the basins of concern in this study (Uintah, Cache, Salt Lake, and Utah) remained clear of fog during the period from 1-8 February 2016 (Figure 33). As shown in ceilometers backscatter, periods of light precipitation was observed in the Cache and Salt Lake Valleys from 1-4 February (Figs. 34-35).

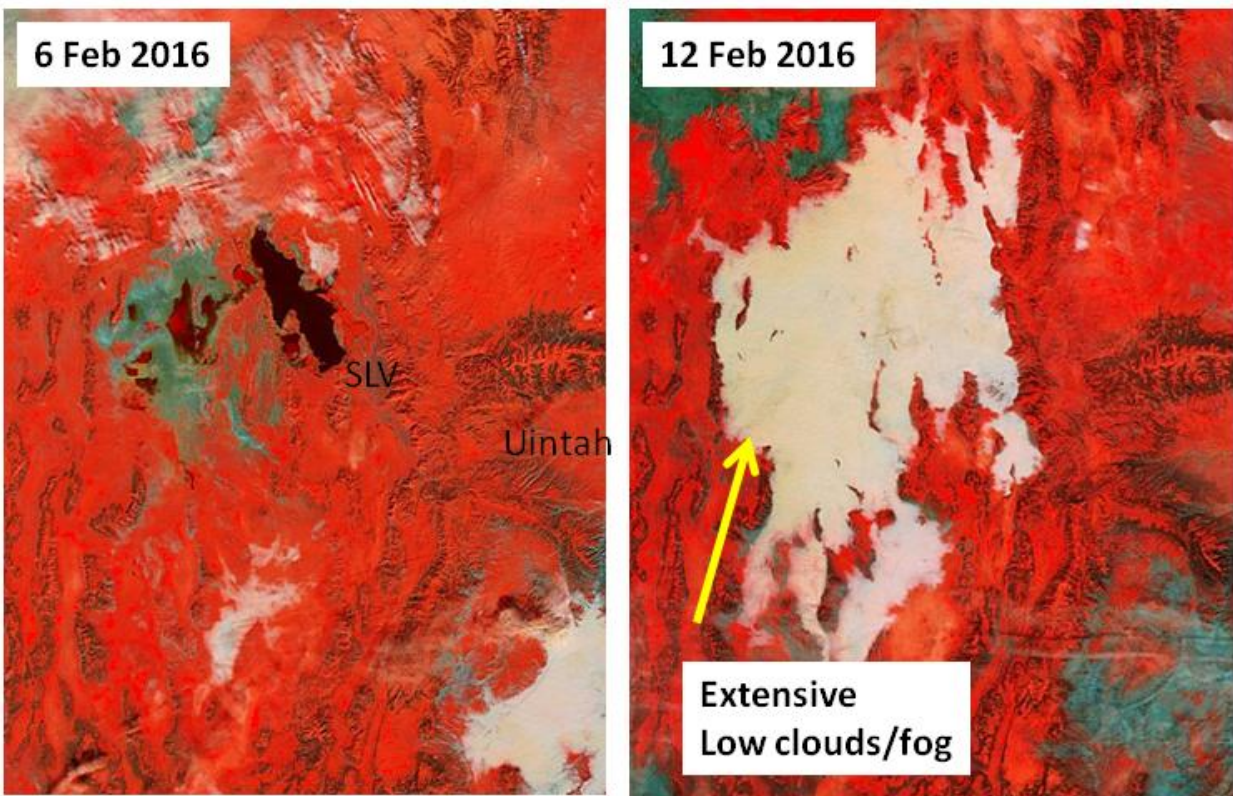


Figure 33. MODIS 3-6-7 satellite image from 6 Feb and 15 Feb 2016. Clouds and fog are represented by white colors, while ground surfaces are represented by green and red colors. The location of the Salt Lake Valley and Uintah Basin are indicated on 6 Feb.

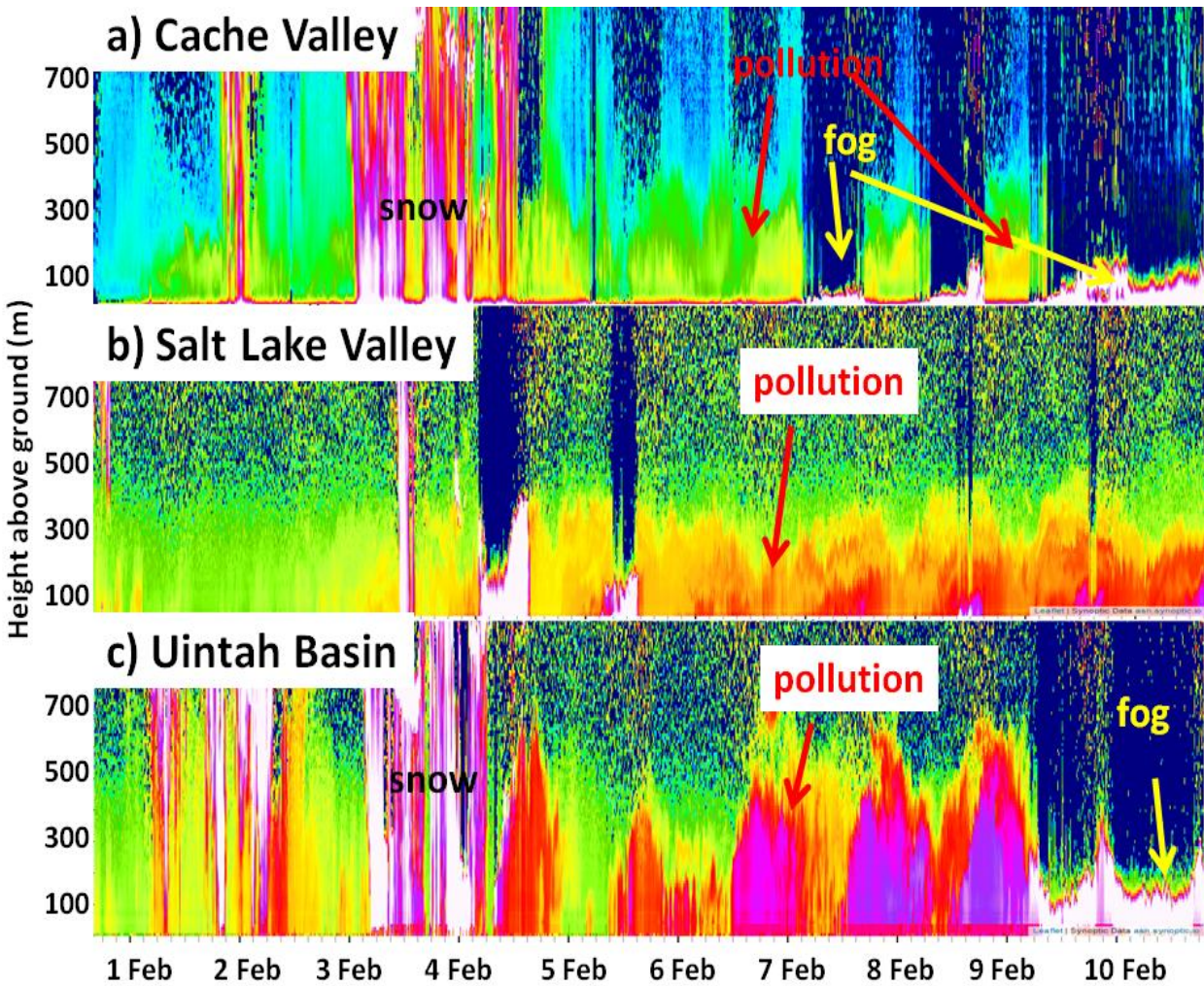


Figure 34. Laser ceilometer backscatter (colors) from the **a** Cache Valley, **b** Salt Lake Valley, and **c** Uintah Basin from 1-10 February 2016. Dark green and yellow colors represent low to moderate PM concentrations. Orange, red, magenta, and purple represent high levels of PM pollution. White color indicated beam saturation from precipitation or fog.

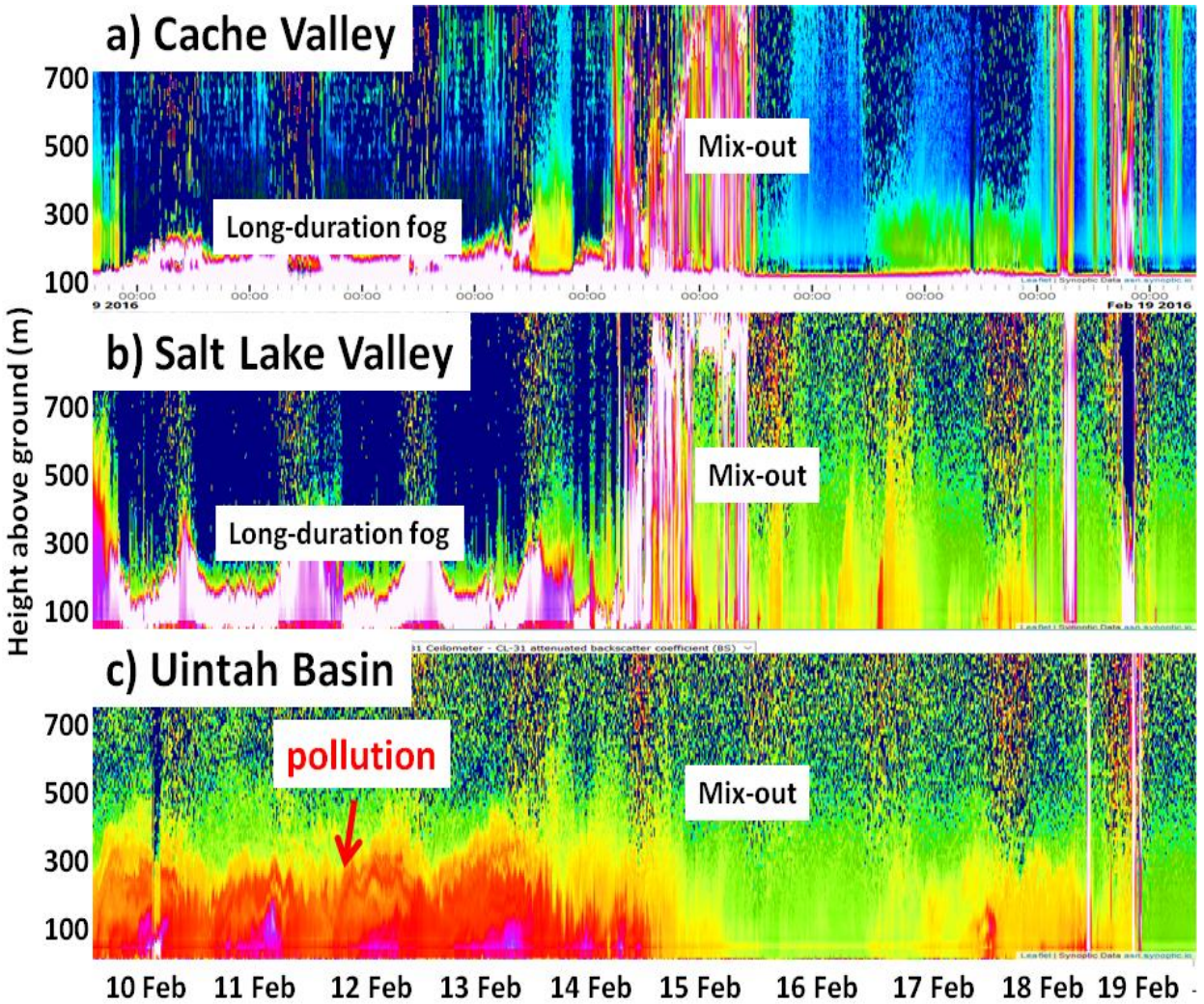


Figure 35. Laser ceilometer backscatter (colors) from the **a** Cache Valley, **b** Salt Lake Valley, and **c** Uintah Basin from 10-10 February 2016. Dark green and yellow colors represent low to moderate PM concentrations. Orange, red, magenta, and purple represent high levels of PM pollution. White color indicated beam saturation from precipitation or fog.

However, from the 5th-9th February, the Salt Lake, Utah, Cache, and Uintah Valleys remained cloud-free, with the exception of some nocturnal fog on the 8th and 9th February in the Cache Valley (Fig. 33). However, late on the 9th of February, the Great Salt Lake Basin and surroundings became covered in low clouds and fog (Fig 33). The fog lasted until the initial mix-out period on the 15th of February. The spatial extent of the fog across central and northern Utah can be seen in the MODIS imagery on February 12th. As has been the case in other episodes, the WRF model was unable to properly capture the fog location and timing, although it did better in the Salt Lake Valley than other locations. The fog performance issues resulted in significant model temperature biases and errors at times, as will be discussed next.

The 2-m temperatures were simulated relatively well in the Salt Lake Valley (Table 14). Biases were small and RMS errors were similar to those observed during the more highly validated case in January 2011. Similar to the PCAPS January 2011 case, some of the RMS error in the Salt Lake Valley resulted from the model not properly capturing the cold overnight low temperatures observed. Some errors also occurred when clouds that were observed dissipated prematurely on the 12-13 February in the simulation (Fig. 36).

The 2-m temperatures showed somewhat higher RME errors compared to observations in the other Utah basins. The reasons for these errors in these basins are unknown, as only limited surface observations are available with which to validate the models in these basins for the episodes of interest. Careful analysis of the model output compared to satellite observations of cloud cover and snow cover points to model issues with one or both of these factors (e.g., model melts snow too fast or model has too much or too little cloud cover) likely played a role in these basins.

The warm model temperature bias in the Utah Valley between 10-15 February appears related to early snow melt-out in the model as well as the simulated clouds dissipating too early. A similar situation is noted in the Cache Valley. In the Uinta Basin, both warm and cold model temperature biases occurred during the simulations. During the first half of the cold-air pool, a warm model temperature bias in the Uintah Basin during nighttime between 7-12 February is related to the model creating extensive cloud cover when in reality there was none (Fig. 37). During the second half of the episode, the spurious clouds in the Uintah Basin remain, resulting in less melting of the snow compared to reality, so the surface temperatures modeled at the end of the episode between 14-17 February are biased somewhat warm (Fig. 37)

Table 14. WRF performance for **2-m temperature (°C)** for 1-17 February 2016 cold-air pool

Station	Bias (°C)	RMS Error (°C)
Hawthorne	0.254	2.627
Salt Lake City	0.395	1.919
Lindon	2.491	4.203
Vernal	-0.598	3.597
Logan	5.405	6.469

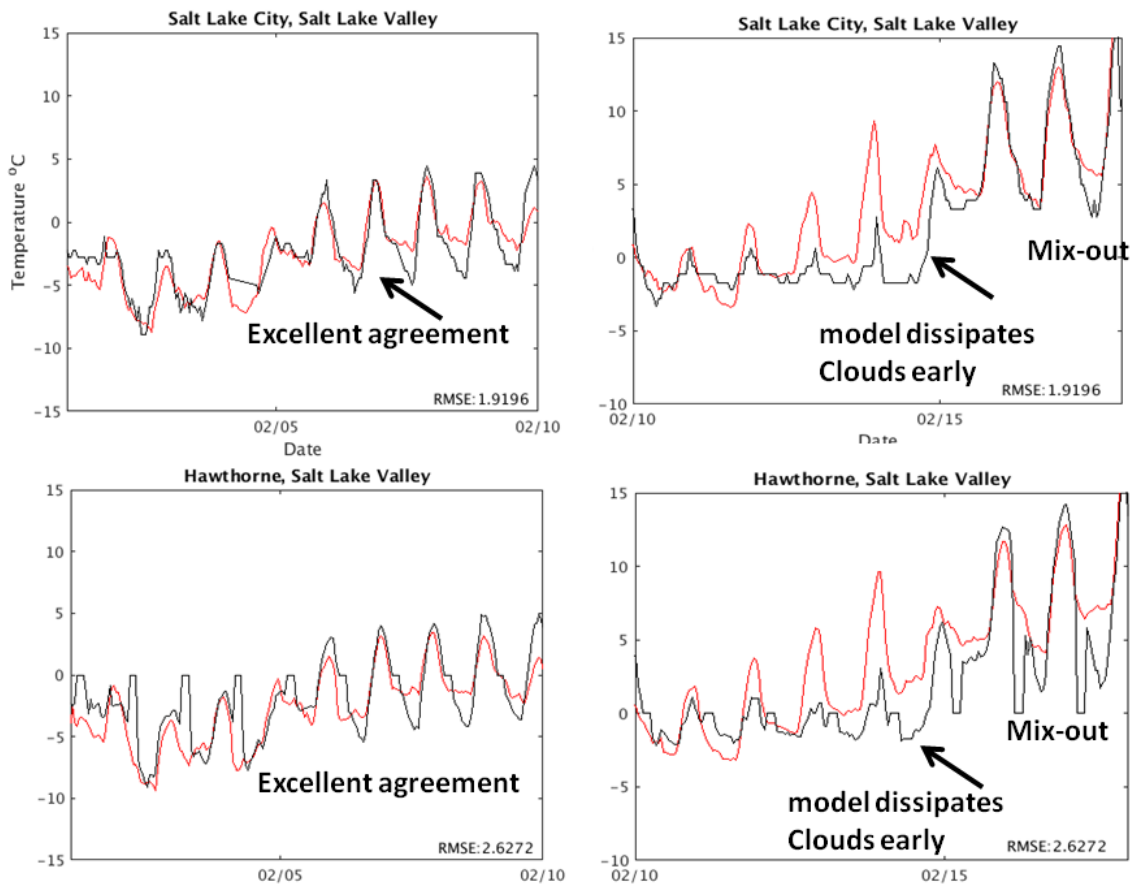


Figure 36. Comparison of model (red line) and observed (black line) 2-m temperature in the Salt Lake Valley at the Salt Lake City International Airport (top) and the UDAQ Hawthorne Elementary (bottom) between 1-18 February 2016.

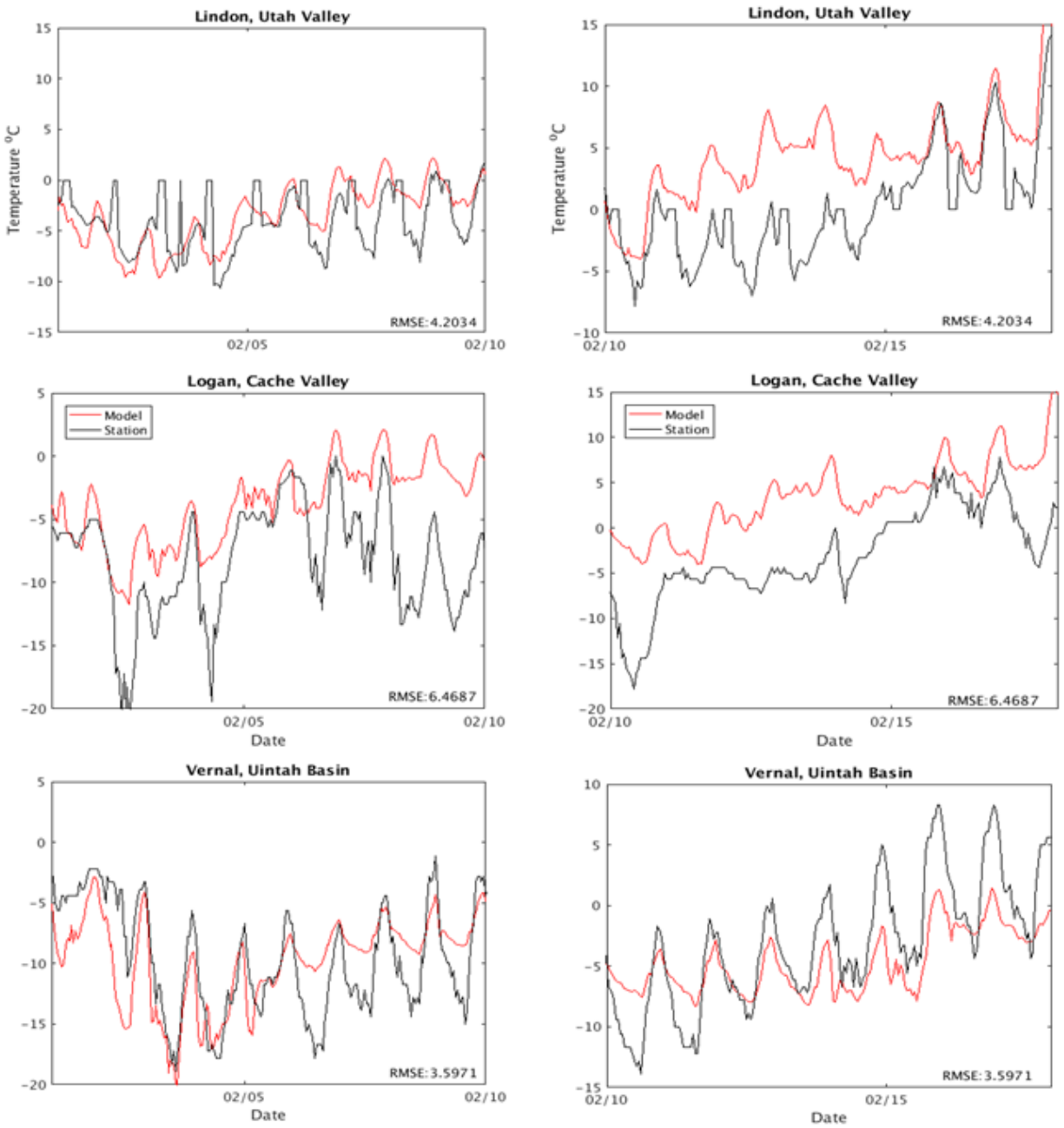


Figure 37. Comparison of model (red line) and observed (black line) 2-m temperature (°C) in the Utah Valley (top panel), Cache Valley (middle panel), and Uintah Basin (bottom panel) for 1-18 February 2016.

10-m wind speeds biases and errors were generally low for all basins (Table 15), as the model reproduced the light winds associated with cold-air pool conditions. Wind speeds in the model and observed generally remained below 3 m s^{-1} at all observation locations during the duration of the cold-air pool. The weakest winds were observed and simulated at Vernal, with the strongest winds, presumably because of lake breezes and drainage flows, were observed at the Salt Lake International Airport (Figures 38 and 39). While the numerical simulations in general captured the very light wind speeds, the numerical simulations were unable to simulate winds below around 0.75 m s^{-1} . At extremely light or calm (0 m s^{-1}) wind speeds, the model continued to simulate a $0.5\text{-}1 \text{ m s}^{-1}$ flow.

Wind directions were also analyzed but are not shown here as they were not deemed important. Wind directions are highly irregular, sporadic, and controlled by small unrepresentative terrain and building features during such light speeds.

Table 15. WRF performance for 10-m wind speed for 1-17 February 2016 cold-air pool

Station	Bias (m s^{-1})	RMS Error (m s^{-1})
Hawthorne	-0.126	0.921
Salt Lake City	-1.094	1.862
Lindon	0.072	0.995
Vernal	-0.261	1.445
Logan	0.508	1.620

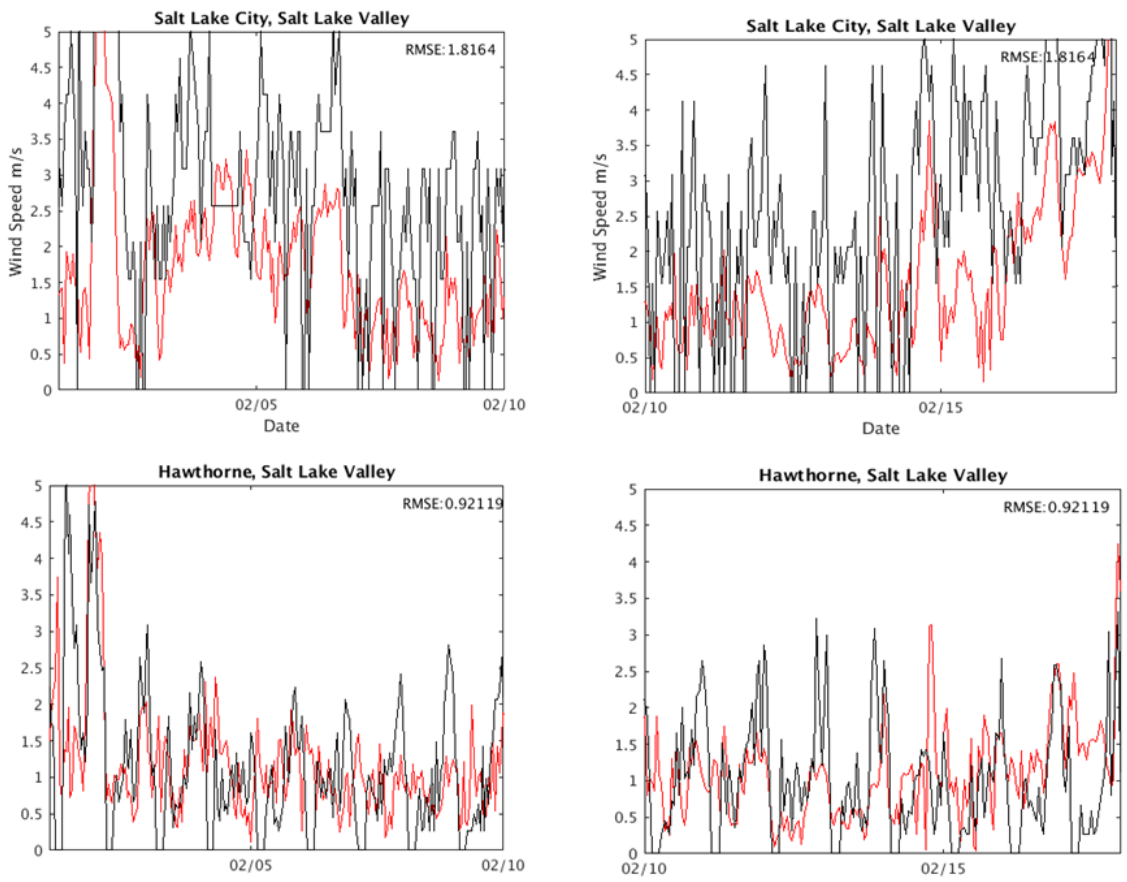


Figure 38. Comparison of model (red line) and observed (black line) 10-m wind speed (m s^{-1}) in the Salt Lake Valley at the Salt Lake City International Airport (top) and the UDAQ Hawthorne Elementary (bottom) between 1-18 February 2016.

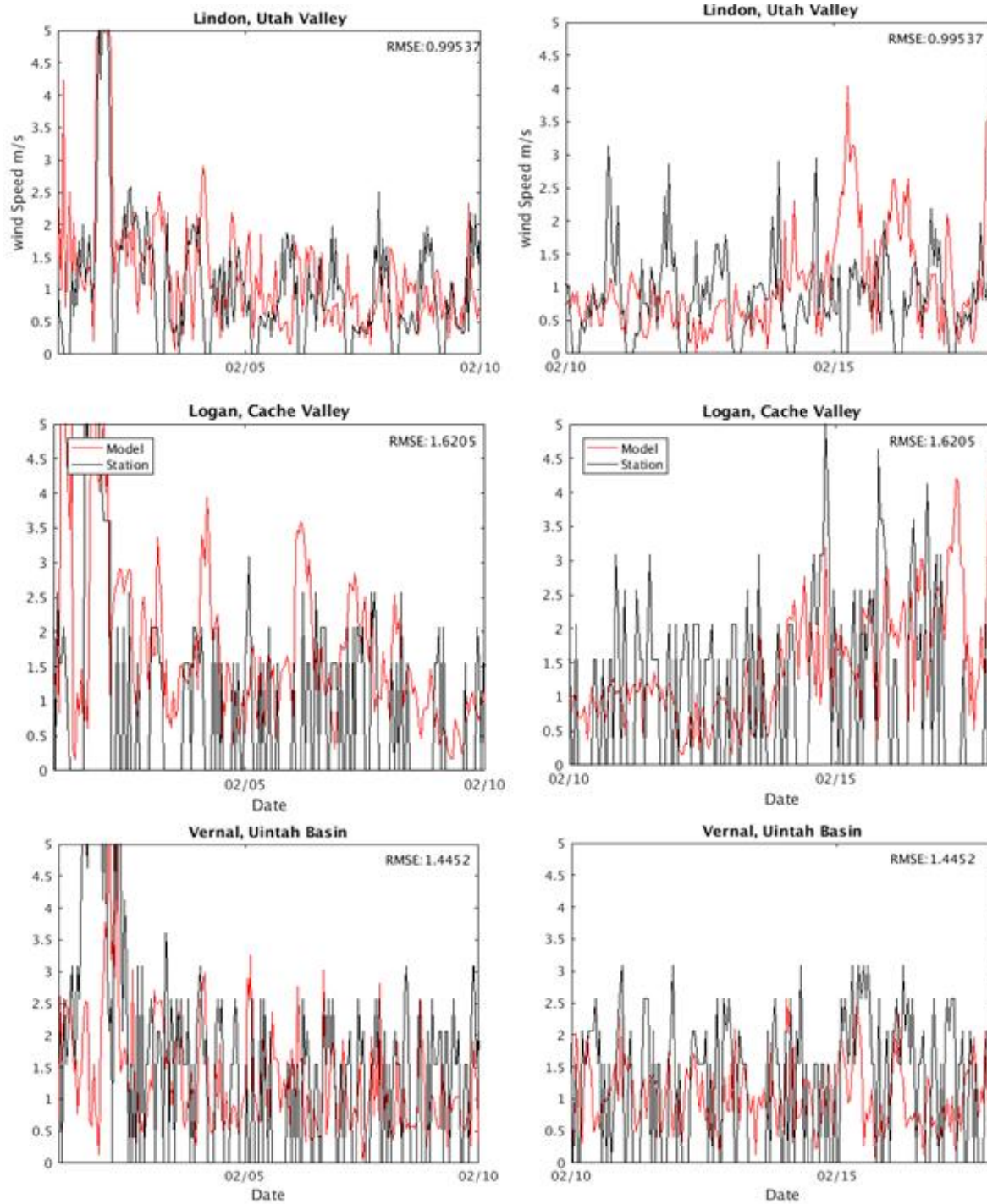


Figure 39. Comparison of model (red line) and observed (black line) 10-m wind speed (m s^{-1}) in the Utah Valley (top panel), Cache Valley (middle panel), and Uintah Basin (bottom panel) for 1-18 February 2016.

4. Summary

Improved WRF meteorological modeling of cold-air pools was developed for the Utah Division of Air Quality by the University of Utah. The modeling framework described in this study that was used by the UDAQ (the BASE simulation) resulted in overall improvements of the ability of the model to accurately simulate the cold-air pool as compared to the standard 'default' WRF configuration as validated against PCAPS observations. Less validation data existed with which to validate the December 2013 and February 2016 cold-air pools.

Three cold-air pools were simulated with the WRF model:

- 1-11 January 2011
- 7-21 December 2013
- 1-17 February 2016

The improved final WRF "BASE" configuration used by UDAQ was shown to generally simulate the following characteristics of the January 2011, December 2013 and February 2016 cold-air pools well:

- Synoptic large-scale evolution (i.e., passage of weather systems, wind speeds at mountaintop level, subsidence capping inversion above 1500 m above ground level)
- Surface and boundary-layer temperature evolution
- Snow cover, snow depth over all surfaces
- Cloud cover in the Salt Lake Valley
- Snow albedo over barren surfaces
- Boundary-layer flow timing and location

The simulations struggled with modeling of the following characteristics of the cold-air pools:

- Boundary-layer flow intensity and height above surface
- Extremely light or calm winds (less than $0.5\text{-}1.0\text{ m s}^{-1}$) are always over-predicted by the models
- Boundary-layer cloud occurrence and depth in all basins but Salt Lake Valley
- Depth of vertical mixing during the afternoon transition period

Further fundamental research is needed to improve these problems, including improved surface snow cover evolution and physics, planetary-boundary layer, and cloud microphysical schemes.

5. References

- Avey, L., 2013: PM_{2.5} State Implementation Plan: Meteorological Modeling. Utah Division of Air Quality.
- Crosman, E., and J. Horel, 2009: MODIS-derived surface temperature of the Great Salt Lake. *Remote Sensing of Environment*, **113**, 73-81.
- Crosman, E.T., and J.D. Horel, 2016: Wintertime Lake Breezes near the Great Salt Lake. *Boundary-Layer Meteorology*. **159**(2), 439-464
- Crosman, E.T., and J.D. Horel, 2017: Large Eddy-Simulations of a Salt Lake Valley cold air pool. Submitted to *Atmospheric Research*.
- Foster, C., 2015 MS Thesis. University of Utah Available in online archive at: <http://content.lib.utah.edu/cdm/ref/collection/etd3/id/4007>
- Foster, C., E.T. Crosman, and J.D. Horel, 2017: Simulations of a Cold-Air Pool in Utah's Salt Lake Valley: Sensitivity to Land Use and Snow Cover. Accepted, *Boundary-Layer Meteorology*
- Joseph A. Grim, Jason C. Knievel, Erik T. Crosman, 2013: Techniques for Using MODIS Data to Remotely Sense Lake Water Surface Temperatures. *Journal of Atmospheric and Oceanic Technology* **30**:(10), 2434-2451
- Lareau NP, Crosman ET, Whiteman CD, Horel JD, Hoch SW, Brown WOJ, Worst TW, 2013: The Persistent Cold-Air Pool Study. *Bull Am Meteorol Soc.* 94, 51-63.
- Lareau NP, Horel JD, 2015a: Dynamically induced displacements of a persistent cold-air pool. *Boundary-Layer Meteorol.* 154, 291-316.
- Lareau NP, Horel JD, 2015b: Turbulent erosion of persistent cold-air pools: numerical simulations. *J Atmos Sci* 72:1409-1427
- Lyman, S., Mansfield, M., Shorthill, H., Anderson, R., Mangum, C., Evans, J., and Shorthill, T.: Distributed measurements of air quality and meteorology, in: Final report: 2013 Uinta Basin winter ozone study, edited by: Stoeckenius, T. and McNally, D., ENVIRON International Corporation, Novato, California, chapter 3, 1–35, available at: http://www.deq.utah.gov/locations/U/uintahbasin/ozone/docs/2014/06Jun/UBOS2013FinalReport/UBOS_2013Sec_3_DistribMon.pdf, last access: 15 November 2016.
- Lu W, Zhong S, 2014: A numerical study of a persistent cold-air pool episode in the Salt Lake Valley, Utah. *J Geophys Res Atmos* 119:1733-1752
- Neemann, E.M., Crosman, E. T., Horel, J. D., and Avey, L, 2015: Simulations of a cold-air pool associated with elevated wintertime ozone in the Uintah Basin, Utah, *Atmos. Chem. Phys.*, 15, 135-151.